OXYGEN DIFFUSION
IN DISLOCATIONS AND GRAIN BOUNDARIES
IN MAGNESIUM OXIDE

by

LEONARD E. DOLHERT

B.S. Massachusetts Institute of Technology
(1979)

Submitted to the Department of
Materials Science and Engineering
in Partial Fulfillment of the
Requirements of the
Degree of

DOCTOR OF PHILOSOPHY

at the

MASSACHUSETTS INSTITUTE OF TECHNOLOGY

September 1985

Signature of Author________________________________
Department of Materials Science and Engineering
August 9, 1985

Certified by________________________________
W. D. Kingery
Thesis Supervisor

Accepted by________________________________
Bernhardt J. Wuensch
Chairman, Departmental Committee on Graduate Students

OXYGEN DIFFUSION
IN DISLOCATIONS AND GRAIN BOUNDARIES
IN MAGNESIUM OXIDE

by

LEONARD E. DOLHERT

Submitted to the Department of
Materials Science and Engineering
on August 9, 1985 in partial
fulfillment of the requirements for the
Degree of Doctor of Philosophy

Abstract

Oxygen-18 gas exchange followed by concentration profile determination by Secondary Ion Mass Spectrometry (SIMS) was performed on single crystals, deformed single crystals and polycrystals of MgO. The following results were obtained for the temperature range 1200 °C-1500 °C for undoped MgO.

$$D=(3.9\ {}^{+10.5}_{-2.9}) \times 10^{-6}\ \exp(-\frac{3.45 \pm 0.17\ \text{eV}}{kT})\ \text{cm}^2/\text{sec} \qquad 1200\text{-}1500\,^\circ\text{C}$$

$$D'_d a^2 = 10^{-(15.9\pm1.9)}\ \exp(-\frac{3.20 \pm 0.58\ \text{eV}}{kT})\ \text{cm}^4/\text{sec}$$

$$D'_b \delta = 10^{-(6.5\pm2.2)}\ \exp(-\frac{4.06 \pm 0.78\ \text{eV}}{kT})\ \text{cm}^3/\text{sec}$$

where D = bulk diffusion coefficient
D'_d = diffusion coefficient within a dislocation
a = dislocation core radius
D'_b = diffusion coefficient within a grain boundary
δ = grain boundary thickness

Error intervals are for 68% confidence calculated from standard deviations from linear regression of Arrhenius plots. Activation energies for oxygen diffusion in the bulk, dislocations, and grain boundaries are the same within the experimental error. At 1200 °C it was found that $D'_b = D'_d = 10^{5.3} D$ and that δ and a are both less than 10 angstroms.

Thesis Supervisor: W. D. Kingery
Title: Professor of Ceramics

Table of Contents

List of Abbreviations

a = dislocation core radius

A = a constant approximately equal to 1 in dislocation diffusion equations

C = concentration of oxygen-18 = #18/(#18+#16)

channel = period of time during which the SIMS mass spectrometer is switched to each mass for a given amount of time until all the desired masses have been sampled. This whole process is repeated any number of times.

C_b = concentration of oxygen-18 beyond diffusion zone = 0.00204

CN = channel number

C_s = surface oxygen-18 concentration, assumed equal to oxygen-18 concentration in the exchange system's oxygen, 0.9554

$C' = (C-C_s)/(C_b-C_s)$

d = dislocation density

D = bulk or "lattice" diffusion coefficient of oxygen

D' = diffusion coefficient of oxygen in a grain boundary or dislocation

D'_b = diffusion coefficient of oxygen in a grain boundary

D'_d = diffusion coefficient of oxygen in a dislocation

F center ≡ oxygen vacancy with 2 associated electrons $Vo^{++} + 2e'$ in Kroger Vink notation

g = grain size

I = SIMS primary ion beam current

k = Boltzmann constant = 8.62×10^{-5} eV/°K

N = number of experimentally determined values

Oxygen-16 = Oxygen of mass 16

Oxygen-18 = Oxygen of mass 18

O-16 = Oxygen of mass 16

O-18 = Oxygen of mass 18

p = SIMS sputter pit depth

S = an entropy factor assumed to be unity

SIMS = Secondary Ion Mass Spectrometry

t = time, usually diffusion time at a constant temperature

t_s = total sputtering time for a sputtered pit.

x = distance perpendicular to sample in same direction as oxygen diffusion

x_p = estimated diffusion penetration depth

Z = the number of ways a vacancy pair can orient itself in the lattice.

δ = grain boundary thickness

ϵ_t = true strain

σ = standard deviation

$\mu m = 10^{-6}$ meters

#CN = total number of channels for a sputter pit

#16 = number of counts of oxygen-16 from mass spectrometer

#18 = number of counts of oxygen-18 from mass spectrometer

List of Figures

List of Tables

Acknowledgements

First I would like to thank my thesis advisor Prof. Kingery for his guidance, patience, and desire to teach me how to solve problems in a logical way.

I would also like to thank my wife Diana Healy for her continued encouragement and for the excellent word processing and computer plotting she has done.

Many thanks are due to members of my research group--Emilio Giraldez for his help with experiments, Emilio Giraldez and Alexana Roshko for the polycrystal used in experiments, and Dunbar Birnie III and Yet-Ming Chiang for many helpful discussions.

I also thank Han-Ill Yoo for many helpful discussions.

I am grateful to Pat Kearney for technical help in setting up experiments. I am grateful to Carol Handwerker for supplying MgO powder and Na doped polycrystals, and also to Scott Wuthrich for his help in transferring data from an HP computer to an IBM computer.

Prof. A. Mocellan and his students at the Ecole Polytechnique Federale de Lausanne deserve thanks for deforming some MgO samples.

I thank Masayuki Fujimoto for TEM pictures of my samples.

I would also like to thank Professors Bernhardt J. Wuensch, Robert L. Coble, and Kenneth C. Russell for helpful discussions and critical review of this thesis.

I also thank Susan Rosevear for her help with office matters.

Secondary Ion Mass Spectrometry was carried out in the Center for Microanalysis of Materials, University of Illinois, which is supported by DOE under contract DE-ACo2-76ER 01198. I'd like to thank Judy Baker and Chris Loxton for their technical assistance and helpful discussions regarding SIMS.

The support of Department of Energy contract DE-ACo2-76ER02390 is gratefully acknowledged.

1.0 INTRODUCTION

This is a study of oxygen diffusion in magnesium oxide. Secondary Ion Mass Spectrometry (SIMS) was used to measure oxygen-18 concentration gradients. Effort was concentrated on analyzing the low concentration, deep penetration part of the diffusion profile, often called a "tail", which is dominated by dislocation and grain boundary diffusion.

Fast grain boundary and dislocation diffusion has been best characterized in metals, and those results offer a useful comparison when studying diffusion in ceramics. These results have been reviewed by Balluffi[1] for dislocations and Martin and Perraillon[2] for grain boundaries. Some of the general results are:

1. The diffusion coefficient within the core of the grain boundary or dislocation is about 10^4 to 10^6 times that of lattice diffusion.
2. The grain boundary thickness (δ) and dislocation core radius (a) are about 5-10 angstroms.
3. The activation energy for grain boundary or dislocation diffusion is on the order of 0.5 to 0.7 times that of bulk diffusion.

Diffusion in ceramic grain boundaries and dislocations is more complicated than in metals. Boundaries and dislocations generally have associated space charge and impurity segregation which may affect diffusion of the anion and cation in different manners. Most ceramics are not available in as pure a form as most metals so that in many cases intrinsic behavior cannot be observed. Results for oxides, alkali halides, and carbides have been reviewed by Atkinson[3].

MgO offers some advantages as a model ceramic system, even though its high melting point (2800 °C) and lack of purity make studying intrinsic properties very difficult. Its rock salt structure has often been used to model dislocation and grain boundary structure. Because of its cubic structure many bulk properties, such as diffusion, are isotropic. Its bond type is mostly ionic and it has a high degree of stoichiometry.

2.0 LITERATURE REVIEW

2.1 OXYGEN DIFFUSION IN MAGNESIUM OXIDE

There have been many studies of oxygen diffusion in magnesium oxide. (Ref's 4-28) The data are summarized in Table 1 and the bulk diffusion data is plotted in Figure 1. There is not a consensus on activation energies. These have been reported over a range of 1.3 to 5.6eV. Some authors have broken their data into high and low temperature regions while others have not. The reported diffusion coefficients themselves are spread out over more than an order of magnitude at most temperatures. The datas of Shirasaki[20,21,22,23] are particularly difficult to interpret as they were based on gas exchange of "loosely sintered" materials prepared from carbonates or chlorides, while other authors used large grained or single crystal material.

In most of these studies the shape of the oxygen diffusion gradient was not determined. Most of these studies used a technique where the average oxygen-18 concentration of the whole sample or of the gas phase was measured after gas exchange between the sample and O-18 gas. In most gas exchange experiments, stable isotope oxygen-18 was diffused into the sample for a measured time at a measured temperature. Often the sample was crushed before the diffusion anneal, and then the oxygen in it converted to CO_2 afterwards. This gas sample or the diffusion anneal atmosphere was then analyzed in a mass spectrometer. The gas sample analysis was plugged into an equation[29] to arrive at a "Bulk Diffusion Coefficient". The gas concentration at time t divided by the gas concentration at equilibrium with the sample, is proportional

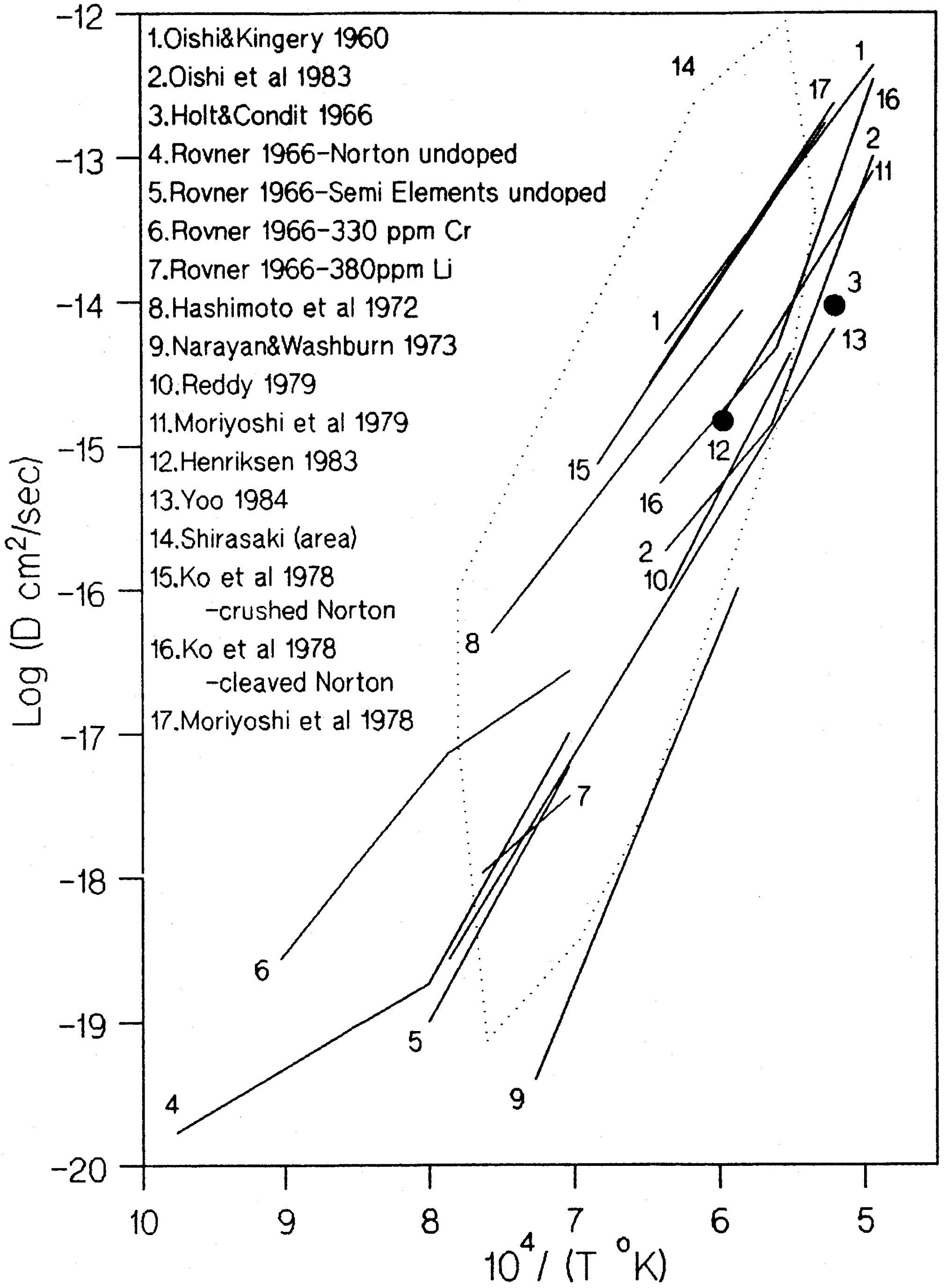

Fig. 1 Previous bulk oxygen diffusion data for MgO.

Table I

Oxygen Diffusion Data in MgO

Literature Survey

Authors	Ref.	Technique	P_{O_2} Torr	T °C	$^*D_o$ Cm^2/sec	$^*E$ ev	Sample**
Bulk Diffusion							
Oishi & Kingery 1960	4	O-18 gas exchange with solid, gas mass spectrometry	150	1300-1750	2.5×10^{-6}	2.71	Low purity (~100ppm Si) Crushed single crystals
Oishi et al. 1983	5	O-18 gas exchange with solid, gas mass spectrometry	150	1300-1500	2.2×10^{-9}	2.21	Norton Co. chemically polished
Oishi & Ando 1984	6			1500-1750	6.76	5.55	(50u removed) single crystals
Ando et al. 1983 Oishi & Ando 1984	7 6	gas exchange, mass spectrometry	150	1400-1700			Chemically polished Fe doped (310,2300, and 12900 ppm) Spicer single
Results agree with Oishi et al. (1983), ie, no effect of Iron							
Condit & Holt 1964	8	O-18 gas exchange & proton activation autoradiography	?	1610	---	--	MgO bicrystal
Bulk penetration depth 2um, 17 hours, therefore $D\sim10^{-13} cm^2/sec$							
Holt & Condit 1966	9	O-18 gas exchange, proton activation autoradiography	120	1650	---	--	Fused Semi Elements polycrystal
$D=10^{-14}$ cm^2/sec							
Rovner 1966	10	O-18 gas exchange with solid, gas mass spectrometry	1	975-1150	4.3×10^{-5}	3.56	Crushed? Norton single crystals
				750-975	4.8×10^{-14}	1.31 ±0.13	
				975-1150	2.4×10^{-5}	3.56 ±0.13	Crushed? Semi Elements single crystals
				1000-1150	4.8×10^{-12}	1.47 ±0.17	Norton Co, Cr 330ppm doped crushed?
				834-1000	1.5×10^{-8}	2.36 ±0.13	
				1040-1150	1.4×10^{-11}	1.85 ±0.22	Semi Element Li 380ppm doped crushed?

Table 1 (cont.)

Hashimoto et al. 1972	11	O-18 gas exchange with solid, gas mass spectrometry	40	1050-1438	4.5×10^{-7}	2.61	Crushed polycrystals made from carbonate
Narayan &Washburn 1973	12	TEM observation of dislocation loop shrinkage	air	1100-1427	$1.37\pm0.26\times10^{-2}$	4.78 ±0.18	Muscle Shoals single crystals
Ko et al. 1978	13	Gas exchange, mass spectrometry	?	1190-1630	1.1×10^{-5}	2.95	Crushed Norton single crystals
			?	1510-1760	5.42	5.33	Cleaved Norton single crystals
				1290-1510	4.61×10^{-8}	2.46	
Moriyoshi et al. 1978	14	Gas exchange, mass spectrometry	?	1273-1650	9.8×10^{-6}	2.92	Crushed single crystals and chemically polished single crystals
Reddy 1979	15 16	O-18 gas exchange, proton activation, alpha particle energy analysis	760-800	1310-1550	$1.9^{+4.8}_{-1.4}\times10^{-4}$	3.84 ±0.21	Mechanically polished ORNL single crystals
Moriyoshi et al. 1979	17	Polygonization of dislocations observed by TEM	air	1400-1750	1.35×10^{-5}	3.28	Mechanically damaged Tateho single crystal sheets
Henriksen et al. 1983	18	Mg(O-18)/Mg(O-16) interdiffusion, SIMS diffusion profile determination	---	1400	---	--	Chemically polished ORNL

$D=(1.6\pm0.3)\times10^{-15}$ cm^2/sec, no effect of adding 1400ppm Sc.

Yoo 1984	19	O-16 gas exchange with Mg(O-18) epitaxial layer, Mg(O-18)/Mg(O-16) interdiffusion, SIMS diffusion profile	air	1000-1650	$1.81^{+2.9}_{-1.1}\times10^{-6}$	3.24 ±0.13	Epitaxial MgO-18 layer on Norton substrate

Table 1 (cont.)

Shirasaki &Oishi 1971	20	gas exchange, mass spectrometry	8	1415			Crushed polycrystalline MgO
D=2×10^{-13} cm^2/sec							
Shirasaki &Hama 1973	21	gas exchange mass spectrometry	35	1020-1450	2.4×10^{-7}	2.42 ±0.22	Crushed well sintered polycrystal prepared from carbonate
				1020-1260	1.6×10^{-7}	2.61 ±0.26	Crushed loosely sintered polycrystal prepared from carbonate
				1260-1450	9.9×10^{-1}	4.46 ±0.43	
Shirasaki et al. 1973	22	gas exchange mass spectrometry	40	1190-1420	4.5×10^{-7}	2.61	Crushed polycrystal
					5.2×10^{-7}	1.93	3.5% Li crushed polycrystal
10-100 increase in D due to Li							
Shirasaki et. al. 1984	23	gas exchange mass spectrometry	40	1209-1466	3.0×10^{-7}	2.62	Polycrystals prepared from chloride, sintered at 1400°C and crushed
				1466-1570	3.5×10^{-3}	3.99	
				1043-1136	1.1×10^{-8}	2.93	Polycrystals prepared from chloride, sintered at 1250°C, and crushed
				1136-1330	1.2×10^{-3}	4.24	
				1043-1156	1.2×10^{-8}	26.59***	Crushed polycrystals prepared from Johnson Matthey powder sintered at 1450°C and gently crushed and annealed (1450°C, 4 hr.) polycrystals prepared from same powder sintered at 800°C
				1156-1513	1.5×10^{-5}	3.47	
				1380-1540	5.0×10^{-5}	2.73	2000ppm Si polycrystals prepared from chloride, sintered at 1550°C, & crushed

Table 1 (cont.)

				1340- 1466	4.4×10^{-5}	2.90	Same as above except sintered at 1450°C
				1466- 1540	9.8×10^{5}	6.94	
				1330- 1370	2.0×10^{8}	7.80	Same as above except sintered at 1250°C
				1250- 1451	6.9×10^{9}	7.98	100 ppm Ca polycrystals prepared from chloride, sintered at 1550°C, & crushed
				1116- 1242	2.0×10^{-7}	2.94	Same as above except sintered at 1250°C
				1242- 1340	2.1×10^{9}	8.07	

Grain Boundary Diffusion

Condit & Holt 1964	8	O-18 gas exchange & proton activation autoradiography	?	1610	---	--	MgO bicrystal

Grain boundary diffusion penetration depth >20um, t=17 hours

Holt & Condit 1966	9	O-18 gas exchange, proton activation autoradiography	120	1650	---	--	Fused Semi Elements polycrystal

$$\frac{D'_b\delta}{D} > 4.8\times10^{-4}$$

McKenzie et al. 1971	24	O-18 gas exchange, proton activation autoradiography	115	1621- 1743	---	--	Polycrystalline Semi Elements

$$\frac{D'_b\delta}{D^{1/2}} = (1\text{-}81)\times10^{-10}\ \mathrm{cm}^2/\mathrm{sec}^{0.5}$$

factor of 5 increase with 7000 ppm Fe, included in listed range

Table 1 (cont.)

Dislocation Diffusion

Groves &Kelly 1962	25	TEM examination of dislocation dipole break-up & conservative climb	---	910-1360	---	3.1	Cleaved & bent Norton Co single crystals
Narayan &Washburn Phil. Mag. 1972	26	TEM examination of self climb of dislocation loops	---	1100-1250	$^*D'_{d,o}$(Area)= $7.5\pm4.3 \times 10^{-18}$ cm^4/sec	2.62 ±0.15	Cleaved & bent large grained polycrystalline Muscle Shoals (Al~600ppm)
Narayan &Washburn Crystal Lattice Defects 1972	27	TEM examination of shrinking loop connected to foil surface by a screw dislocation	---	1167-1376	$^*D'_{d,o}$= 3.0×10^{-3} cm^2/sec	2.72 ±0.22	Same as above
		IEM observation of edge dislocation dipole breakup	---	927	---	2.60 ±0.22	Same as above

Notes:

*Pre-exponential D_o and activation energy energy E for bulk diffusion equation

$$D=D_o \exp(-E/kT) \text{ cm}^2/\text{sec}$$

except where noted for Narayan & Washburn's pre exponentials for dislocation diffusion.

$$D'_d = D'_{d,o} \exp(-E/kT) \text{ cm}^2/\text{sec}$$

and

$$D'_d(\text{Area}) = D'_{d,o}(\text{Area}) \exp(-E/kT)$$

"Area" is the area of a cross section of the dislocation core.

**Manufacturers of MgO in this column are as follows:

Norton Co.,	Worcester, MA
Semi-Elements, Inc.,	Saxonburg, PA
Oak Ridge National Laboratory,	TN
Taheto Corp.,	Japan
Muscle Schoals Electro-Chemical Corp.,	Tuscumbia, AL
W&C Spicer Ltd.,	England
Johnson Matthey Co.,	New York, NY

***The activation energy of 26.59 must be a misprint.

to $(Dt/a)^{1/2}$, where D is the bulk diffusion and a is the particle radius. This method cannot determine the effectiveness of dislocations and grain boundaries as paths for diffusion because their effect, if any, is averaged in with the "Bulk Diffusion Coefficient". Errors can be introduced in choosing the particle radius a and by dislocations and cracks introduced during crushing.

Narayan & Washburn[12] obtained oxygen diffusion coefficients by studying dislocation loop shrinkage by transmission electron microscopy. They do not present an Arrhenius plot of diffusion coefficients so it is hard to compare the reliability or scatter of their data with that of others. They obtained the lowest measured oxygen diffusion coefficient and one of the higher activation energies. However, it is based on the assumption that the dislocation loop can maintain the oxygen potential around itself for it to shrink at a rate determined by oxygen diffusion alone. At extremely high rates of oxygen vacancy annihilation or creation, this may not be a valid assumption. For a given oxygen flux, the source or sink rate per unit dislocation line length must increase as the loop becomes smaller.

$$\text{Source/Sink rate} = \frac{\text{Oxygen flux}}{2\pi r} \tag{2.1}$$

r = dislocation loop radius

As r becomes very small, the source or sink rate becomes very high. In order to calculate a diffusion coefficient from dislocation loop shrinkage, one must determine the shrink rate and its time and radius dependence. Then one must make assumptions to create an equation relating loop shrinkage to oxygen diffusion and extract a diffusion coefficient. This indirect method, however elegant, depends on many assumptions and never actually measures an oxygen potential or concentration gradient. Also, the loop radius shrink rate may be controlled by impurities. These may concentrate at the shrinking loop, creating a unique chemical environment which might change as the loop radius becomes very small. Impurity drag may slow the loop from shrinking (i.e., creeping). Lastly, one may have to consider cation diffusion or cation vacancy creation/annihilation. For a MgO dislocation loop to shrink, vacancies of oxygen and magnesium must be created someplace, diffuse, and then be anihilated.

Yoo[19] performed a very thorough oxygen bulk diffusion study. He grew low dislocation density single crystal MgO-18 material. Gas exchange was performed with O-16 atmosphere (air) and then concentration profiles were determined using Secondary Ion Mass Spectrometry (SIMS). He studied a wider temperature range than other authors. Therefore his activaion energy of 3.24eV may be considered more accurate than those of other authors. Also, the fact that epitaxially grown low dislocation density material was studied rather than mechanically polished or crushed material means that dislocations and grain boundaries probably did not enhance the measured bulk diffusion coefficient. This may be why Yoo's oxygen diffusion coefficient is at the lower end of all other authors except Narayan and Washburn[12].

Yoo[19] also concluded that overall gas exchange and diffusional kinetics are not slowed by surface exchange down to 1100°C and probably to 1000°C. Reddy and Cooper[15,16] also found that surface exchange does not influence kinetics in the 1300 to 1600°C temperature range which they studied.

In oxide ceramics, there is not much quantitative data for grain boundary or dislocation oxygen diffusion. There are several reasons for this. First, oxygen diffusion is generally much slower than cation diffusion, making measurements difficult. Second, there is no suitable radioactive isotope for tracer oxygen diffusion measurements. Third, the techniques used to study fast oxygen diffusion have generally not examined deep concentration profiles but have inferred fast grain boundary or dislocation diffusion from overall kinetics--such as oxidation-reduction rates or total oxygen uptake during gas-solid exchange.

In Al_2O_3, Oishi and Kingery[30] found faster oxygen diffusion in polycrystalline particles than for single crystal particles. When these results were recalculated using grain size rather than sample particle size in determining surface area for oxygen gas exchange, the diffusion coefficients for both types of sample were the same[31]. It was reasoned that oxygen grain boundary diffusion was fast enough to equilibrate the grain boundaries with the atmosphere in a very short time and subsequent diffusion was from the grain boundaries into the grain.

There is some evidence for fast grain boundary diffusion in MgO. There are a number of papers on oxygen gas exchange experiments[11,20,21,22] in which the grain sizes rather than the particle size was used to calculate diffusion coefficients. Fast diffusion in grain boundaries was reasoned as in the case of Al_2O_3[30,31] mentioned above. Proton activation and autoradiography[8,9,24] has been used to show deep penetration of oxygen-18 in MgO grain boundaries. McKenzie et. al.[24] analyzed some MgO bi-crystal boundaries by this technique. They obtained data in the range

$$\frac{D'_b \delta}{D^{0.5}} = (1\text{-}81) \times 10^{-10}\ \mathrm{cm^2/sec^{0.5}} \qquad 1621\text{-}1743^\circ\mathrm{C} \tag{2.2}$$

where D'_b = diffusion coefficient of oxygen in a grain boundary
D = bulk diffusion coefficient of oxygen
δ = grain boundary thickness

They claim $D'_b \delta/\sqrt{D}$ increased by a factor of 5 when samples were doped with 7000 ppm

Fe. Their data are consistent with $D'_b/D = 10^5-10^6$ and a 5-10 angstrom grain boundary thickness.

Oishi et.al. [5] studied oxygen self diffusion in MgO by the previously mentioned isotope gas exchange technique which averages in grain boundary and dislocation effects in determining a "Bulk Diffusion Coefficient". They found higher measured bulk diffusion coefficients in crushed and cleaved samples than in chemically polished samples. Much of the scatter in oxygen bulk diffusion literature may be due to mechanically introduced dislocations or grain boundaries.

Henriksen et. al. [18] demonstrated the feasibility of using secondary ion mass spectrometry on MgO to observe deep O-18 concentration "tails" due to grain boundary diffusion. They found enhanced oxygen bulk diffusion in a deformed MgO sample which showed a diffusion "tail".

There is also evidence for fast oxygen diffusion in MgO dislocations, sometimes referred to as oxygen pipe diffusion. Holt and Condit [9] observed enhanced oxygen-18 diffusion in dislocations by proton activation and autoradiography, but no quantitative analysis was done. They found dislocations to be less effective than grain boundaries, but their Semi Elements MgO material was relatively impure and may have had a second phase at the grain boundaries. Their attempts to increase the amount of diffusion by increasing the dislocation density gave inconclusive results.

Groves and Kelly [25] analyzed edge dislocation dipole breakup in MgO by transmission electron microscopy. By measuring the wave length of dipole spacing fluctuations and the spacing of dislocation loops after the dipole breaks up, they obtained an activation energy for the motion of point defects in the core of an edge dislocation of approximately 3.1eV.

Narayan and Washburn[27], using the same technique, obtained an activation energy of 2.60±0.22eV. They also examined a shrinking loop connected to the foil surface by a screw dislocation. They obtained the following equation for motion of point defects in a screw dislocation.

$$D'_d = 3.0 \times 10^{-3} \exp\left(\frac{-2.72 \pm 0.22 \text{ eV}}{kT} \right) \text{cm}^2/\text{sec} \quad 1167\text{-}1367^\circ\text{C} \qquad (2.3)$$

They attributed this to oxygen diffusion. In a different TEM study[26] Narayan and Washburn looked at self climb of dislocation loops where coplanar dislocation loops move closer together by means of pipe diffusion due to their interacting strain fields. They obtained the following result for diffusion in dislocations.

$$D'_d A = (7.5 \pm 4.3) \times 10^{-18} \exp\left(\frac{-2.62 \pm 0.15 \text{ eV}}{kT} \right) \text{cm}^4/\text{sec} \quad 1100\text{-}1250^\circ\text{C} \qquad (2.4)$$

where A is the cross-sectional area of a dislocation.

This agrees with their previous results[27] at 1208°C (the center of the overlap of their temperature ranges) if a core radius of 4×10^{-8} cm is assumed and A is calculated as $\pi(4\times10^{-8}\text{cm})^2$. As in the case of determining a bulk diffusion coefficient by dislocation climb, these TEM studies must relate the TEM observations to diffusion coefficients through a complex equation. Assumptions must be made as to the form of that equation and to the values for constants within it. This method of studying diffusion is very indirect and perhaps inaccurate.

In the case of MgO there are some anomalies which may relate to fast oxygen grain boundary and dislocation diffusion. As has been already mentioned McKenzie et. al.[24] found greater enhanced grain boundary diffusion in samples doped with 7000ppm Fe compared to undoped samples. Cheng[32] found redox rates in iron doped MgO faster than could be explained by known bulk diffusion coefficients. Chen et. al.[33] have found that the very fast formation of lithium color centers in lithium doped MgO under oxidizing conditions is enhanced by surface abrasion deformation. Shirasaki et.al.[22] found enhanced oxygen diffusion in lithium doped polycrystalline MgO. White et.al.[34] found very fast F center removal with activation energy of 3.4eV upon oxidation of MgO which was previously reduced in magnesium metal vapor. White et. al. interpreted this result as due to rapid oxygen pipe diffusion.

2.2 IMPURITIES AND DEFECT ENERGIES IN MAGNESIUM OXIDE

Magnesium Oxide is very difficult to make in a pure enough form to study intrinsic properties. Typically there is at least 100ppm impurity in a sample of Magnesium Oxide. Some chemical analyses of MgO materials are listed in Table 2. Perhaps the purest MgO single crystals ever made are those made at Oak Ridge National Laboratory. This material as well as the Spicer material was prepared by melting pure MgO powder under carbon electrodes.

Table 3 lists some relavent calculated defect energies for MgO. The high Schottky energy of 7-8 eV combined with the high level of impurities means that many properties, such as cation diffusion, are impurity controlled. Since MgO is

Table 2

Major Impurities in Various MgO Materials

(Weight ppm unless otherwise noted)

reference	5	16	37	38
maker	ORNL			
		appm		
Al	15	57	10	10
Ca	50	24	50	5
Cr	1	<2	1	--
Cu	--	--	<.1	5
Fe	7	3	7	10
Mn	<1	0.4	<1	10
Na	<1	--	<1	--
P	13	--	10	--
Si	22	21	15	50

reference	5	7	39	38
maker	Norton			
Al	37	--	5-25	10
Ca	210	30	300-500	50
Cr	4	10	--	10
Cu	<1	--	--	10
Fe	70	--	10-30	50
Mn	7	--	--	5
Na	<2	--	--	--
P	46	--	--	--
Si	<3	70	200-300	10

reference	9	24	38	17	40	41
maker	Semi Elements			Taheto		
		appm				
Al	30	750	10	650	55	30-60
Ca	300	300	50	330	--	40-300
Cr	5	4	--	--	32	10-130
Cu	<5	--	10	--	--	10-20
Fe	10	7	50	70	80	30-50
Mn	--	--	10	<10	4	--
Na	--	--	--	<10	135	--
P	--	--	--	<10	--	--
Si	50	70	50	300	--	--

Table 2 (cont.)

reference	27	42	43	43
maker	Muscle Shoals		Monocrystal	Ventron
Al	600	40	30	20
Ca	300	1000	250	190
Cr	20	10	15	12
Cu	<10	--	--	--
Fe	300	100	200	200
Mn	20	--	10	8
Na	--	--	20	15
P	--	--	--	--
Si	<50	100	11	<3

reference	38	44
maker	Spicer	
Al	10	20-62
Ca	5	24-72
Cr	--	--
Cu	10	--
Fe	50	3-10
Mn	--	--
Na	--	.5-3
P	--	--
Si	5	10-40

Table 3

Calculated Defect Energies in MgO

Enthalpy (eV)

Reference #'s

Process	Abbr.	45	46	47	48	49	50
Schottky defect formation	H_s	7.5	7.72	7.4-7.9	7.7	7.5	
free cation vacancy migration	H_m^c	2.16	2.07			2.1	
free anion vacancy migration	H_m^a	2.38	2.11			2.4	
cation/anion vacancy pair formation	H_f^p	-2.55			-2.67		
vacancy pair migration	H_m^p					2.5	$H_m^p \geq H_m^a$ $H_m^p \geq H_m^c$
anion Frenkel formation	H_f^F	15.2			12.1	17.6	
anion interstitial migration	H_m^i	1.35					
cation Frenkel formation		11.9			12.42	13.0	

highly stoichiometric and because most often multivalent cation impurities far outnumber monovalent ones, the generally accepted defect structure is an excess of magnesium ion vacancies proportional to cation impurities of valance 3 or greater.[35,36]

Also due to the high Schottky energy, it will be difficult to see intrinsic Schottky anion vacancies in MgO. If we assume the entropy pre-exponential term to be unity, the fractional concentration of anion vacancies will be

$$\exp\left(\frac{-H_s}{2kT}\right). \qquad (2.5)$$

If we take the temperature of 1750°C, the highest temperature at whigh oxygen diffusion has been measured in MgO, the concentration of intrinsic anion vacancies would be $10^{-9.34}$ or 0.0005ppm if the Schottky energy H_s is 7.5eV. Even if the Schottky energy is 5.5eV, the concentration of intrinsic anion vacancies would only be $10^{-6.85}$ or 0.14ppm at 1750°C. These concentrations are extremely low, and are depressed even further by the presence of cation impurities of valence 3 or greater. Cation vacancy and impurity concentrations will be much higher than the Schottky anion vacancy concentration.

3.0 THEORY

3.1 DIFFUSION EQUATIONS

The model used for the present study is that of constant surface concentration, C_s, of oxygen isotope 18, O-18, diffusing into flat MgO of uniform bulk concentration C_b of O-18 starting at time zero, t=0. The diffusion coefficient D of O-18 is assumed to be concentration independent.

$$@\ t=0,\quad C=C_s \quad x\leq 0,\quad C=C_b \quad x>0$$

$$@\ t>0,\quad C=C_s \quad x\leq 0,\quad C=C(x,t) \quad x>0$$

Basic equations for this model can be found in Crank[29]. In subsequent equations, $C(x,t)$ will be simplified to C.

If we define a relative concentration as

$$C' = \frac{C-C_s}{C_b-C_s} \tag{3.1}$$

then the solution of Fick's laws for the aforementioned boundary conditions is

$$C' = \mathrm{erf}\left(\frac{x}{2\sqrt{Dt}} \right). \tag{3.2}$$

Values for the "error function" erf can be found in tables or through a digital computer with proper software.

A plot of the average concentration at distance x into the sample versus distance x will have a slope from which the diffusion coefficient D can be calculated. First the inverse error function of each side of the previous equation is taken.

$$\mathrm{erf}^{-1}\, C' = \frac{x}{2\sqrt{Dt}} \tag{3.3}$$

Differentiate with respect to x.

$$\frac{d\ \mathrm{erf}^{-1}\, C'}{dx} = \frac{1}{2\sqrt{Dt}} \tag{3.4}$$

Solve for D.

$$D = \frac{1}{t}\left(2\,\frac{d\ \mathrm{erf}^{-1}\, C'}{dx}\right)^{-2} \tag{3.5}$$

This equation will be true for any diffusion time in which the diffusant has had a statistically significant number of jumps where Fick's Laws are true and other factors, such as dislocations or grain boundaries, are not influencing diffusion in a significant way.

A less accurate way to estimate D is by measuring a diffusion depth of diffusing material, X_p, and using the equation

$$D_p = \frac{X_p^{\,2}}{4t} \tag{3.6}$$

For the present boundary conditions model this equation is only exact if X_p is the distance where $C'=0.84$ or, in other words, when the concentration is 16% of the difference between the surface concentration and the bulk concentration. A factor of 2 error in measuring X_p will result in a factor of 4 error in D_p. This is especially a consideration when noise levels are high in measuring C'. High noise level will make the diffusion depth appear shorter.

The generally accepted models for dislocation and grain boundary enhanced diffusion assume appreciably higher diffusion coefficients within those defects compared to the bulk diffusion coefficient. After LeClaire and Rabinovitch[51], dislocation diffusion is modeled as a cylinder of radius a perpendicular to the surface with a diffusion coefficient D'_d, greater than the bulk diffusion coefficient D. After Leclaire[52], grain boundary diffusion is modeled as a slab of thickness δ perpendicular to the surface with a diffusion coefficient D'_b much greater than D.

In order to discuss fast dislocation and grain boundary diffusion, it is useful to define the concepts of short, intermediate, and long diffusion times. If diffusion time is very short, called type C diffusion by Harrison[53], diffusion takes place mostly in the dislocations or grain boundaries and follows bulk diffusion kinetics in sectioning experiments. Measured diffusion coefficients will be those of dislocation or grain boundary material. For intermediate or type B diffusion times, diffusion takes place both in the dislocations or grain boundaries and the bulk. Near the surface, bulk diffusion kinetics are observed due to the relatively large area for surface exchange with matrix material compared to the area of dislocations or grain boundaries intersecting the surface. Farther in from the surface, diffusion takes place down the dislocations and grain boundaries and then into the bulk. At long or type A diffusion times, diffusant has time to enter and leave many dislocations and grain boundaries. Bulk kinetics are observed with an effective diffusion coefficient proportional to the dislocation or grain boundary diffusion coefficient, the bulk diffusion coefficient, and the dislocation density or grain size. As pointed out by Martin & Perraillon in their review[54], there is some disagreement in the literature as to how these factors are combined in the effective diffusion coefficient. At very long diffusion times in polycrystalline samples bulk kinetics might be observed at a measured "bulk diffusion coefficient" closer to the grain boundary diffusion coefficient than the bulk coefficient. These three regimes are summarized below. For dislocation diffusion,

short time	$\sqrt{Dt} < a$
intermediate time	$a \ll \sqrt{Dt} \ll \sqrt{d}$
long time	$\sqrt{Dt} > d^{-1/2}$

where

D = bulk diffusion coefficient
t = diffusion time
a = dislocation core radius
d = dislocation density.

For grain boundary diffusion,

short time	$\sqrt{Dt} < \delta$
intermediate time	$\delta \ll \sqrt{Dt} \ll g$
long time	$\sqrt{Dt} > g$

where g = grain size.

Samples with fast dislocation diffusion during intermediate time diffusion anneals will exhibit a deep penetration, low concentration diffusion profile "tail". LeClaire and Rabinovitch[51] have solved for the linear tail slope on a natural log of concentration versus penetration distance plot.

$$\frac{d \ln C}{dx} = -A \left(\left(\frac{D'_d}{D} -1 \right) a^2 \right)^{-1/2} \qquad (3.7)$$

where A = $f(a/\sqrt{Dt})$, a constant approximately equal to 1
D'_d = dislocation core diffusion coefficient
D = bulk diffusion coefficient
a = dislocation core radius

The constant A may be graphically estimated from Figure 4 in LeClaire & Rabinovitch[51]. From this equation we can solve for $D'_d a^2$.

$$D'_d a^2 = A^2 D \left(\frac{d \ln C}{dx} \right)^{-2} + Da^2 \qquad (3.8)$$

If dislocation diffusion is significant, the second term is insignificant. Thus $D'_d a^2$ may be estimated from the tail slope and estimates of A and D.

Information may also be obtained from the concentration intercept $C_{x=0}$ of the back-extrapolation of the diffusion tail on a log of concentration versus penetration distance plot. In principle, the dislocation core radius a could be calculated:

$$a = \left(\frac{C_{x=0}}{C_s \pi d (Dt)^{0.92}} \right)^{6.25} \qquad (3.9)$$

where d = dislocation density

LeClaire & Rabinovitch[51] point out that this equation is of little practical significance - if a measured dislocation density is one third of the true dislocation density, the core radius calculated by means of this equation will be 10^3 times the actual value. However if this equation is solved for d, an estimate of d within a factor of 2 will result even with a 10^2 uncertainty in a.

$$d = \frac{C_{x=0}}{C_s \pi a^{0.16} (Dt)^{0.92}} \qquad (3.10)$$

LeClaire[52] has reviewed the mathematics of grain boundary diffusion measurement. For intermediate diffusion times the tail slope is linear on a log of concentration versus diffusion distance to the 1.2 power. From this slope, the diffusion time t and an estimate of D, $D'_b\delta$ may be calculated.

$$D'_b\delta = .66 \left(\frac{d \ln C}{dx^{1.2}} \right)^{-5/3} \left(\frac{4D}{t} \right)^{1/2} \qquad (3.11)$$

where D'_b = grain boundary diffusion coefficient
δ = grain boundary thickness
D = bulk diffusion coefficient
t = diffusion time

However, this equation will only be accurate

if

$$\beta \geq 10$$

where

$$\beta = \frac{D'_b\delta}{2\, D\, (Dt)^{1/2}} \qquad (3.12)$$

The practical significance of this restriction is that diffusion times should not be too long if $D'_b\delta$ estimates are desired.

Atkinson and Taylor[55] describe a difference in time dependence between the dislocation diffusion tail slope and the grain boundary tail slope. In the case of dislocation diffusion, it is independent of diffusion time.

$$\frac{d \ln C}{dx} \neq f(t) \text{ for dislocation diffusion} \qquad (3.13)$$

In the grain boundary case, the relevent tail slope is proportional to diffusion time to the -0.3 power.

$$\frac{d \ln C}{dx^{1.2}} \propto t^{-.3} \quad \text{for grain boundary diffusion} \qquad (3.14)$$

Therefore a plot of the log of the tail slope, $\log(d \ln C/dx^{1.2})$ versus $\log t$ will have a slope of -0.3 for grain boundary diffusion in a set of diffusion anneals at the same temperature. This should offer an experimental means of distinguishing between measured tails dominated by dislocation diffusion and those dominated by grain boundary diffusion.

If there is segregation, defined by the segregation coefficient γ equal to the concentration of diffusant in the fast diffusion region divided by concentration in the bulk, one obtains $\gamma a^2 D'_d$ or $\gamma \delta D'_b$ from equations 3.8 and 3.11 respectively. In this study γ is not used for simplicity, but it must be understood that in a ceramic system segregation is an important phenomenon [3].

3.2 ERROR MEASUREMENT

There are two types of error in scientific measurement-systematic and random. Systematic errors are those which arise from sources such as inaccurately calibrated instruments or unaccounted for impurities. Random error manifests itself when repeated measurements of the same quantity show variability not caused by systematic errors. Theoretically one can eliminate systematic errors by performing flawless experiments. However there will always be random error to a greater or lesser extent in any type of measurement.

Systematic errors are treated by always striving to eliminate them in all phases of experimentation and data analysis. Philosophically this is the only way to eliminate systematic error. If one sees a source of systematic error one can either take it into consideration and then treat all affected data in a systematic way or redo the experiment and the measurements after eliminating that source of error.

Random error, most of which is dealt with by Gaussian distribution theory, is characterized by a number called the standard deviation. For the ideal case of no systematic error and a near infinite number of <u>experimentally determined</u> values X_i, the mean of those <u>experimentally determined</u> values is the <u>actual</u> value being sought, and 68% of those <u>experimentally determined</u> values fall within one <u>real</u> standard deviation, σ, of the mean or actual value. If there is systematic error the mean of the experimentally determined values will be displaced from the actual value by the systematic error. In practice one calculates a sample mean and a sample standard deviation, σ_X, from a limited number of experimentally determined values. The sample mean is used as an estimate of the actual value and the sample standard deviation is used as an estimate of the real standard deviation. The sample mean is defined as

$$\bar{X} = \frac{\Sigma X_i}{N} \qquad (3.15)$$

where X_i is the i^{th} experimentally determined value and N is the number of experimentally determined values. The sample standard deviation is defined as

$$\sigma_x = \frac{\Sigma (\bar{X}_i - x)^2}{\sqrt{N - 1}} \qquad (3.16)$$

Theoretically the sample standard deviation is an estimate of the standard deviation which is independent of N. Therefore the sample standard deviation should be independent of N. The standard deviation of the mean is defined as

$$\sigma_{\bar{x}} = \frac{\sigma_x}{\sqrt{N}} \qquad (3.17)$$

For small N, Student's t statistics can be used to improve the reliability of these calculated standard deviations by multiplying them by a factor greater than 1. As more experimental values are determined, the range of those values will increase but the standard deviation of the mean will decrease due to the $\sqrt{N}$ factor in the denominator of equation 3.17. For practical reasons, about 5-10 experimental values are required to calculate a standard deviation of the mean. To reduce the standard deviation of the mean by 1/2, four times as many samples must be used.

In some cases standard deviations are calculated by other methods. For instance counting statistics defined by the Poisson distribution are used to calculate the standard deviation for the number of counts #, which a mass spectometer or Geiger counter measures.

$$\sigma_{\#} = \sqrt{\#} \tag{3.18}$$

If enough counts are measured, random error in # might be insignificant. However, random error in some other part of a scientific experiment may increase the overall standard deviation of actual values being sought.

In many cases people make informed guesses to estimate a standard deviation. This may be the only way to arrive at a standard deviation for a single measurement. However if this method is used, one must be careful not to base experimental conclusions on overly optimistic assumptions about error. For example, one must be careful when interpreting diffusion Arrhenius plots;[5 6] a few experimentally determined values which seem to deviate from the rest may be a manifestation of random or even systematic error rather than a change of diffusion mechanism.

Standard deviations for the slope and intercept of a linear regression are analytic. This is true for simple linear regression which assumes no error in the independent variable and equal standard deviations for all dependent variables. It is also true for weighted linear regression which weights each data pair by the standard deviation of the dependent variable.

In contrast, standard deviations for constants in non-linear regression cannot be solved for explicitly. They must be estimated through iterative calculations. In many cases, one can model a non-linear regresson with a linear regression. This is done in Arrhenius plots, for example, when D versus T data are plotted as log(D) versus 1/T data.

In general, one must measure more than one quantity, q_i, in order to calculate a particular physical quantity q_p through a function f

$$q_p = f(q_i) \tag{3.19}$$

Each of those measured quantities, q_i, will have an associated error σ_{qi}. If errors are random and independent, the error in the physical quantity being determined, σ_{qp}, is[57]

$$\sigma_{qp} = [\Sigma (\frac{\partial f}{\partial q_i} \sigma_{qi})^2]^{1/2} \tag{3.20}$$

The errors are said to be added in quadrature. Whether the errors are random and independent or not random and independent, the ordinary sum of errors is a limiting case[57] for the error in the physical quantity being determined.

$$\sigma_{qp} \leq \Sigma \left| \frac{\partial f}{\partial q_i} \right| \sigma_{qi} \tag{3.21}$$

Since this is a limiting case it is almost always an overestimation of the error.

In most studies involving Arrhenius plots, one experimental value of a diffusion coefficient is used to calculate an actual value at each temperature. In this study many values were usually used to calculate actual diffusion coefficient values at each temperature. This is especially true at 1200 °C where 22 experimental values of D, 11 of $D'_d a^2$, and 10 of $D'_b \delta$ were determined for undoped samples.

4.0 EXPERIMENTAL PROCEDURE

4.1 SAMPLE PREPARATION

The following is a list of MgO materials from which all samples were taken.

One 21.5 gram piece of Oak Ridge National Laboratory single crystal, undoped, Fig. 2.

One piece of OR single crystal doped with 300-500 atom ppm Li[58].

Two pieces of Norton Company undoped single crystals.

Two pieces of Spicer 4N single crystals doped with 310ppm Fe.

One piece of Spicer 4N single crystal doped with 370ppm Ni.

One piece of Spicer 4N single crystal doped with 800ppm Cr.

One piece of undoped polycrystalline material made by Emilio Giraldez and Alexana Roshko at MIT.

Several small pieces of Na doped material ready to be sintered made by Carol Handwerker at MIT.

One of the Fe doped Spicer crystals was supplied by Yasumichi Oishi from a piece studied by him[7]. From this list, intermediate samples were made that were deformed, doped, or used as received. From these intermediate samples, 88 diffusion samples were made. Out of these 88 samples, 46 came from one Oak Ridge single crystal (Fig. 2).

The defect structure of the single crystals consisted of widely spaced (>100μ) subgrain boundaries and a free dislocation density measured by etch pits of 3×10^{6} cm^{-2}. Table 4 lists microstructure information for other samples as well.

---

[*] Oak Ridge National Laboratory, Oak Ridge, TN 37830

[**] Norton Research Corp. (Canada) Ltd., Niagara Falls, Ontario, Canada

[***] W&C Spicer Ltd., 25 St. Georges Place, Cheltenham, England

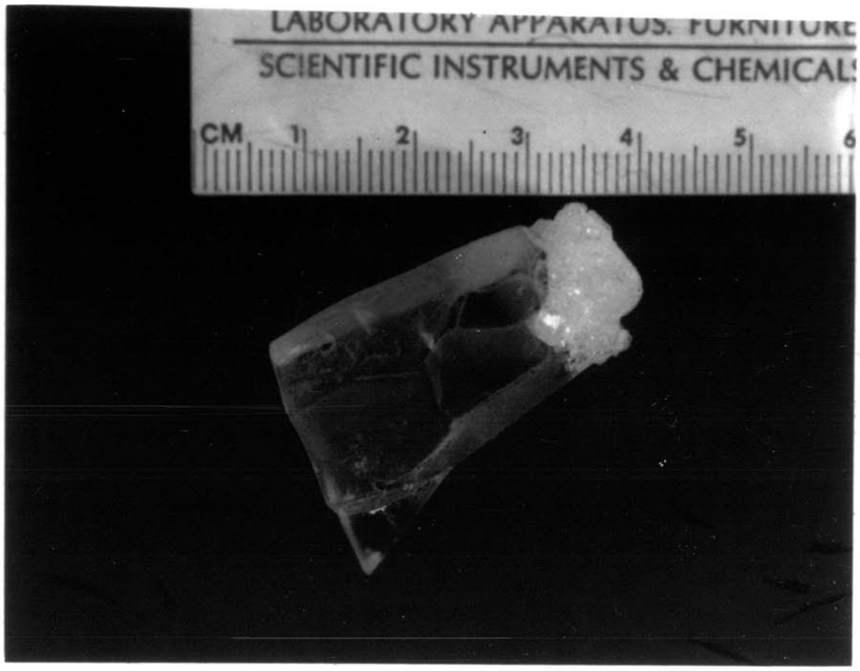

Fig. 2 Oak Ridge National Laboratory 21.5 gram undoped starting crystal. Undoped single crystals and single crystals deformed 6% and 55% were taken from this piece. Out of the 88 diffusion samples made in this study, 46 came from this piece.

Table 4

Microstructure and Sample Deformation Information

Sample original dimensions (in.) Weight (gm)	True strain	Temp. ^{o}C	Time min.	Stress PSI	Grain Size um	Dislocation Etch Pit Density cm^{-2}
ORU Oak Ridge (Fig. 2) 21.5 gm	zero undeformed	N/A	N/A	zero undeformed	500	3×10^{6}
MIT polycrystal	"	"	"	"	11	----
Na doped polycystal	"	"	"	"	18	----
OR6 Oak Ridge .415x.415x.188 1.9 gm	6%	1400	11	8,000	500	50×10^{6}
OR55 Oak Ridge .467x.455x.200 2.4 gm	55%	1500	23	10,600	6	13×10^{6}
NC62 Norton Co. .539x.560x.199 3.5 gm	62%	1700	4	6,600	13	1.8×10^{6}
NI27 Spicer 370ppm Ni .406x.368x.064 0.5 gm	27%	1500	20	14,000	10	----
FE35 Spicer 310ppm Fe .223x.220x.136 0.376 gm	35%	1530	22	11,300	9	8×10^{6}

The etchant used was 1 part by volume H_2SO_4, 1 part distilled H_2O, 5 parts NH_4Cl saturated solution. Etching is useful to correlate deformation with microstructure. Transmission electron microscopy can reveal more dislocations than etching[59], but dislocations can be easily introduced during TEM sample preparation due to the softness of MgO. Also only miniscule volumes of material can be observed, requiring many samples to calculate an average dislocation density. Extremely accurate dislocation densities were not required in this study so etch pit dislocation densities were adequate.

The undoped polycrystalline sample had an average grain size of 11 microns. The sodium doped polycrystal had an average grain size of 18 microns, Fig. 3. The sintered samples were prepared as follows. The undoped sample was prepared from powder prepared in a clean room and containing under 100ppm total impurity. The powder was cold pressed into a pellet 5/8" dia. x 3/16" thick at 200,000 psi and then placed in a platinum envelope. This envelope was suspended in a previously baked out Morganite alumina tube furnace in flowing oxygen at 1250°C for 24 hours. The temperature was then increased to 1400°C for 48 hours. The sample was greyish, probably from platinum, and translucent. The small sodium doped samples were made from reagent magnesium carbonate containing 500 µg/g Na/Mg, 30 µg/g Ca/Mg, and approximately 50 µg/g of other impurities. This was converted to the oxide and then filter cast into small flakes. The flakes were sintered in a platinum envelope in a previously baked out Morganite furnace tube at 1450°C for 116 hours.

All of the above samples except the already small Na doped pieces were divided into intermediate pieces for various treatments and then divided into diffusion samples (5-10mm. x 5mm. x 2-3mm.) by diamond sawing.

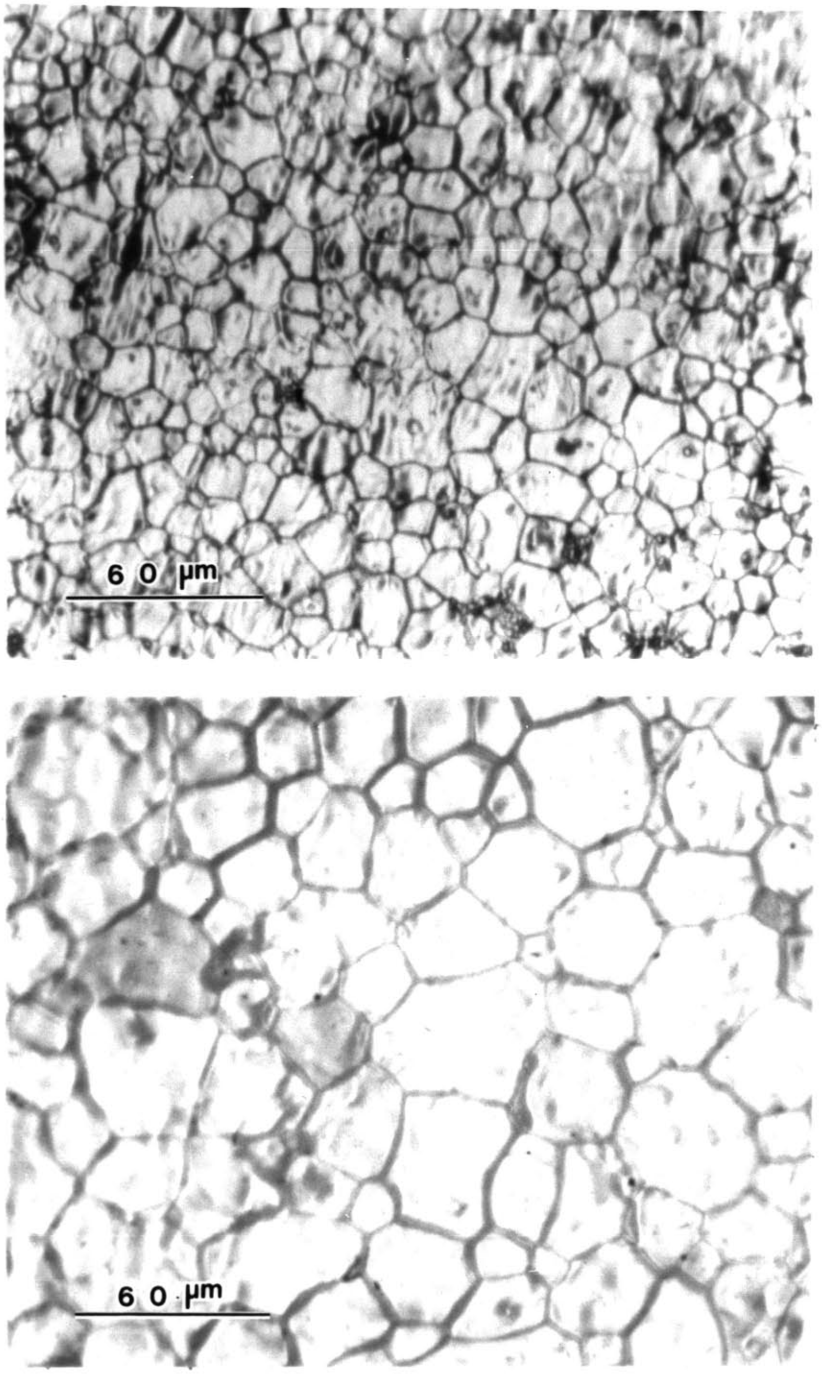

Fig. 3 Microstructures of polycrystalline samples. Top undoped. Bottom sodium doped.

Cleaving was not done. This insured many small, uniform samples from the starting material-an improper cleave could destroy the sample or severely damage it. Previously the present author has found Oak Ridge material particularly difficult to cleave. Others[60] have also observed this phenomenon. Presumably its relatively high purity results in a softer material which can plastically deform before a cleavage plane is initiated. All cutting was done with an approximately 240 grit 0.012" thick diamond saw blade using light weight (approximately 20 grams) at slow speed (approximately 10 inches per second). The light weight and slow speed are necessary to avoid excessive mechanical damage to the sample. The gentleness of the cut was indicated by the fact that a sample 2mm x 2mm took an average of one hour to cut through. Isopropyl alcohol was used as a cutting lubricant. Compared to kerosene, its use reduced blade clogging and significantly increased cutting speed.

Some samples were deformed to introduce extra dislocations and subgrain boundaries. High temperature compression of MgO along a [100] axis introduces dislocations which, as deformation proceeds above about 10% true strain, knit to form low angle grain boundaries[59]. These boundaries, lying on (110) planes, are parallel to each other and the pressing direction. They are spaced from 1 to 40 microns apart. As deformation proceeds past about 50% true strain the grains become more equiaxed. Table 4 lists the deformed samples and relevent information. Samples to be pressed were rectangular parallelopiped shaped with (100) faces. They retained this shape even after pressing. For pressing they were cleaned with methanol, wrapped with graphite foil, and inductively heated in graphite dies under vacuum. Temperature was measured with an optical pyrometer sighting through a hole in the die insulation. When the desired strain was achieved power was shut off and the samples cooled rapidly, around 100°C in the first minute. All samples except the Oak Ridge 6% deformed sample were pressed by the author and had well developed low angle grain boundaries. The 6% sample was deformed by Professor A. Mocellan and colleagues (Ecole Polytechnique Federale de Lausanne, Switzerland) in a similar manner. It had no subgrain boundaries and an etch pit dislocation density of $5 \times 10^7/\text{cm}^2$, Fig. 4. This was done by design so the sample would have a high free dislocation density. For all deformed samples diffusion profiles were measured parallel to the pressing direction, so many low angle grain boundaries were perpendicular to the diffusion sample surface.

Figure 5 shows low angle grain boundaries in the 370ppm nickel doped sample deformed 27%. Other more deformed samples had more closely spaced low angle grain boundaries. Also shown in Figure 5 is an optical micrograph of the Oak Ridge sample deformed to 55% true strain. Figure 6 shows a TEM micrograph of the undoped Oak Ridge sample deformed to 55% strain. This sample had grain boundaries composed of nets of dislocations as shown and some boundaries of parallel dislocations. The Norton Co. sample deformed to 62% strain had a similar microstructure but many precipitates were on the boundaries, Fig. 7. Precipitates containing Ca and Al[61] and precipitates containing Si were observed[62]. Atomic absorption analysis determined the Al content of 70 weight ppm and Ca content of 240ppm.

A sample from the 6% pressing and a sample from the 55% pressing were doped with calcium. After chemical polishing, which will be described later, the samples were buried in 2600 mole ppm Ca doped MgO powder (Prepared by Alexana Roshko, MIT) in a packet

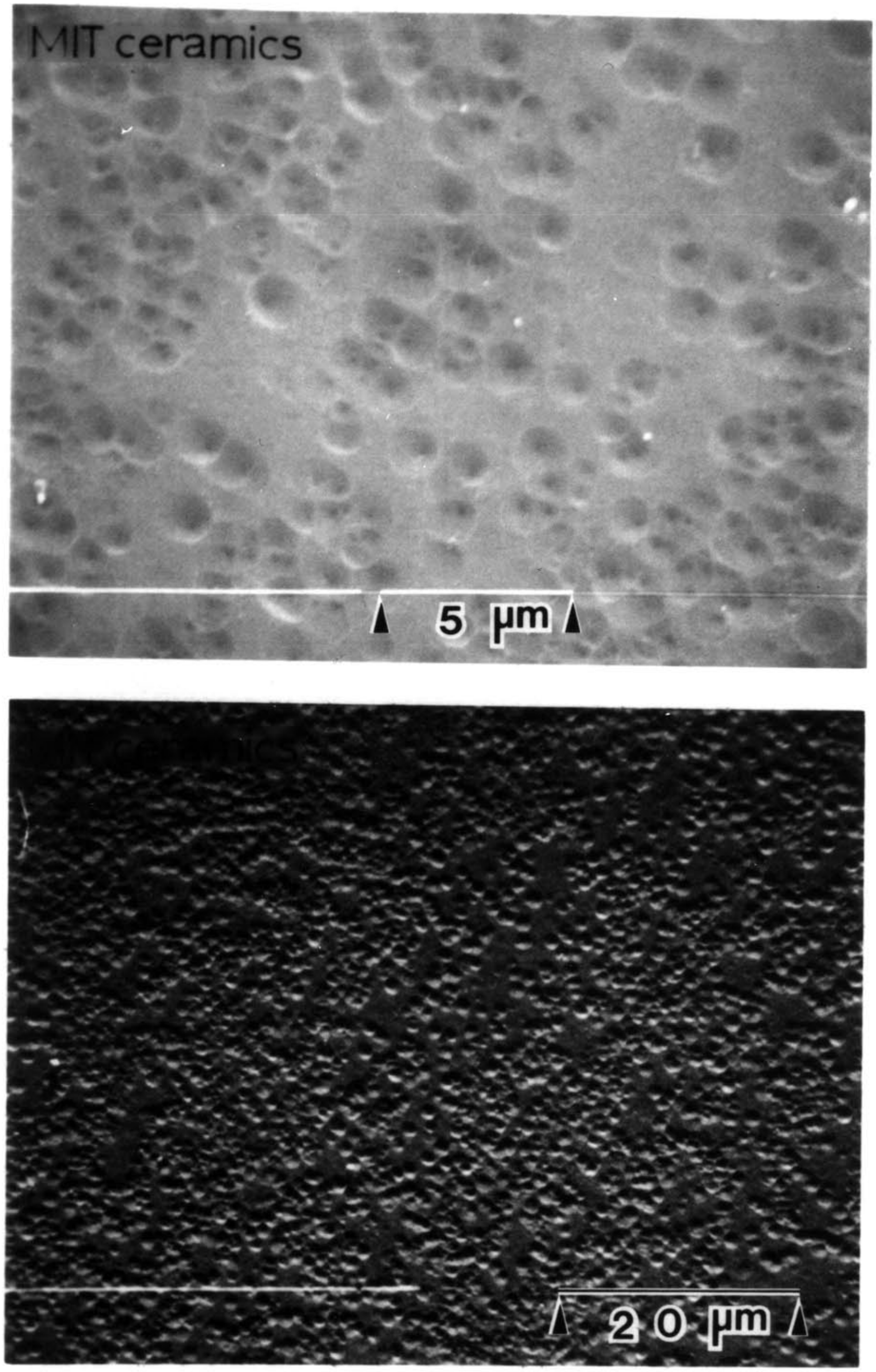

Fig. 4. Oak Ridge MgO deformed 6%. SEM pictures of etched sample.

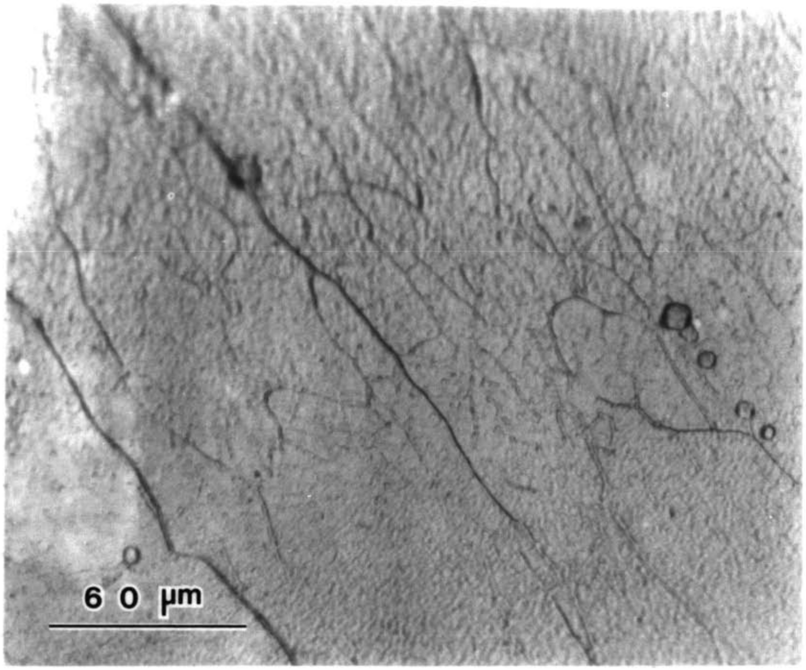

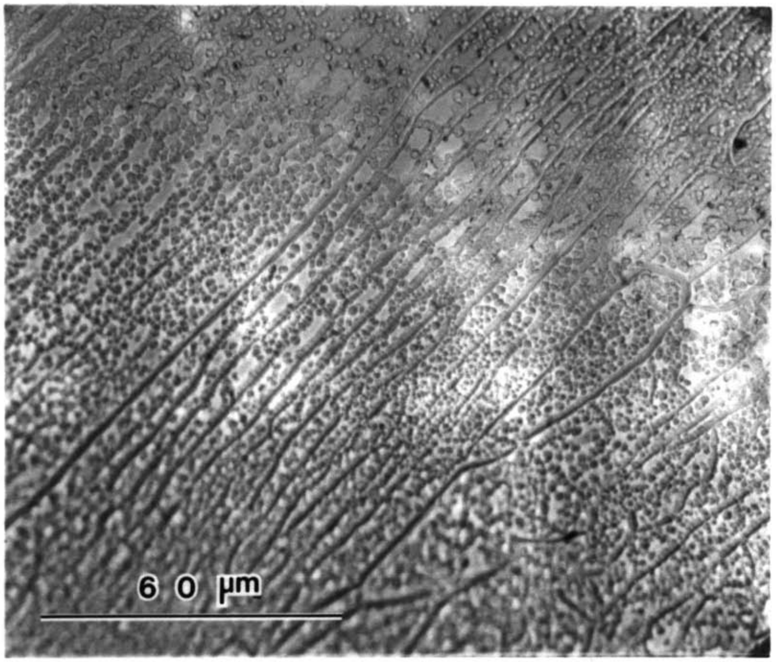

Fig. 5. Optical micrographs of two deformed samples. Top-Spicer 370ppm Ni doped MgO sample deformed to 27% true strain. Bottom-Undoped Oak Ridge sample deformed to 55% true strain.

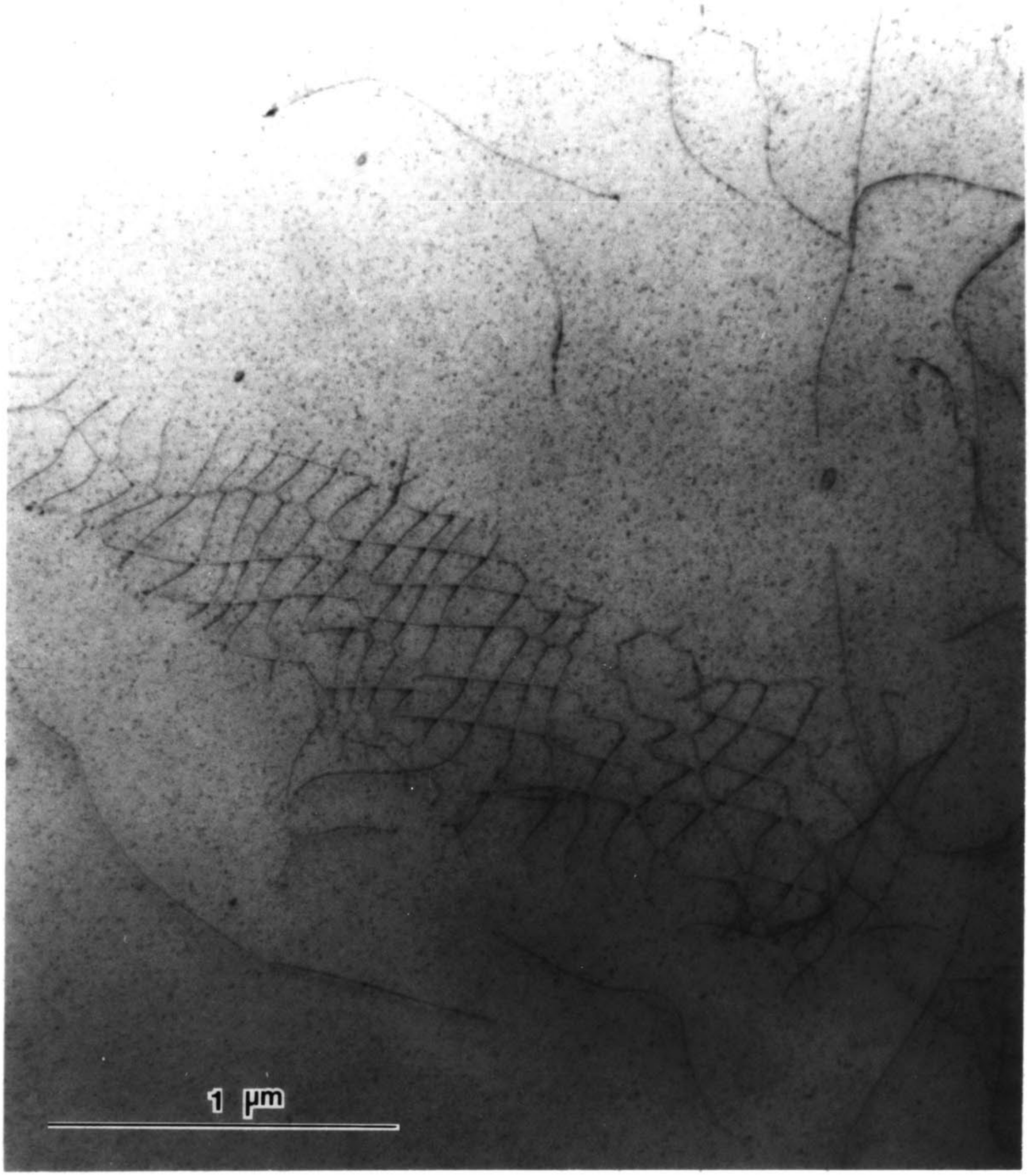

Fig. 6 TEM micrograph of grain boundary in undoped Oak Ridge MgO deformed to 55% true strain. Taken by M. Fujimoto.

Fig. 7 TEM micrograph of precipitates on a grain boundary in a Norton Co. crystal deformed to 62% true strain. Taken by M. Fujimoto.

made from clean 0.001" platinum. The platinum was cleaned with successive rinses of detergent (PEX Laboratory Glass Cleaner, Pecks Products Co., St. Louis, MO)/ water solution, then distilled water, followed by overnight soaking in HCl, followed by rinses of distilled water and methanol. Two other samples from the 6% and 55% pressings were prepared in the same manner, except they were buried in high purity MgO powder (made from $MgCO_3$ made by Carol Handwerker, MIT). These were made as a control to distinguish between the effect of doping and the effect of the doping anneal. Both packets were annealed for 22 days at 1400 °C in a Morganite alumina tube furnace previously baked out at 1700 °C in air for 36 hours. These four samples were later sawed in half to make a total of eight samples.

All samples except sintered samples were chemically polished in 100 °C hot phosphoric acid before use as diffusion samples. The acid was heated in a teflon beaker which itself was suspended in hot phosphoric acid. The teflon was used to avoid impurity dissolution from a glass beaker. The teflon beaker was suspended in hot fluid to reduce convection within the polishing bath so as to produce very smooth polished surfaces. Phosphoric acid was simply a convenient fluid to use. The acid temperature was measured with a teflon coated thermometer. The samples were manipulated with teflon tweezers while resting on platinum gauze. After each 10-30 minute period in the hot acid, the samples were rinsed about 30 seconds in clean, distilled (<1ppm residue after evaporation) water heated to near boiling in a teflon beaker, followed by a cold distilled water rinse. The hot water was replaced after each rinse, the acid a couple of times, always before the last period of time the samples were in it. During the first 10-30 minute polishing all sample surfaces were polished in order to clean them. Then, in order to save material on the thin samples, one surface of each sample was polished by gluing the samples to the platinum with an acid-proof lacquer ("Miccrostop" stop-off lacquer, Miccro Products, Pyramid Plastics Inc., Tolber Div., Hope, Arkansas). The lacquer was removed with acetone followed by thorough methanol rinsing before the final period of polishing. Samples were in the hot acid for an accumulated time of 3 hours. This removed 300 microns of material, which was found to be more than enough to remove damage from diamond sawing. After the final water rinses, the samples were rinsed with methanol and then air dried before use. Sometimes the samples were stored in dry pure methanol in HCl cleaned glass beakers for a few days before heat treatment. Chemically polished surfaces were extremely smooth-slight roughness was observed only at magnifications above 20,000X.

Some samples were cleaned instead of or after chemical polishing. Sintered samples were not polished because this results in surfaces with unacceptable roughness (~ 0.5-1μ) for Secondary Ion Mass Spectrometry. The small sodium doped samples were not cleaned or polished, but used as sintered. However, the undoped polycrystalline samples, the calcium doped samples, and the undoped samples annealed like the calcium doped samples all had to be cleaned because they were sawed. Cleaning was done in previously cleaned glassware. Samples were first rinsed with trichloroethylene then soaked in it for a few days. Then they were rinsed with acetone and distilled water. Next they were soaked in detergent and water solution on a hot plate for 20 minutes, rinsed under tap water for 10 minutes, soaked in hot distilled water for 5 minutes, rinsed about 8 times with distilled water and then rinsed with acetone and stored in it until needed for annealing. Then they were rinsed with acetone a few times, then with methanol, then air dried. It was hoped that this sequence would remove any oils or other cutting residues like impurity agglomerates which may have come from the diamond saw apparatus.

All cleaning and polishing was done in an acid fume hood. Virgin, talc free polyethylene gloves (Vanlab Poly Gloves, VWR Scientific, San Francisco, CA) were used and changed frequently, not only on hands but on counters to provide a clean working surface. Other than fluids, the only materials to touch samples before annealing were teflon, polyethylene, clean platinum and clean glassware while being cleaned or stored in liquids. Glass had to be used because some of the heating or solvent treatments would dissolve polyethylene or overheat teflon.

Samples of Oak Ridge material were tested for impurity pickup in both the oxygen-18 exchange system and a McDanel alumina tube furnace. Samples were placed in a new solvent cleaned McDanel 998 alumina boat and then covered with MgO powder. Samples were also placed on top of the powder. This assembly was placed in a horizontal McDanel 998 alumina tube furnace at 1350°C for 16.5 hours. Figure 8 illustrates the results. The sample surface in contact with the MgO powder was clean at least when viewed by SEM. Some powder particles stuck to it. The surface exposed to the furnace atmosphere showed silicon containing lumps on its surface. The surface facing the alumina showed a very rough surface with many silicon containing lumps. Silicon containing precipitates may have come out of the sample, but silicate evaporation from the McDanel 998 Al_2O_3 furnace tube and deposition of a silicate onto the MgO surface seems more likely. This could produce a liquid phase which might facilitate evaporation of the MgO surface. Samples annealed in the oxygen-18 exchange apparatus appeared clean in scanning electron micrographs.

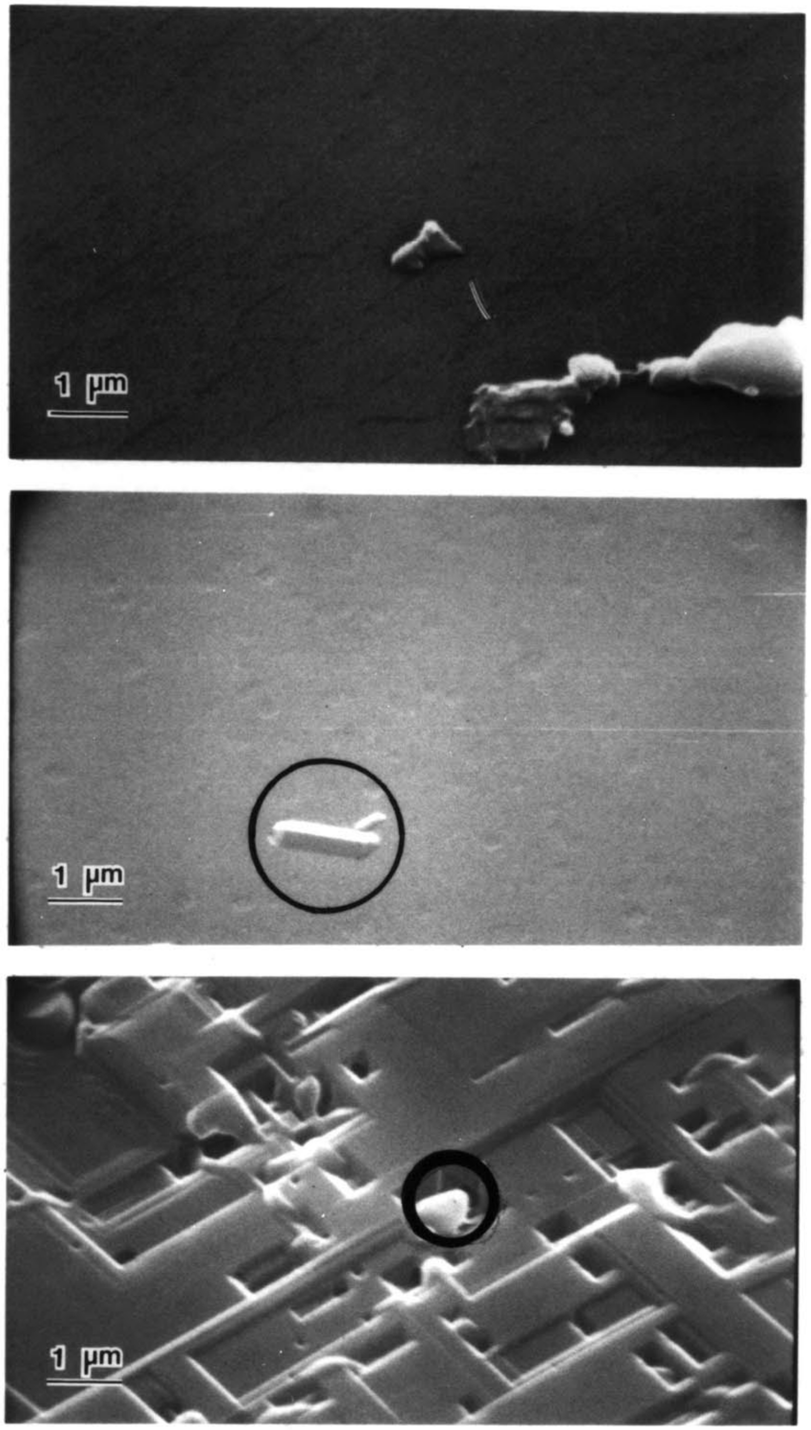

Fig. 8. SEM pictures of MgO samples annealed in a McDanel 998 alumina tube at 1350 °C for 16.5 hours. Top - sample surface buried by MgO powder. Middle - Sample surface exposed to furnace atmosphere. Bottom - sample surface facing new McDanel 998 alumina boat. Circled lumps showed Si X-ray signals.

4.2 EQUILIBRATION AND DIFFUSION ANNEALING

After chemical polishing or cleaning, samples were heat treated. They were given an equilibration anneal and then a diffusion anneal. All samples, except the sodium doped samples which were sintered in air at 1400 °C, were first given a 1/2 hour 1400 °C anneal in air. The purpose of this anneal was to equilibrate the samples with air so all samples would have the same thermal and oxygen partial pressure history. Oxidation-reduction in MgO doped with iron takes place as fast or faster than magnesium vacancy diffusion[63]. Magnesium vacancy diffusion in MgO is faster than magnesium, impurity, or oxygen diffusion[36]. The calculated $\sqrt{Dt}$ for vacancy diffusion for the equilibration anneal is 0.1 mm. This was deemed enough since oxygen diffusion depths in the present work were under a micron. Samples were buried in pure MgO powder (made by calcining pure $MgCO_3$ made by Carol Handwerker, MIT) and held in a clean platinum bucket (1" dia. X 1.5" tall) with an acid leached polycrystalline MgO lid. The sample holder, suspended by a clean platinum wire was lowered into and pulled from a vertical Al_2O_3 (Morganite) tube furnace at temperature. The bottom of the furnace was blocked off with a piece of alumina held there by a spring to reduce convection. The new furnace tube had been previously cleaned and then baked out at 1700 °C in air for 36 hours. The only things which touched samples, holder, and hang-down wire were talc-free polyethylene gloves. Samples later referred to as contaminated were equilibrated in a different sample holder exposed to the furnace atmosphere in a different furnace.

After the samples were pre annealed, they were used immediately for oxygen isotope 18 gas exchange diffusion anneals. The samples and MgO powder were dumped onto a polyethylene glove. The MgO powder did not stick to the samples and was reused for other equilibration anneals. The samples were rinsed with methanol to remove any MgO powder then air dried, then placed in the diffusion sample holder with teflon tweezers. This sample holder was a 1/2" diameter by 3/4" tall bucket made of previously cleaned platinum sheet. Inside it were divisions made of platinum gauze so samples would not touch each other but be exposed to the oxygen-18 containing atmosphere. The sample holder lid was a piece of single crystal MgO with a 1/8" hole in the middle. This arrangement was used to keep the samples out of the direct flow of the system atmosphere which might cause excessive sample evaporation. For short time, "Type C" diffusion anneals the lid was not used. Samples later referred to as contaminated had a separate similar sample holder. The atmosphere in the closed system diffusion apparatus was artificial air, 80% Nitrogen and 20% Oxygen at 5-20 torr above atmospheric pressure so any leaks would be out, not in. The oxygen was 95.54% oxygen isotope 18. (Monsanto Research Corp., Mound Facility, Miamisburg OH 45342) Gas samples taken after 7 random diffusion anneals showed it did not change composition. The sample holder was placed in the cool zone of the furnace while the furnace was at 800 °C or less. The system, except for stored gas, was evacuated then backfilled with atmosphere. Then the furnace was brought up to temperature. The sample holder was lowered into or pulled from the furnace while the furnace was at temperature. It was lowered 0.5" every 30 seconds until centered in the hot zone, at which time the timing of the anneal was begun. The sample holder was quickly pulled completely out of the exchange system, at which time the timing of the anneal was ended.

Figure 9 shows a schematic of the gas exchange apparatus. Gas exchange took place in a closed loop. The gas was continuously mixed by convection due to the hot furnace on one side of the loop. Most of the loop was 3/4" glass

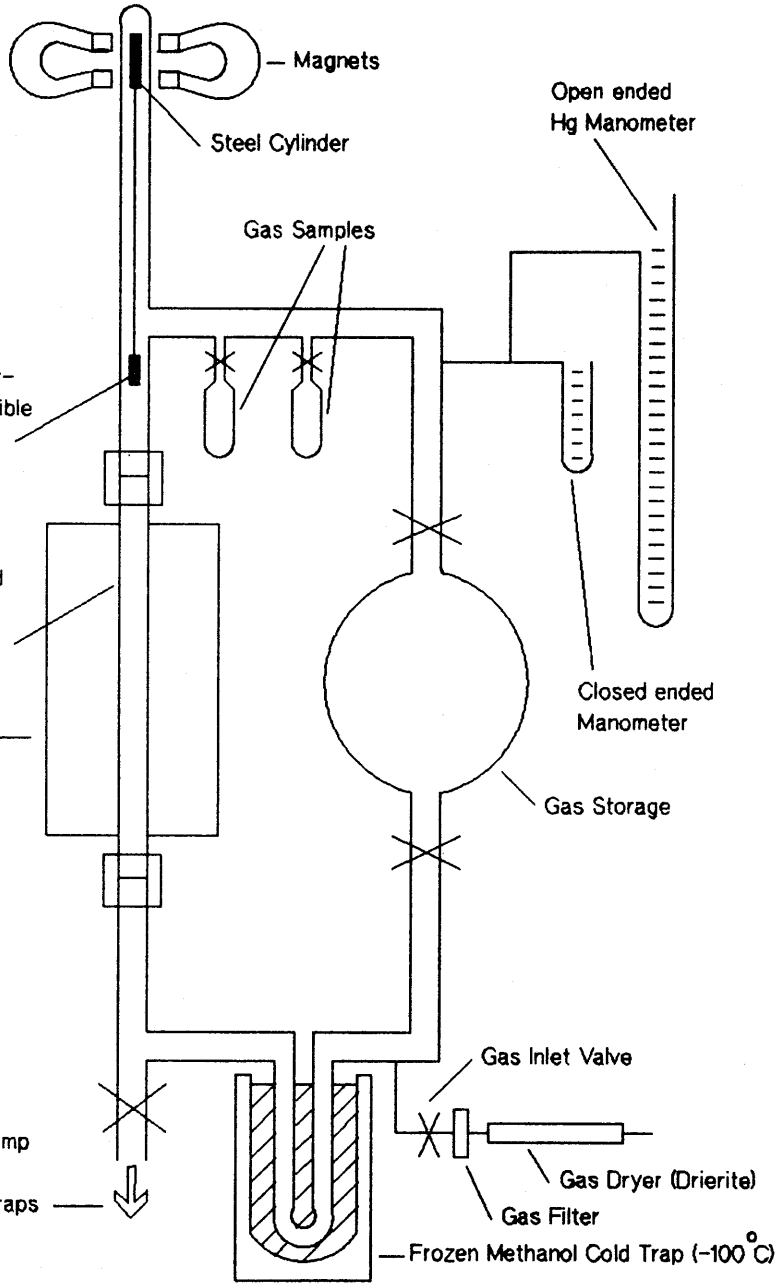

Fig. 9 Schematic diagram of oxygen-18 gas exchange apparatus.

tubing. Teflon tubing was used to connect manometers and gas inlets by means of brass fittings. Apiezon grease was used to seal joints. The furnace tube was alumina, connected to the glass with brass fittings (Cajon Ultra Torr) which were air and water cooled. The sample holder was lowered and raised suspended by a platinum wire connected to a grease coated solid steel cylinder suspended through the glassware by a torus of 8 strong horseshoe magnets. Temperature was measured with a Pt/Pt10%Rh thermocouple supported by a single crystal sapphire tube which extended into the furnace from below. The sample holder rested on this tube during diffusion anneals, insuring close proximity between the thermocouple bead and the sample holder. Part of the gas loop was a U-tube trap (filled with 1/4" glass beads) suspended in frozen methanol (-100 °C). The methanol was frozen by pouring liquid nitrogen into it while mixing it. This was cold enough to freeze water and common acids which might cause impurity evaporation from the furnace tube. The internal volume of the loop was 2.5 liters, with a 2 liter storage vessel so 80% of the atmosphere could be re-used.

The inlet gas was dried with anhydrous $CaSO_4$ (Drierite Co., Xenia, Ohio) in a glass tube then filtered for dust before entering the system. The vacuum system was a mechanical vane pump which had been flushed and filled with high purity pump fluid (Solvex-10 flushing fluid, Plasma Oil 80 pump oil, CVC Products Inc., Rochester NY.). The pump was connected to the system via a molecular sieve (Linde 13X, Union Carbide) filled tube then a liquid nitrogen trap, both used to trap any pump oil droplets.

All internal parts of the system were cleaned in various ways. Typically new parts were cleaned with detergent and water, tap water rinse, distilled water rinse, acetone rinse, trichloroethylene rinse, acetone rinse, methanol rinse and then air dried. Mercury manometers were also cleaned with nitric acid. The system was dismantled and cleaned a few times as sample contamination was a problem. Originally many fittings were sealed with silicone rubber However it was found that this material, unless of aerospace quality, never completely cures and therefore gives off low molecular weight silicones. Also, it is gas permeable and therefore not a true sealant. This material could be dissolved with a solution of 85% ethyl alcohol and 15% water saturated with potassium hydroxide. The whole exchange system was cleaned with this solution after all visible silicone had been scraped off.

Two different furnace tubes were used. Originally the system was fitted with a McDanel "998" alumina tube. This tube contaminated samples with silicon, and probably other elements from its glassy grain boundary phase (See Figure 8). The final tube was a Morganite "Triangle RR recrystallized" alumina tube which was first cleaned, then fired, then the inside was filled with 50% HF, 50% water for 3 1/2 hours, then thoroughly rinsed with distilled water. Next pure magnesium carbonate (Carol Handwerker, MIT) was calcined in the tube. The MgO from this firing was dispersed in methanol. This dispersion was poured into the tube while it was being rotated to coat the tube with MgO. The tube was fired at 1400 °C by pulling it through a furnace one way at 1" per hour while dried filtered air flowed through it in the other direction. From test samples it was determined that this proceedure resulted in a uniform spinel coating. This coating acted as a barrier layer between the Al_2O_3 tube and the sample atmosphere.

Table 5 lists the diffusion anneals. Most diffusion anneals had from 5 to 8 different samples. In this way, undeformed, deformed, polycrystalline, and doped samples could be given identical diffusion anneals. Higher temperature or longer times were not used so that dislocation rearrangement, recrystallization, contamination and sample evaporation

Table 5

Diffusion Anneals Summary

Run*	time secs	mean temp ±range	relative diffusion**** time	furnace tube
4A	14580	1386±1	I	**McDanel 998 Al_2O_3 Furnace Tube
4B	75780	1386±1	I	"
11	26700	1398^{+3}_{-24}	I	"
12	600	1412±2	S/I	"
A	9690	1410±3	I	Spinel Coated ***Morganite Triangle RR Al_2O_3 Furnace Tube
B	4050	1013±2	S	
C	106560	1216±4	I	"
D	64680	1210±9	I	"
E	42600	1205±4	I	"
F	9720	1205±3	S/I	"
G	605	1127±4	S	"
H	579600	1211^{+3}_{-41}	I	"
I	9710	1411±1	I	"
J	40140	1304±3	I	"
K	2755	1486±2	I	"
L	241	1209±2	S	"
MgO:Na	12015	1411±1	I	"

*Runs 1-3, 5-10, 13-17 were done to check impurity pickup or to equilibrate the exchange system with Oxygen-18 gas.

**McDanel Refractory Porcelain Co. 510 Ninth Ave. Beaver Falls MN

***Morganite Refractories, Morganite Inc 401 N Ashe Ave. Dunn NC 28334

****See text Section 3.1
S=Short, diffusion only in dislocations & grain boundaries
I=Intermediate, dislocation & grain boundary tails observable

would be minimized. Moriyoshi et. al.[17] found dislocations introduced by deformation would rearrange themselves into subgrain boundaries in 15 hours at 1400°C or in 18 minutes at 1700°C. Also, diffusion times should be relatively short so that β is greater than or equal to 10 (equation 3.12). The present author previously found that recrystallization of deformed samples would occur at temperatures above 1500°C.[64] Intermediate time anneals which would show bulk diffusion and dislocation or grain boundary tails were performed at temperatures near 1200°C, 1300°C, 1400°C and 1500°C. A set of anneals were done at 1200°C for different times to determine the time dependence of the diffusion tail slope. A set of short time anneals which would allow diffusion only in dislocations and grain boundaries were done at temperatures near 1000°C, 1100°C and 1200°C. Lastly, two diffusion anneals were done in short to intermediate time ranges as control experiments, even though the solutions in Section 3.1 could not be applied due to the ambiguity of solutions in these time ranges. Diffusion coefficients calculated from samples from these anneals did not agree with other data. However a "bulk" and a "tail" region were observed in their concentration profiles. No recrystallization or polygonization was observed. Deformed and undeformed Oak Ridge crystals as well as deformed Norton crystals were used in almost every time/temperature combination. Doped samples were included in selected diffusion anneals to compare to the undoped materials.

4.3 SECONDARY ION MASS SPECTROMETRY

Diffusion profiles were determined by Secondary Ion Mass Spectrometry (SIMS) with a CAMECA ims 3f ionmicroprobe (Center for Micro analysis of Materials, Materials Research Laboratory, University of Illinois). This technique uses a primary ion beam to sputter away surface atoms and combinations of atoms which are then analyzed in a mass spectrometer. A total of 119 SIMS profiles were performed on the 88 samples. The primary ion beam was made of singly charged positive argon ions accelerated to 9.7KeV. They arrived at the sample surface at 4.2KeV after the 4.5KV ion extraction field near the sample is taken into account. The primary ion beam current was about 10^{-7}-10^{-8}A. This beam was rastered in a 500 µm x 500 µm square and a mechanical aperature accepted secondary ions from only a 60 µ diameter at the center of the raster. Some samples used a 250 µ raster and a 150 µ analysis area. This produced a flat bottomed sputter crater and insured level depth profiling and minimal sputter pit edge effects. Surface charging of highly insulating MgO was eliminated by use of an electron beam. First, all samples were coated with 300 angstroms of gold. The sample surface was exposed to an electron beam accelerated through 4KV plus the 4.5KV extraction field. The electron beam current was adjusted to maximize the secondary ion signal. Presumably, the electron gun heats the sample surface which allows charge dissipation[6,5].

Positively charged secondary ions $(O-16)^+$, $(O-18)^+$, $(Mg-24)^+$, and $(Si-28)^+$ were usually measured. Sometimes a dopant was also measured. The silicon signal was monitored as an indicator of surface contamination. Samples from short diffusion time anneals which would allow oxygen diffusion only in dislocations and grain boundaries had a very low $(O-18)^+$ signal. The sensitivity of the machine was increased, but this allowed the $(O-16)^+$ signal to saturate the detector. For these samples the weaker $(O-32)^+$ signal was monitored instead of the $(O-16)^+$ signal so that all oxygen signals would be measured in the same detector.

The mass spectrometer was cycled through the desired masses, analyzing each one for a period of about 1 second. After each mass was analyzed, the cycle was repeated. Each cycle is called a channel. Usually 300-400 channels were accumulated during 30-60 minutes of sputtering, during which time about 1 micron of material was removed. At this depth a bulk concentration very close to the world's ambient level of 0.002 was usually observed. Sputter pits of all samples were smooth except the polycrystals. These sputtered preferentially at grain boundaries and certain grains sputtered more than others.

One experiment on the SIMS was tried. While a sample was running, first the primary ion beam was turned off. An oxygen signal continued to be seen, at a significantly lower level, until the electron beam was shut off. This shows that the electron gun alone might cause emission of atoms from the surface.

4.4 DATA REDUCTION

This section describes how the equations of Section 3 on theory were actually employed. As stated previously, the model used in this study is of constant surface concentration C_s of diffusant diffusing into material of originally uniform concentration C_b. Furthermore, it is assumed that there is no surface gas exchange inhibition as was discussed in the Literature Survey. Also, due to the chemical similarity of oxygen-18 and oxygen-16, it is assumed that the oxygen diffusion coefficient is independent of the oxygen-18 concentration.

For the relative concentration C', equation 3.1, the surface concentration C_s used is that of the oxygen-18 concentration of the oxygen in the exchange system gas, 95.54%. The bulk concentration used is that of the world's ambient O-18 concentration, 0.204%. The concentration of O-18, C, in the sample at a given depth after a constant temperature diffusion anneal is taken as

$$C = \frac{\#18}{\#18 + \#16} \tag{4.1}$$

where #18 and #16 are the number of counts of oxygen isotopes 18 and 16 which are measured by the mass spectrometer in the same channel. So C is the average O-18 concentration during the channel. Thus the relative concentration used in calculations is

$$C' = \frac{\dfrac{\#18}{\#18 + \#16} - 0.9554}{0.00204 - 0.9554} \tag{4.2}$$

In order to calculate a bulk diffusion coefficient, a plot of $\mathrm{erf}^{-1}(C')$ versus channel number, CN, was made for each sample. Linear least squares regression was performed on the linear part of this plot near the surface of the sample where bulk diffusion dominates. The calculated slope, $d\ \mathrm{erf}^{-1}(C')/d\ CN$ was then converted to a slope referenced to diffusion depth, $d\ \mathrm{erf}^{-1}\ (C')/dx$, by dividing it by the depth per unit channel number.

$$\frac{d\ \mathrm{erf}^{-1}\ C'}{dx} = \frac{d\ \mathrm{erf}^{-1}\ C'}{d\ CN}\ \frac{d\ CN}{dx} \tag{4.3}$$

If we assume the sputter rate during secondary ion mass spectrometry is constant, then

$$\frac{d\ CN}{dx} = \frac{\#CN}{p} \tag{4.4}$$

where #CN = total number channels in the sputter pit
p = sputter pit depth

If we insert this into equation 4.3 we arrive at

$$\frac{d\ \mathrm{erf}^{-1}(C')}{dx} = \frac{d\ \mathrm{erf}^{-1}\ C'}{dCN}\ \frac{\#CN}{p} \tag{4.5}$$

This is used in equation 3.5 to calculate D.

$$D = \frac{1}{t}\left(2\ \frac{d\ \mathrm{erf}^{-1}(C')}{dCN}\ \frac{\#CN}{p}\right)^{-2}\ \mathrm{cm}^2/\mathrm{sec} \tag{4.6}$$

After the bulk diffusion coefficients were calculated, a linear least squares regression of

$\ln(D\ \mathrm{cm}^2/\mathrm{sec})$ versus $1/(T\ ^\circ K)$ was performed.

Sputter pit depths were measured with a profilometer ("Dektak II", Sloan Technology Corp, Santa Barbara, CA). Interference microscopy was not used because chemical polishing resulted in curved, undulating surfaces which made interference patterns difficult to interpret. Each sample's measured pit depth was not used directly in equation 4.6 because they were difficult to measure with precision. Pits on flat samples could be measured more easily. The 15 flattest deformed and undeformed single crystal samples were chosen and their 500 µm square sputter pits measured 3-7 times and averaged. Polycrystal pit depths agreed with single crystal pit depths but had more scatter due to their less smooth surfaces. A plot was made of the average sputter pit depth p divided by primary ion beam current I versus sputtering time t_s in seconds, Figure 10. Linear least squares regression was performed on this plot and the results used to calculate pit depths. In this way the error in pit depth measurement was reduced by averaging it over a set of more reliable pit depth measurements. The result of this regression is

$$\frac{p}{I}\ (\mathrm{cm/nA}) = (8.2 \pm 6.5) \times 10^{-9} + (4.67 \pm 0.31) \times 10^{-11}\ t_s \qquad (4.7)$$

The non zero intercept does not indicate sputtering at zero time but is a manifestation of error. The present author could have forced the linear regression to have a zero intercept but chose to let the data control the regression. Since most samples were sputtered for similar times, far away from $t=0$ this procedure should produce the best sputter pit depth estimates. However if equation 4.7 does not result in the actual values for sputter pit depths, even at the sputter times used, this will result in systematic error in diffusion coefficients.

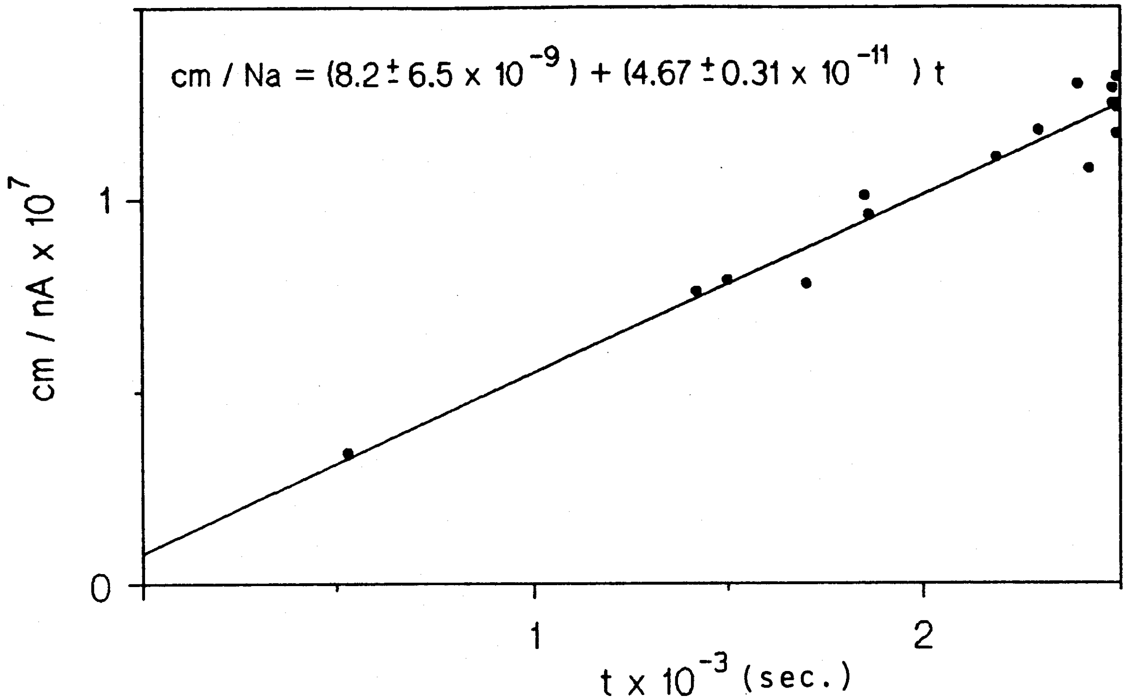

Fig. 10 SIMS sputter pit depth per unit primary ion beam current as a function of sputtering time. Primary beam 9.7KV Argon-40 positive ions, 500 μm square raster.

For the 250 μm square sputter pits, Equation 4.7 multiplied by 4 was used to calculate p. The samples with 250 μm pits had less flat surfaces, making the error in measuring the pit depths higher than the possible error from using the factor of 4.

In order to calculate the dislocation diffusion coefficient parameter $D'_d a^2$, a plot of $\ln(C-C_b)$ versus diffusion distance x was made. The bulk concentration C_b must be subtracted from the measured concentration C to eliminate the effect of the bulk concentration on C as C approaches C_b. On this plot, the dislocation diffusion "tail" will be linear. As in the case of bulk diffusion we assume sputter rate is linear and equation 4.4 is true, then

$$\frac{d \ln(C-C_b)}{dx} = \frac{d \ln(C-C_b)}{dCN} \frac{\#CN}{p} \tag{4.8}$$

If we insert this into theory equation 3.8 we arrive at

$$D'_d a^2 = A^2 D \left(\frac{d \ln(C-C_b)}{dCN} \frac{\#CN}{p} \right)^{-2} + Da^2 \quad cm^4/sec \tag{4.9}$$

Therefore $D'_d a^2$ is calculated by measuring $d \ln C-C_b/dCN$ from a plot, estimating the constant A (approximately equal to 1) from figures 4 in LeClaire & Rabinavitch[51], calculating the sputter pit depth p, estimating the bulk diffusion coefficient D and the dislocation core radius a. The constant A ranged from 0.70 to 1.08 for intermediate diffusion time samples. The bulk diffusion coefficient equation is calculated from the ln D versus 1/T regression. The dislocation core radius a is assumed to be $5X10^{-8}$cm. The factor Da^2 represents a limiting case of equal or slower dislocation diffusion compared to bulk diffusion. Logically, if any tail is to exist, the Da^2 term must be small. In practice, if any tail slope is seen, the Da^2 term is insignificant unless it is assumed that a is very large (~1/2µm). The slope $d\ \ln(C-C_b)/dCN$ is calculated by means of a weighted linear least squares regression of $\ln(C-C_b)$ on CN in the tail slope region. The weight factor used was

$$\sigma = \sqrt{\frac{(\#16)(\#18)}{(\#18 + \#16)(\#18 - C_b(\#18 + \#16))^2}} \qquad (4.10)$$

This was calculated using Poisson distribution counting statistics, assuming negligible error in the bulk concentration C_b=0.00204 and using conventional propagation of error methods[57] (Equation 3.20). An unweighted linear regression assumes equal error for all dependent variables. In this case, as measured C approaches C_b, the number of counts of oxygen-18 is reduced and error in this measurement increases (equation 3.18). After the $D'_d a^2$ parameters were calculated, a linear regression of $\log\ D'_d a^2$ versus $1/(T°K)$ was performed for samples with dislocations and few grain boundaries.

In order to calculate the grain boundary diffusion parameter $D'_b\delta$, a plot of $\ln(C-C_b)$ versus $x^{1.2}$ was made. On this plot the grain boundary diffusion tail is linear. If we assume sputter rate is linear and equation 4.4 is true then

$$\frac{d\ \ln(C-C_b)}{dx^{1.2}} = \frac{d\ \ln(C-C_b)}{dCN^{1.2}}\ \frac{\#CN^{1.2}}{p^{1.2}} \qquad (4.11)$$

If we insert this into theory equation 3.11 we arrive at

$$D'_b\delta = 0.66\ \left(\frac{d\ \ln(C-C_b)}{dCN^{1.2}}\ \frac{\#CN^{1.2}}{p^{1.2}}\right)^{-5/3}\left(\frac{4D}{t}\right)^{1/2} \quad cm^3/sec \qquad (4.12)$$

So $D'_b\delta$ is calculated with this equation after measuring $d \ln(C-C_b)/dCN^{1.2}$ and diffusion time t, calculating sputter pit depth p, and estimating D from the ln D versus $1/T\,^\circ K$ regression. In a similar manner as the dislocation diffusion case, $d \ln(C-C_b)/dCN^{1.2}$ is calculated using a weighted linear least squares fit using the same weighting factor Equation 4.10. After the $D'_b\delta$ parameter was calculated, the parameter β (Equation 3.12) was calculated to insure it was large enough (>10) for theory equation 3.11 to be true.

Both for dislocation and grain boundary diffusion calculations, the linear tail slope nearest the surface was used. In a few instances, two linear regions were observed, one nearer to the surface than the other. The slope nearest to the surface was used because this region would have a greater proportion of the diffusing atoms compared to the deeper penetration region.

In order to help determine whether diffusion tails were due to dislocations or grain boundaries, plots of $d \ln C/d(x^{1.2})$ versus log t were made for 1200°C diffusion samples. As discussed in the Theory section, the slope of this plot should be zero for dislocation diffusion and -0.3 for grain boundary diffusion.

The dislocation density d was calculated for all samples from $\ln(C-C_b)$ versus diffusion distance x plots with theory equation 3.10. The intercept $C_{x=0}$ came from the weighted linear regression intercept. The surface concentration C_s was assumed to be 0.9554, the diffusion time t was inserted, and the bulk diffusion coefficient D was calculated from the log D versus 1/T regression. The dislocation core radius a was assumed to be 5×10^{-8} cm. As was mentioned in the theory section, the calculated d is relatively insensitive to error in a. Even though Equation 3.10 is only true for dislocation diffusion, the dislocation density for all samples was calculated.

For very short time diffusion anneals the oxygen-18 signal was too low to calculate D'_b or D'_d from an inverse error function slope. Instead D'_b and D'_d were estimated with the equation

$$D' = \frac{x_p^2}{4t} \tag{4.13}$$

where x_p is the diffusion penetration depth estimated from an $\mathrm{erf}^{-1}(C')$ or $\log(C)$ versus diffusion distance x plot.

A computer was used to manipulate SIMS results. Approximately 7 megabytes of disk storage were necessary to store and manipulate raw data (numbers of mass spectrometer counts) and calculated data.

5.0 RESULTS

5.1 OXYGEN DIFFUSION PROFILE EXAMPLES

This section contains representative examples from more than 500 data plots of the 119 SIMS profiles. The same data is plotted in different ways in each figure in order to illustrate the data completely. Different plots affect different parts of the diffusion profiles in different manners. Also, different plots are useful in comparing data from the different sample types.

Figure 11 shows some data typical of most of the intermediate diffusion time samples except for the polycrystals. The calculated sputter pit depth is 0.70 μm. The concentration profile (C versus channel number) is shown first (Fig. 11-A), but was not necessary for any calculations. The inverse error function plot is shown next (Fig. 11-B). It was used to calculate the bulk diffusion coefficient from the slope of the near surface region. The slope was calculated from a linear regression from channel number 4 to channel number 15. The highest concentration measured for this sample was about 63%. The SIMS instrument could not determine the concentration right at the surface, but the intercept of the near surface linear region of the inverse error function plot was usually very close to zero, usually between 0.1 and -0.1. This indicates that the surface was probably the same concentration as the O-18 exchange atmosphere. The dislocation or diffusion tail was not subtracted from the near surface region when calculating bulk diffusion coefficients because its magnitude did not affect the slope of the near surface region. The next plot (Fig. 11-C) is the natural log of concentration versus channel number. This plot was not necessary for calculations, but is a good

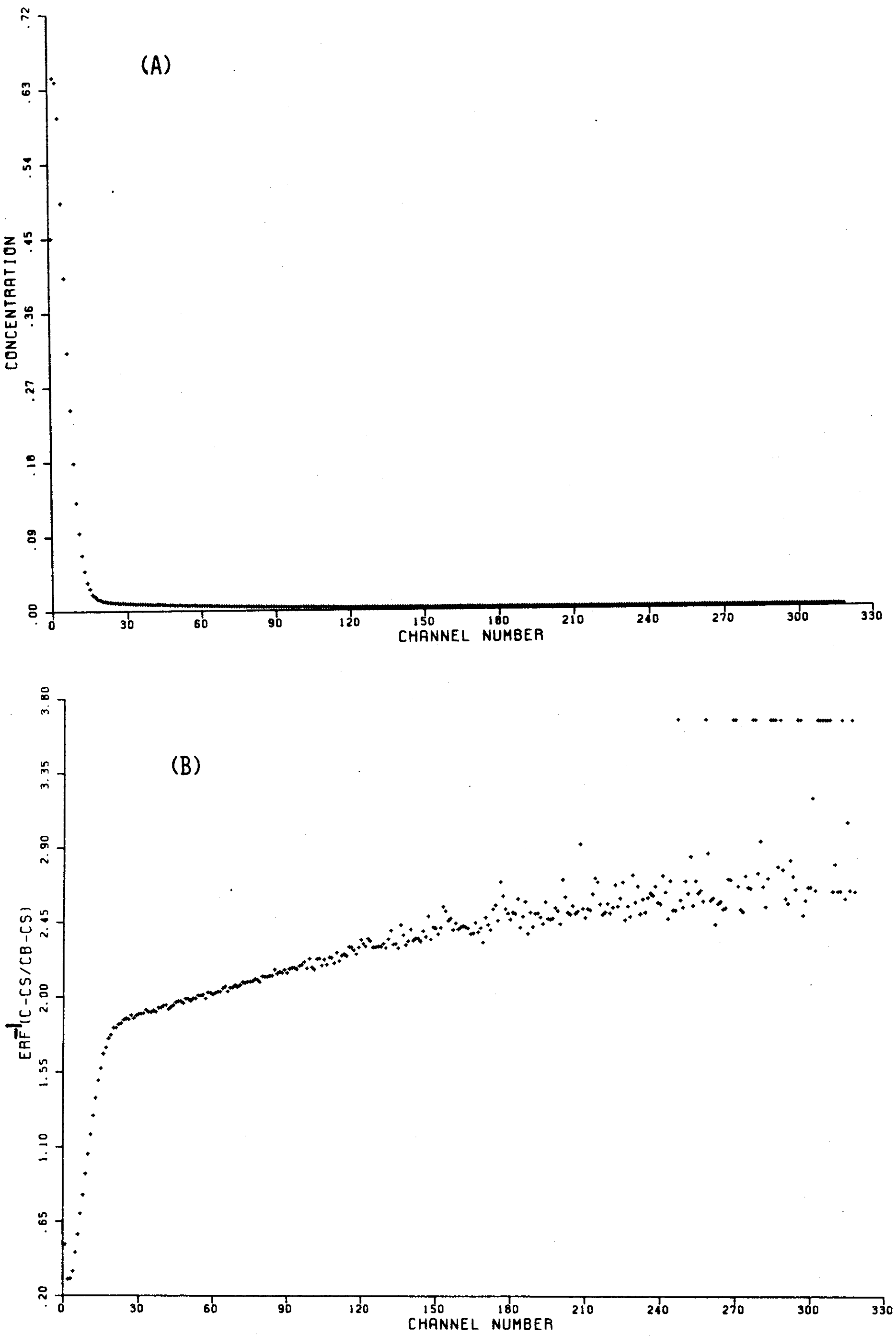

Fig. 11(A-E). Diffusion profile data of an Oak Ridge sample deformed 6% plotted five different ways. Diffusion 1410 °C, 9690 sec. Calculated sputter pit depth is 0.70 µm.

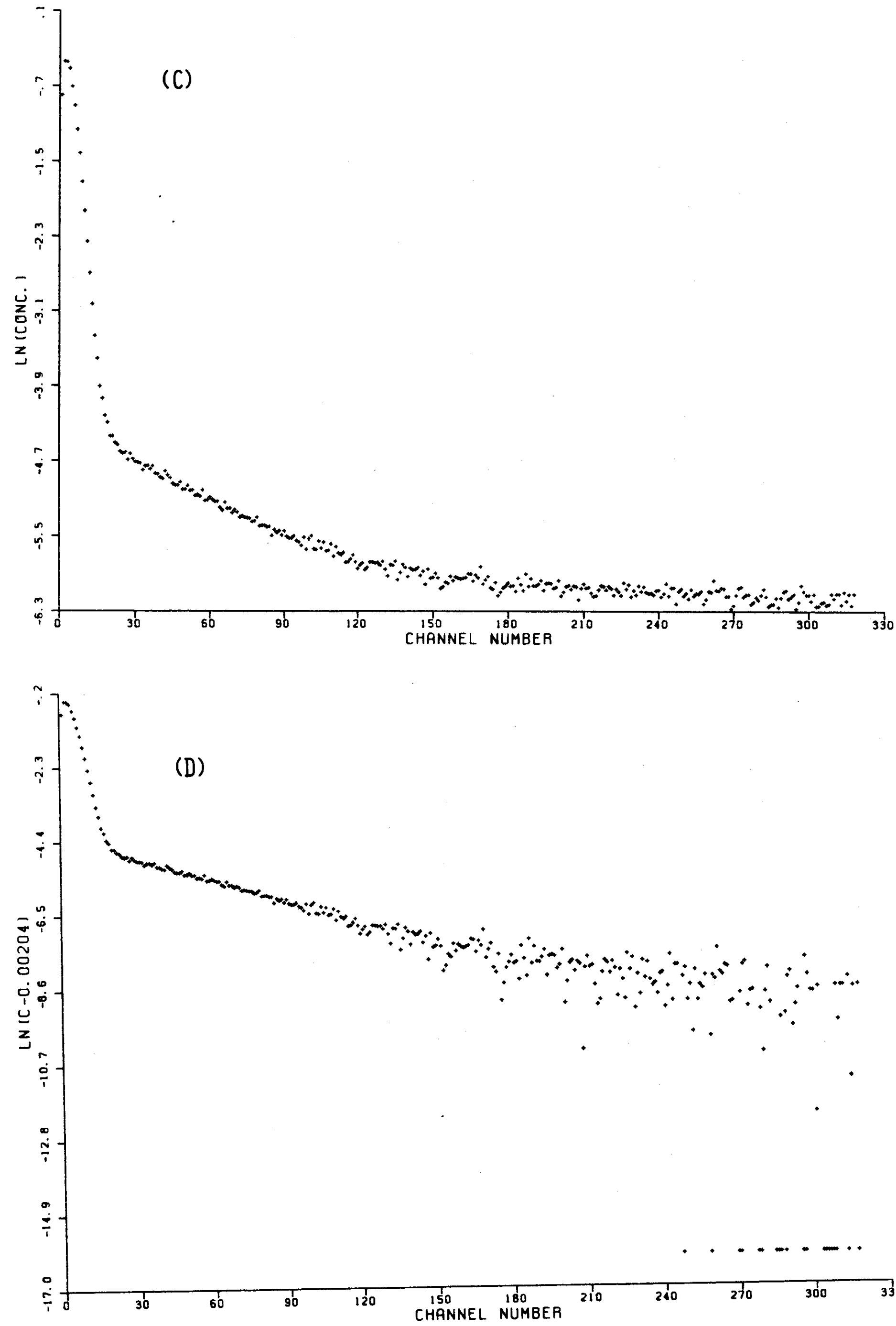

Fig. 11 (continued)

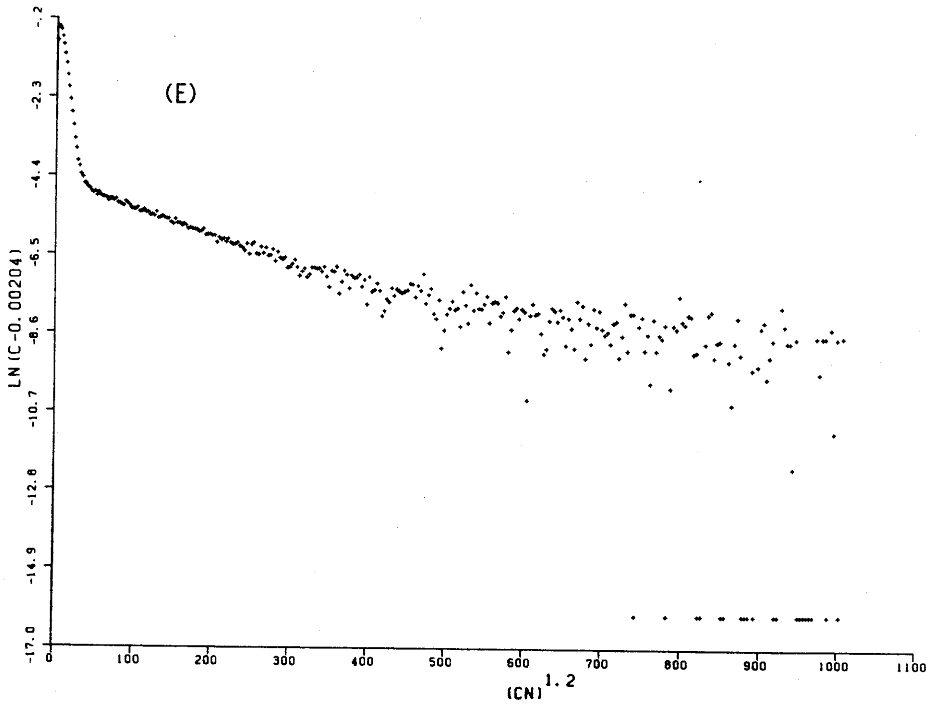

Fig. 11 (continued)

illustration of 3 regions in the data; a bulk diffusion region near the surface, a diffusion "tail" region, and a flat, bulk concentration region farthest from the surface. Two similar plots are shown next (Figs. 11-D,E): Both have the same y axis, $\log_e$ (C-0.00204), but the x axes are slightly different. The first plot has an x axis of linear channel number while the second has an x axis of channel number to the 1.2 power. The slope of the tail region on the linear x axis plot between channel numbers 30 and 150 was calculated by weighted linear regression and was used to calculate a dislocation diffusion parameter $D'_d a^2$. This sample had dislocations and widely spaced subgrain boundaries. The last plot would have been used to calculate a grain boundary diffusion parameter $D'_b \delta$ if grain boundaries were present. It is shown to illustrate that the linearity of the tail slope does not change very much when the power of the x-axis is changed, so this would not be a good method to distinguish between grain boundary or dislocation diffusion. The few points at the top of the inverse error function plot and at the bottom of the $\log_e(C-C_b)$ plots are points where, due to random error, the measured concentration C was less than C_b=0.00204. Since $C-C_b$ is negative the log of $C-C_b$ is undefined, a dummy value is plotted at these points. No regressions were done in the region containing dummy points, and the weighting of the linear regression placed less emphasis on lower values of $\log_e(C-C_b)$ near these points.

Figure 12 shows the same five types of plots as Figure 11 but for a polycrystalline sample. Many of the comments in the preceeding paragraph apply to this figure. The polycrystalline samples showed similar bulk diffusion as other samples but the grain boundary signals were much higher and there was a less sharp transition between the bulk and grain boundary parts of the profiles but a linear region was obtained. FeJ refers to Fe doped samples supplied by Y. Oishi. This might be due to greater effectiveness of high angle grain boundaries for diffusion but is more likely due to preferential sputtering of

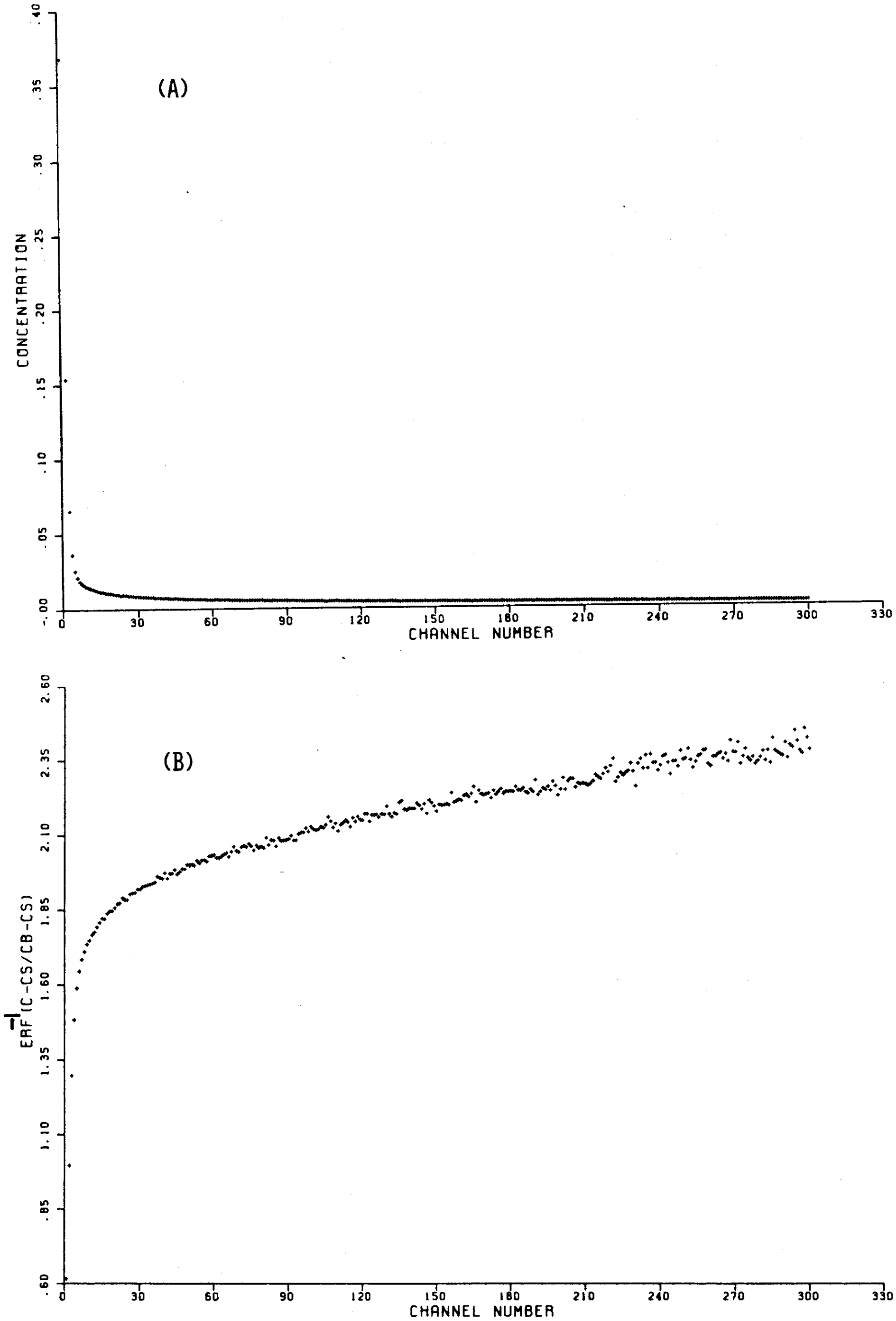

Fig. 12(A-E). Diffusion profile data of a polycrystalline sample plotted 5 different ways. Diffusion 1205 °C, 42600 sec. Calculated sputter pit depth 1.06 µm.

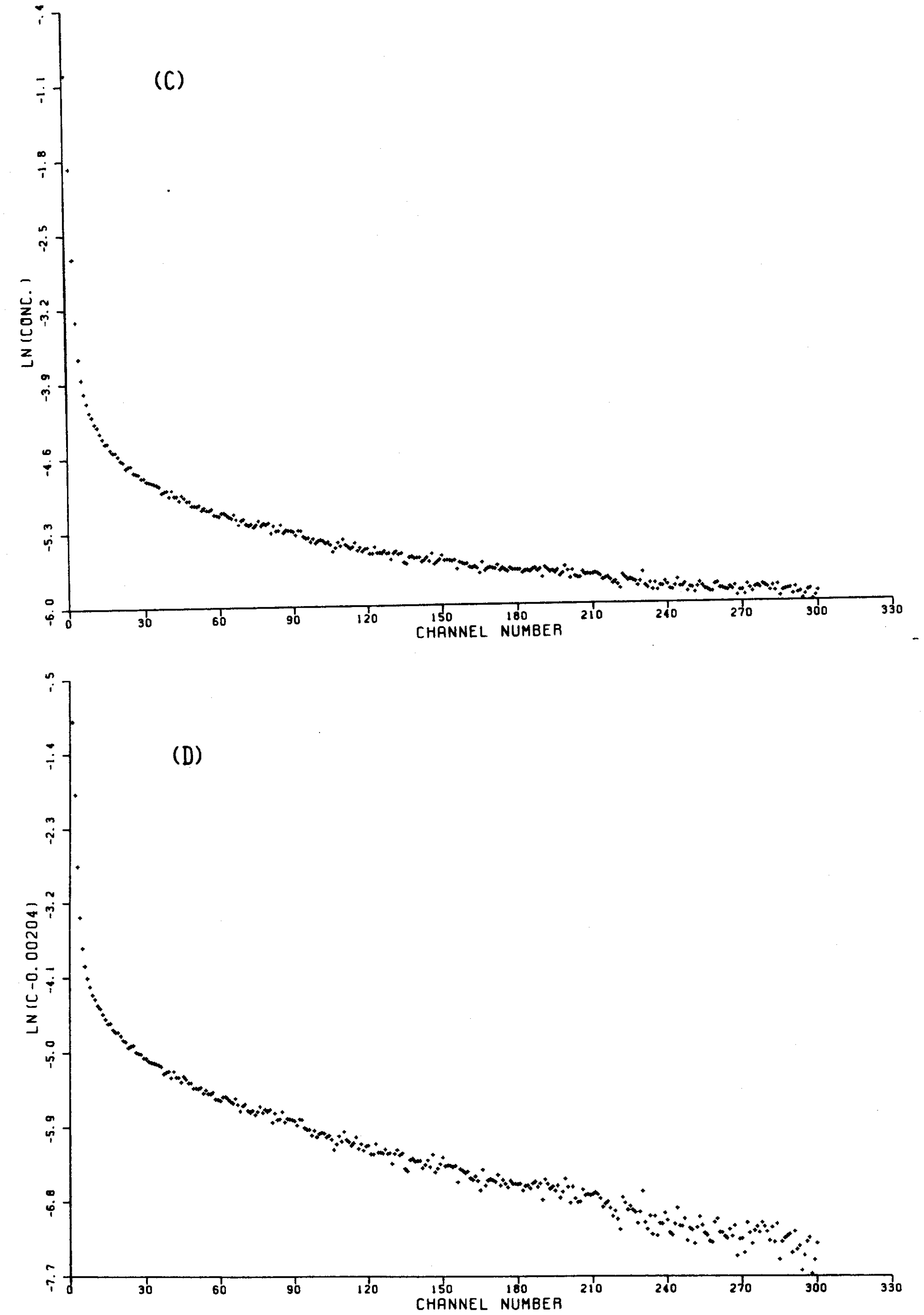

Fig. 12 (continued)

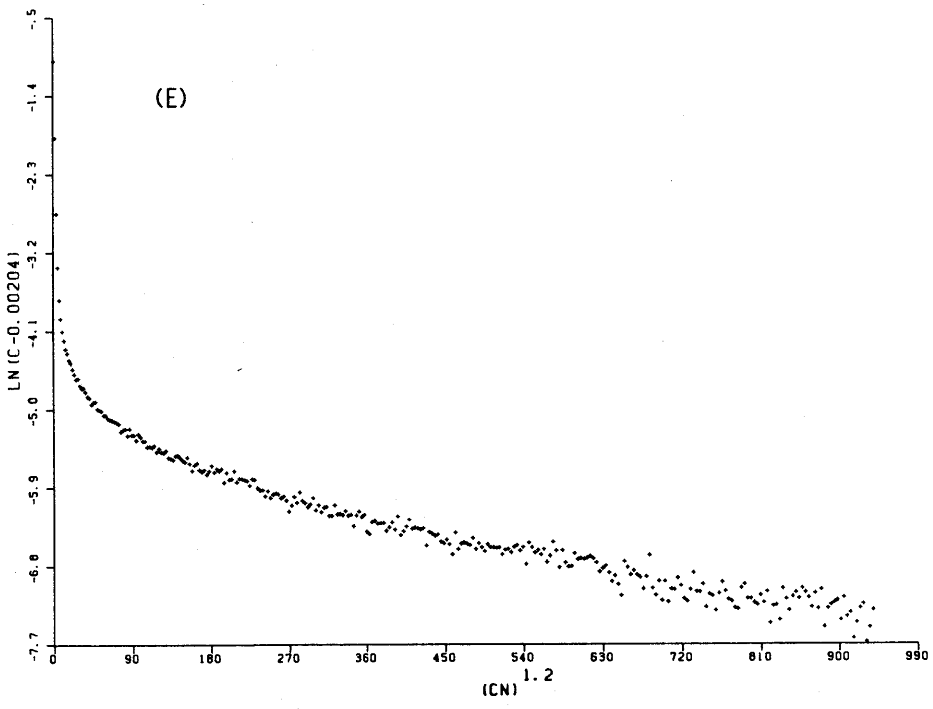

Fig. 12 (continued)

grain boundaries during SIMS. Data from these plots was calculated in a similar manner as for Figure 10, except that a grain boundary diffusion parameter $D'_b\delta$ was calculated from the tail slope of the $\log_e(C-C_b)$ versus channel number to the 1.2 power plot by weighted linear regression.

Figure 13 shows data from a short diffusion time "Type C" diffusion anneal in which $\sqrt{Dt}$ is approximately equal to 4 angstroms. Any diffusant is assumed to follow "bulk kinetics" within the dislocations and grain boundaries. As mentioned in section 4.4, short time samples were analyzed by estimating a diffusion depth, X_p, and inserting it into equation 4.13. For this particular sample the diffusion depth at channel 178 was used, $178/400 \times 1.32\ \mu m = 0.59\ \mu m$. For this sample, X_p was determined on the $\log_e(C)$ versus channel number plot (Fig. 11-C), but for some samples X_p was determined on an inverse error function plot like Figure 11-B.

Secondary ion mass spectrometry was done in a different manner for short diffusion time samples. Since the oxygen-18 signal was so low, the sensitivity of the instrument was increased. This caused the oxygen-16 signal to saturate the detector. The oxygen-32 signal was used (molecular oxygen) instead of the oxygen-16 signal. Since oxygen-18 and oxygen-32 will sputter differently, the concentrations calculated using these signals $C = \#18/(\#18 + \#32)$ are not accurate, but useful in determining the diffusion depth estimate X_p. The data points near the surface of the plots are assumed to be a SIMS artifact upon sputtering through the surface oxygen-18 exchange layer or non-Fickian bulk diffusion due to the short diffusion anneal time.

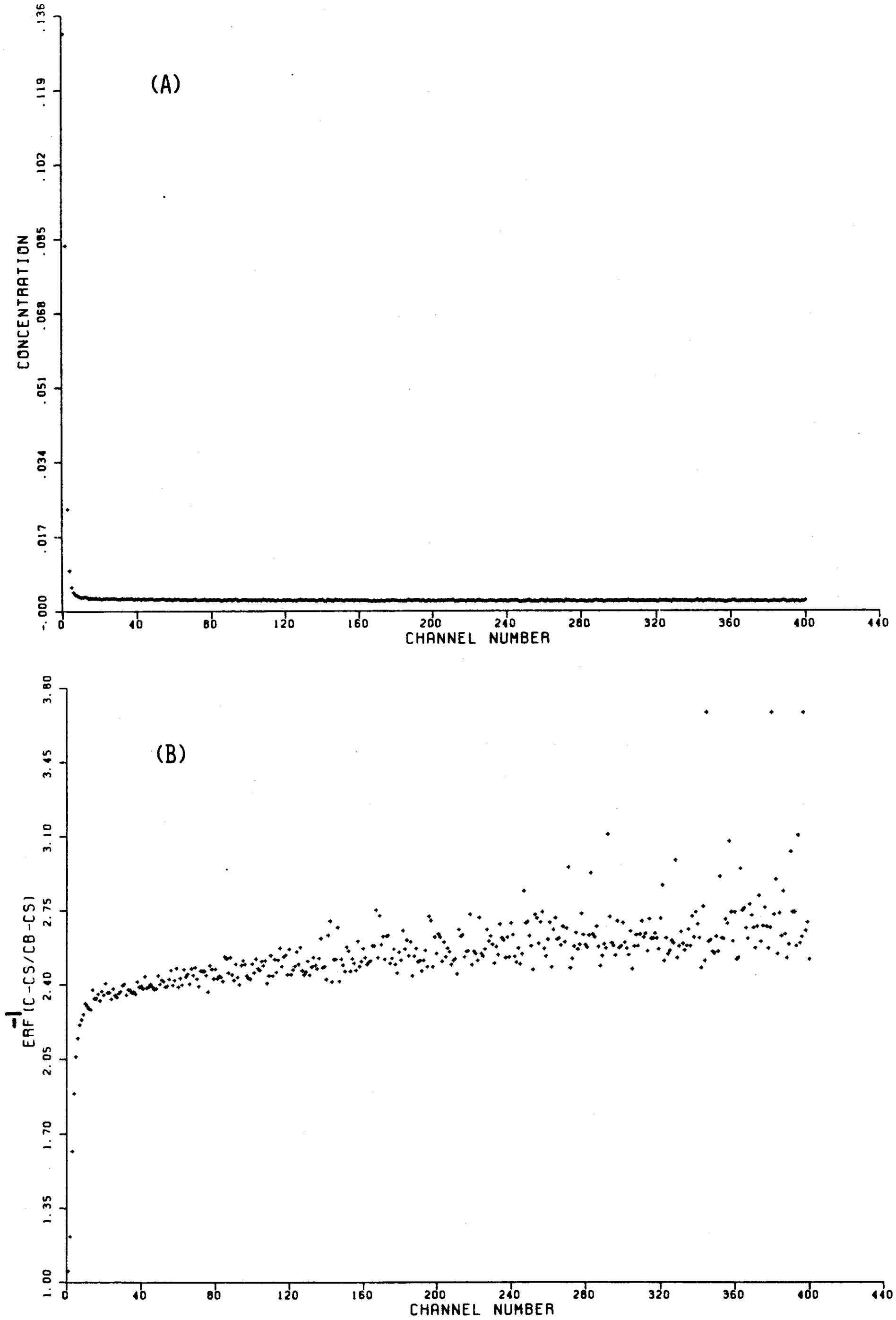

Fig. 13(A-C). Very short time diffusion profile data of a Norton Co. sample deformed to 62% true strain, plotted three different ways. Diffusion conditions 1013 °C, 4050 sec, i.e. very short time "Type C" diffusion, because bulk diffusion penetration is approximately 4 angstroms. Calculated sputter pit depth 1.32 µm. Note that y axis units are not accurate, see text. For this sample, the depth at channel 178 was used to calculate D′.

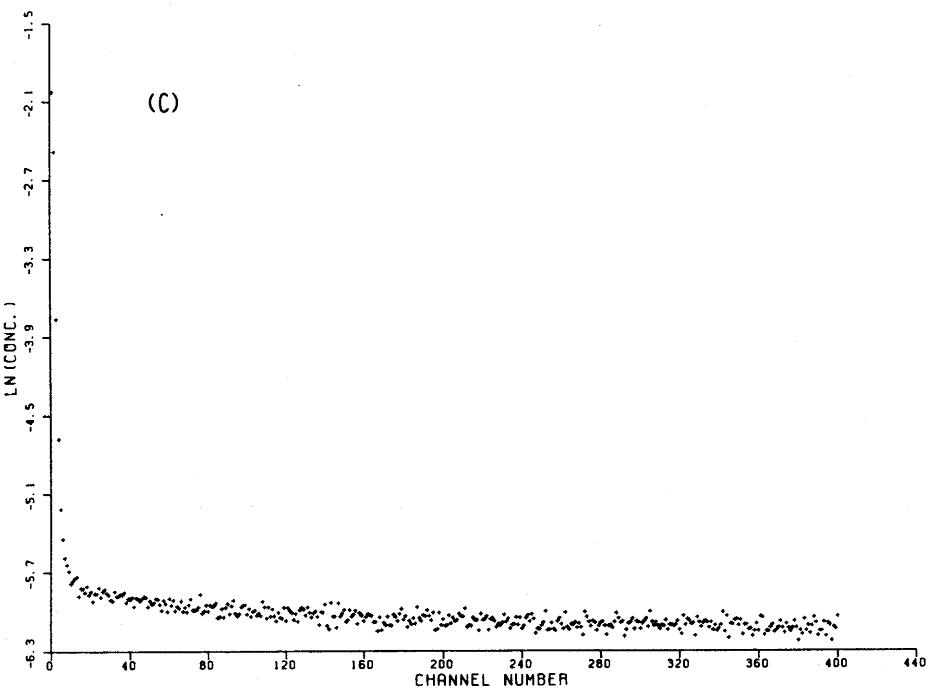

Fig. 13 (continued)

5.2 BULK OXYGEN DIFFUSION IN UNDOPED MgO

This section contains a summary of bulk diffusion data for undoped Oak Ridge, Norton, and polycrystalline (MIT) materials.

Figure 14 illustrates how most of the following data is displayed. The mean of the diffusion measurements or sample mean, sample standard deviation, number of samples used to calculate these quantities, and range of measurements are all displayed at each temperature. Logarithms of these quantities were taken after they were calculated. The number of samples is actually the number of SIMS profiles. Some samples of MgO were analyzed by SIMS on 2 or 3 areas of their surface. Repeat SIMS measurements of the same piece of MgO were not averaged because the 60μ SIMS analysis area is very small and the microstructure or impurity level may be variable between such small areas. The range is shown because it is very useful on log plots of data with large error σ_x, like the dislocation and grain boundary data which follow. If the error σ_x is as large or larger than the mean $\overline{x}$, a not uncommon occurance in diffusion measurements, $\log(\overline{x} - \sigma_x)$ would be unreasonably low on a plot, in fact undefined if σ_x is greater than or equal to $\overline{x}$.

This is just one of the peculiarities of a log plot like an Arrhenius plot. Another peculiarity is how error bars become distorted. Error is usually distributed evenly about a mean. On a linear plot, error bars will extend equal amounts above and below a data point. However, after logarithms are taken, error bars become uneven, extending below a data point more than above it. Conversely, multiplication of data by factors of 1/2 and 2 moves data on a log plot the same amount down or up respectively but are errors of 50% and 100%, respectively.

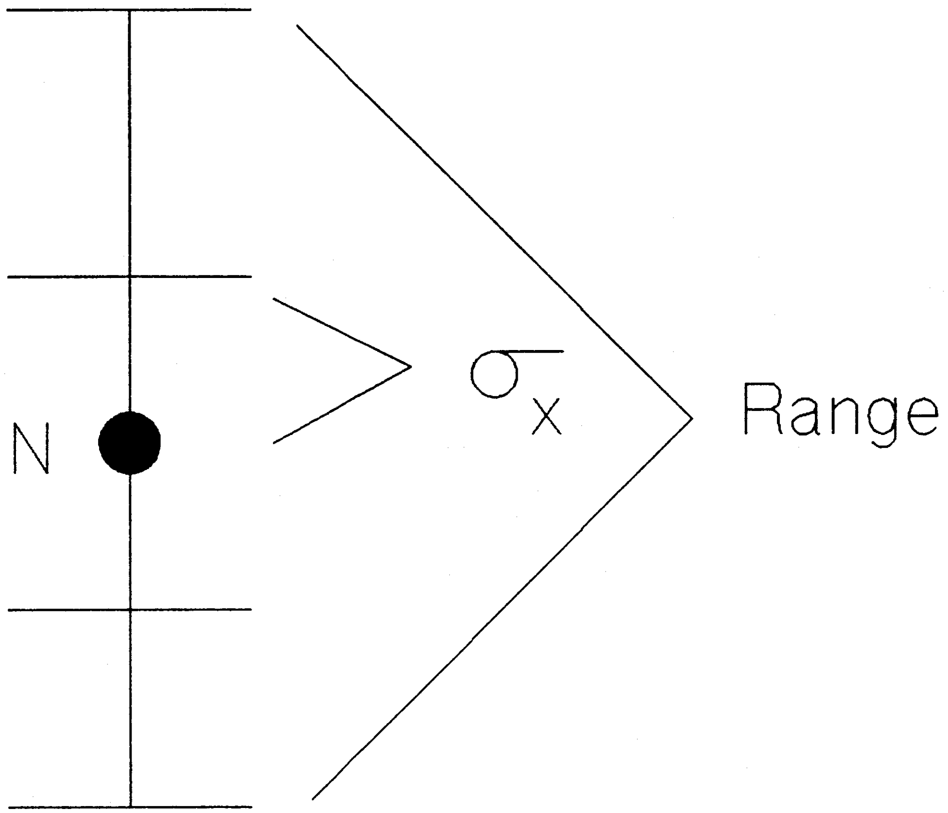

Fig. 14 Schematic diagram of data point notation used in subsequent figures. N is the number of data points used to calculate the sample mean which is indicated by the solid circle. The inner error bars are the sample mean plus and minus the calculated sample standard deviation σ_x, equation 3.15, (not the standard deviation of the mean). Outer error bars indicate the highest and lowest sample measurements. In cases of large σ_x, "inner" error bars are not included if they would extend above or below the range.

The following convention was used in the Arrhenius plots which follow. All data point statistics were calculated based on the actual data, not the log of the data. Logarithms were then computed. If logarithms were computed first, the calculated statistics would be different and not representative of the actual data. Linear regressions on Arrhenius plots were performed on the logarithms of the individual data, not the calculated means or logarithms of means. This automatically weighted the regressions in favor of those temperatures with the most samples. Thus, the regression line predicts the mean of the logarithms while the data displayed are the logarithms of the means.

The linear regression results in an intercept and slope with associated standard deviations. From these quantities, an equation for D as a function of $\exp(1/T)$ is solved. The errors associated with the pre-exponential and activation energy result from the intercept and slope standard deviations. The errors reported are the "one standard deviation"-68% confidence level errors (Section 3.2). This conventional method of performing regressions on Arrhenius plots introduces error. The regression will predict a logarithm of a value near the actual value, not the actual value. This will be clear in the data plots of dislocation and grain boundary diffusion data where the calculated regressions do not go through the means of data with the greatest number of experimentally determined values. This however, is the conventional, easiest, and analytical method. If the mean of the logarithms was displayed (instead of the logarithm of the means) the data points displayed would be closer to the regression lines.

The only way to eliminate this source of introduced error is to perform nonlinear regression of D on T (instead of linear regression of $\log D$ on $1/T$). However, nonlinear regression is usually not analytic and must be done iteratively. The errors associated with nonlinear regression constants are also not analytic. It has been argued that the difference between nonlinear and linear regressions can alter conclusions of a diffusion experiment[66]. In these experiments however, it would make little difference due to the large errors associated with the grain boundary and dislocation diffusion.

Figure 15 is a compilation of bulk oxygen diffusion from undoped Oak Ridge, Norton, and MIT polycrystalline materials. Out of the 39 SIMS profile data used to make this plot, 6 were from the MIT polycrystal, 6 were from the Norton Company crystal deformed 62%, and 27 were from the large Oak Ridge single crystal (Fig. 2) from which undeformed, 6% deformed and 55% deformed samples were made. Therefore, the data are weighted in favor of the purer Oak Ridge material. In any case there was no observable difference among data for different sample types. Slight error is introduced by grouping the 22 samples together at 1210 °C because the samples were from diffusion anneals ranging from 1205 to 1216 °C. However, this grouping facilitates plot viewing and, as mentioned before, the regression line shown was performed on the logarithms of the individual data and not the grouped points. From this line and its associated errors, the following equation was solved.

$$D=(3.9\,^{+10.5}_{-2.9}) \times 10^{-6} \exp\left(-\frac{3.45 \pm 0.17\ \text{eV}}{kT}\right)\ \text{cm}^2/\text{sec} \quad 1200\text{-}1500\,^\circ\text{C} \qquad (5.1)$$

Figure 16 shows how this line compares with those of other authors.

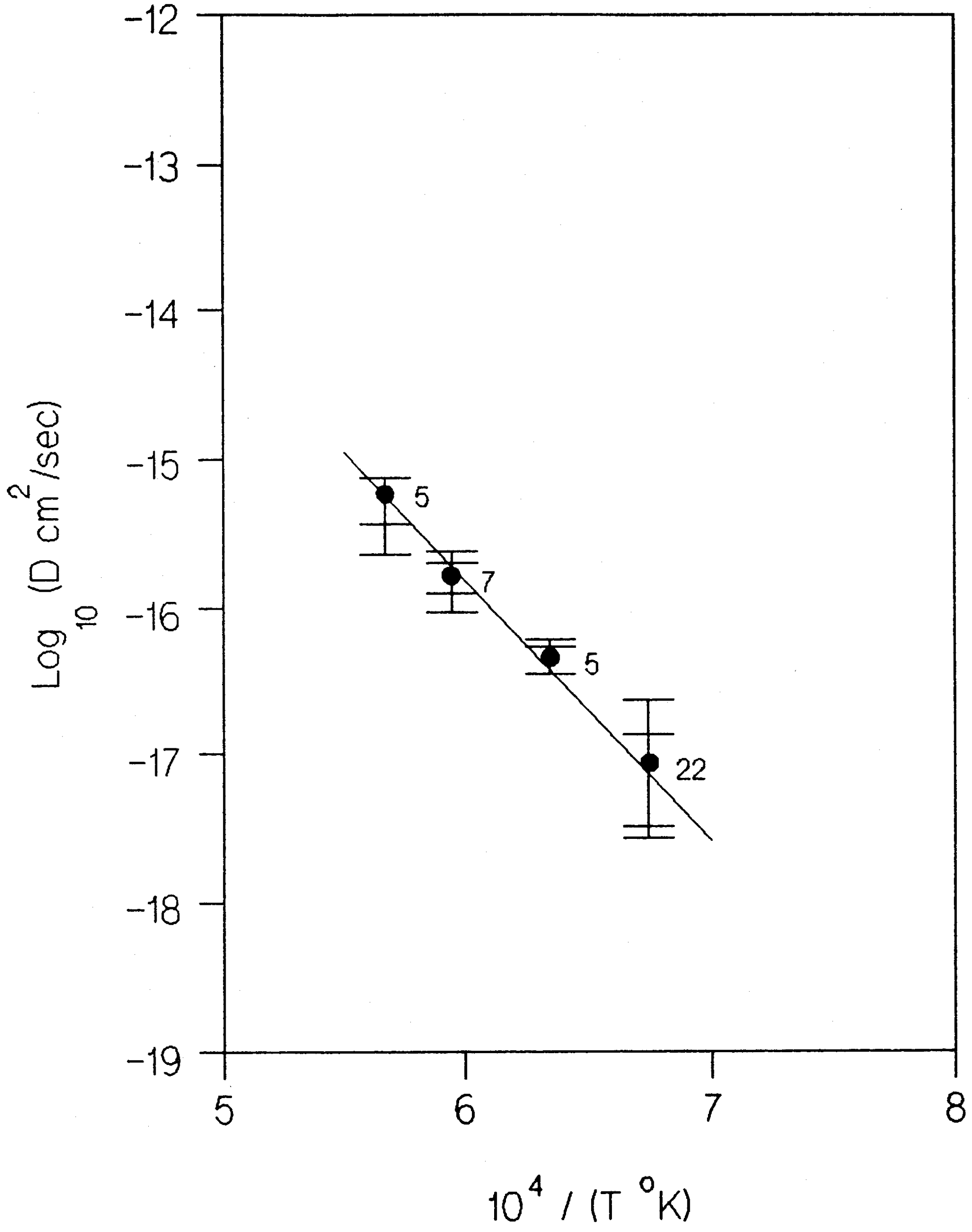

Fig. 15 Bulk oxygen diffusion data of the present study for undoped Oak Ridge, Norton, and MIT MgO. Out of the 39 SIMS profile data used to make this plot, 27 came from one Oak Ridge single crystal.

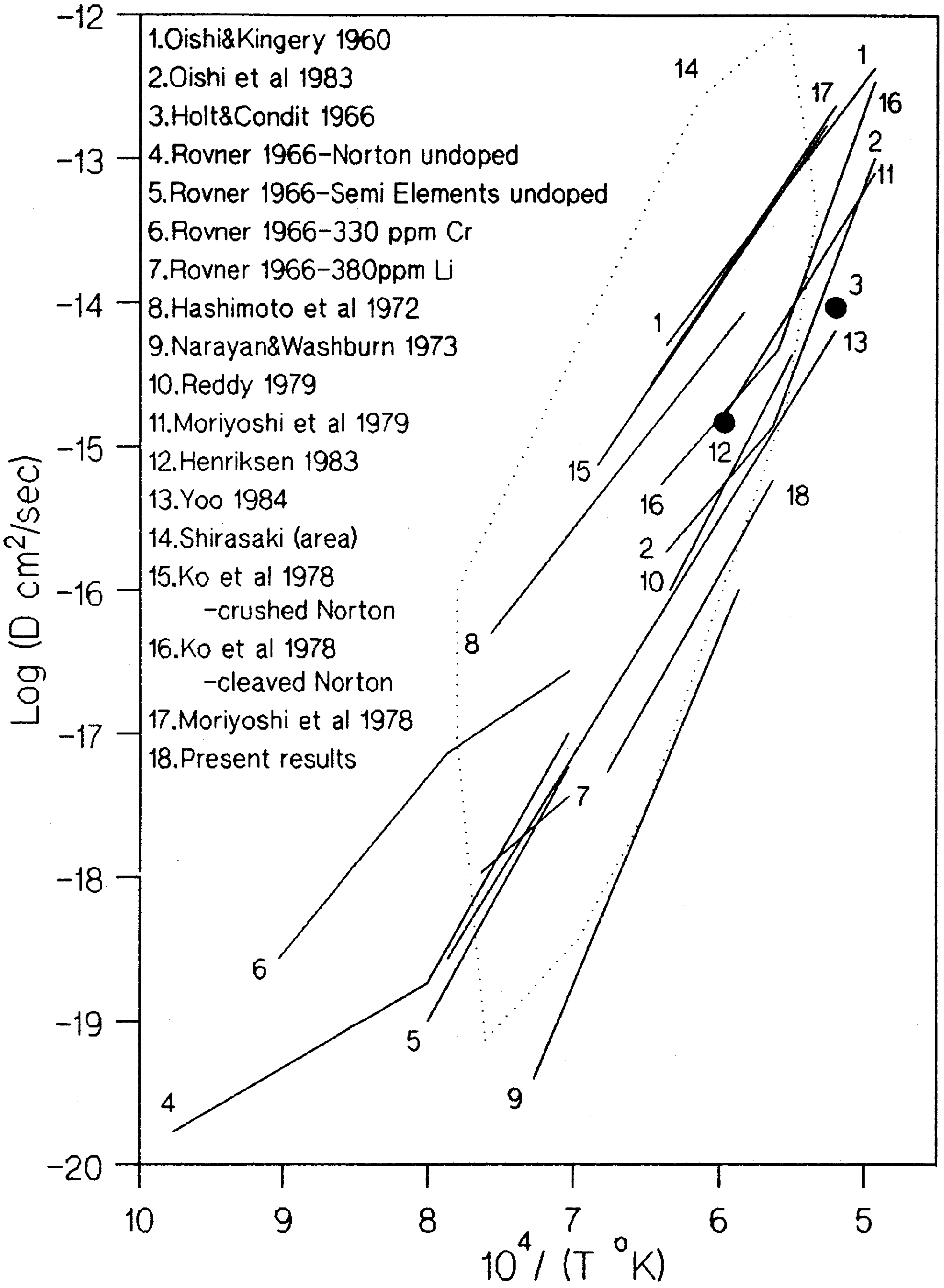

Fig. 16 Bulk oxygen diffusion data of present study along with data of other authors.

5.3 DISLOCATION AND GRAIN BOUNDARY OXYGEN DIFFUSION IN UNDOPED MgO

This section contains various results pertaining to oxygen diffusion in dislocations and grain boundaries. Samples were divided for subsequent analysis on the basis of microstructure. Single crystals and the Oak Ridge sample deformed 6% were analyzed using dislocation diffusion mathematics. Polycrystals and highly deformed samples with low angle grain boundaries were analyzed using grain boundary diffusion mathematics. Figure 17 is a compilation of dislocation diffusion parameter $D'_d a^2$ data for undeformed and 6% deformed Oak Ridge crystals. The regression line in the figure yielded the following result.

$$D'_d a^2 = 10^{-(15.9\pm1.9)} \exp(-\frac{3.20 \pm 0.58 \text{ eV}}{kT}) \text{ cm}^4/\text{sec} \quad 1200\text{-}1500^\circ\text{C} \quad (5.2)$$

Note that the regression resulted in a large error in the pre-exponential term of plus or minus 2 orders of magnitude, even though the range of experiments at 1200 °C was about plus or minus one order of magnitude.

Figure 18 is the same as Figure 17 but with the data of Narayan and Washburn[26] included. The additional data had to be modified to conform with the $D'_d a^2$ axis units. The data from the observation of dislocation loop self climb yielded a $D'_d A$ product where A is the area of a dislocation cross-section. This was divided by π to convert it to $D'_d a^2$ data. The present data agrees very well with that of Narayan & Washburn.

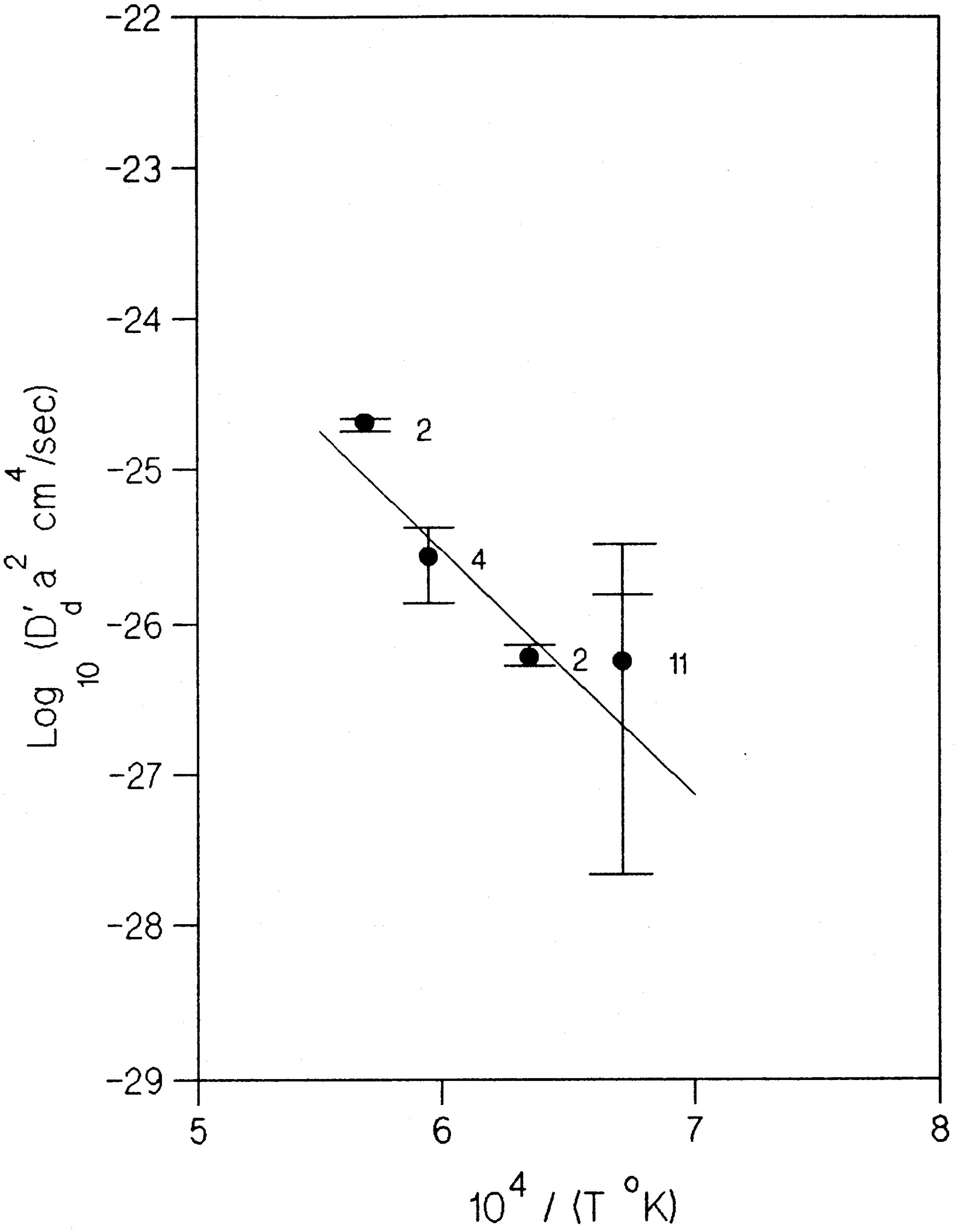

Fig. 17 Dislocation oxygen diffusion parameter $D'_d a^2$ data of the present study for Oak Ridge MgO. All SIMS profile data used to make this plot came from one Oak Ridge single crystal.

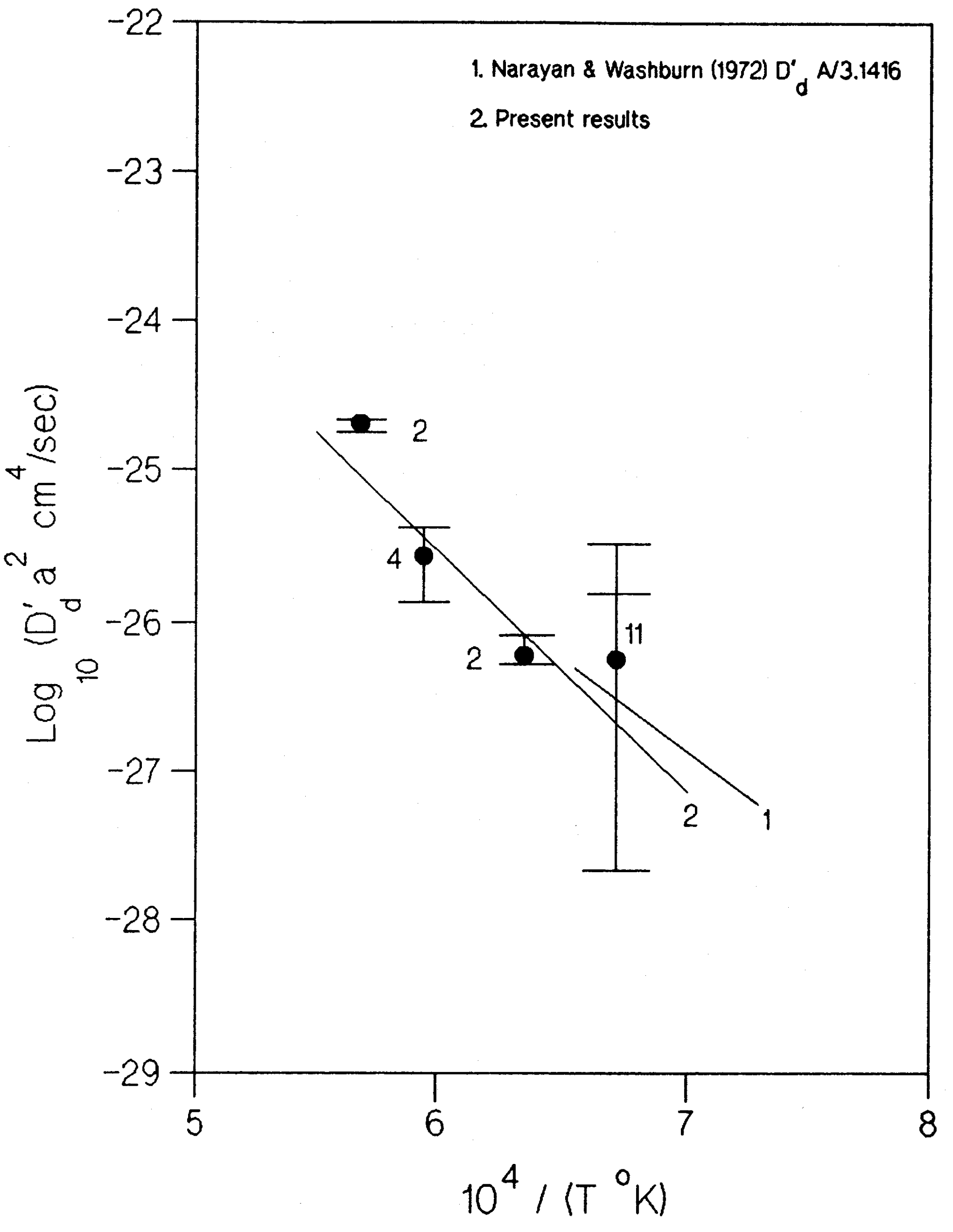

Fig. 18 Dislocation oxygen diffusion parameter data of present study with data of other authors. The data of Narayan & Washburn was divided by π to make it compatible with the plot format.

Figure 19 is a compilation of the grain boundary diffusion parameter data $D'_b\delta$ for undoped samples with grain boundaries. Out of the 19 SIMS profile data used to make this plot, 7 were from the Oak Ridge crystal deformed 55%, 6 were from the Norton company crystal deformed 62%, and 6 were from the MIT polycrystal. No consistent difference between data from the different sample types was observed. The value of β calculated from equation 3.12 should be greater than 10 in order to calculate $D'_b\delta$ from equation 3.11. The value of β was calculated for the SIMS profile data used in this plot by using the experimentally determined value of $D'_b\delta$ for each sample and using the value of D calculated from equation 5.1. The average of β was 1350 and the range was 12–7953. From the regression line on the plot the following equation was solved.

$$D'_b\delta = 10^{-(6.5\pm2.2)} \exp\left(-\frac{4.06 \pm 0.78 \text{ eV}}{kT}\right) \text{ cm}^3/\text{sec} \quad 1200\text{-}1500^\circ\text{C} \qquad (5.3)$$

Figure 20 includes the $D'_b\delta/D$ data of McKenzie et. al. [24] which has been multiplied by the value D found in the present study. The agreement is very good, both studies error ranges overlap. The data of McKenzie et. al. [24] is centered about one order of magnitude above the extrapolated regression line of the present study.

Figure 21 is a summary of very short time "TypeC" diffusion data for all undoped diffusion samples. Out of the 16 SIMS profile data used to make the plot, 9 came from one Oak Ridge single crystal (Fig. 2), 4 from the Norton Company crystal deformed 62%, and 3 from the MIT polycrystal. Therefore the data are weighted in favor of the purer Oak Ridge material. No distinction could be made between dislocation or grain boundary diffusion so values of D'_d and D'_b calculated by means of equation 4.13 were combined on this plot and labelled D'. Because the oxygen-18 SIMS signals were so low for these

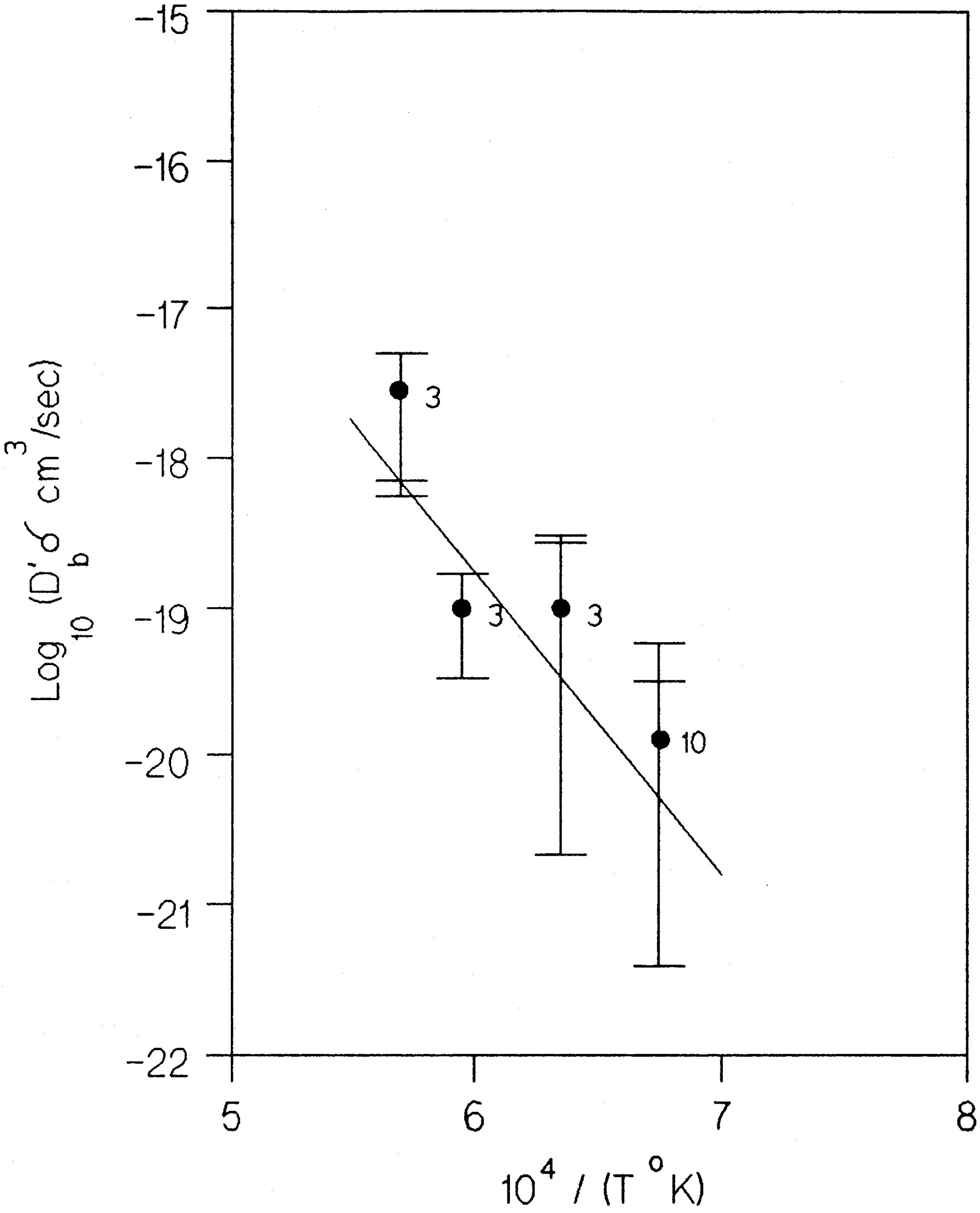

Fig. 19 Grain boundary oxygen diffusion parameter $D'_b\delta$ data for highly deformed Oak Ridge and Norton crystals and MIT polycrystals.

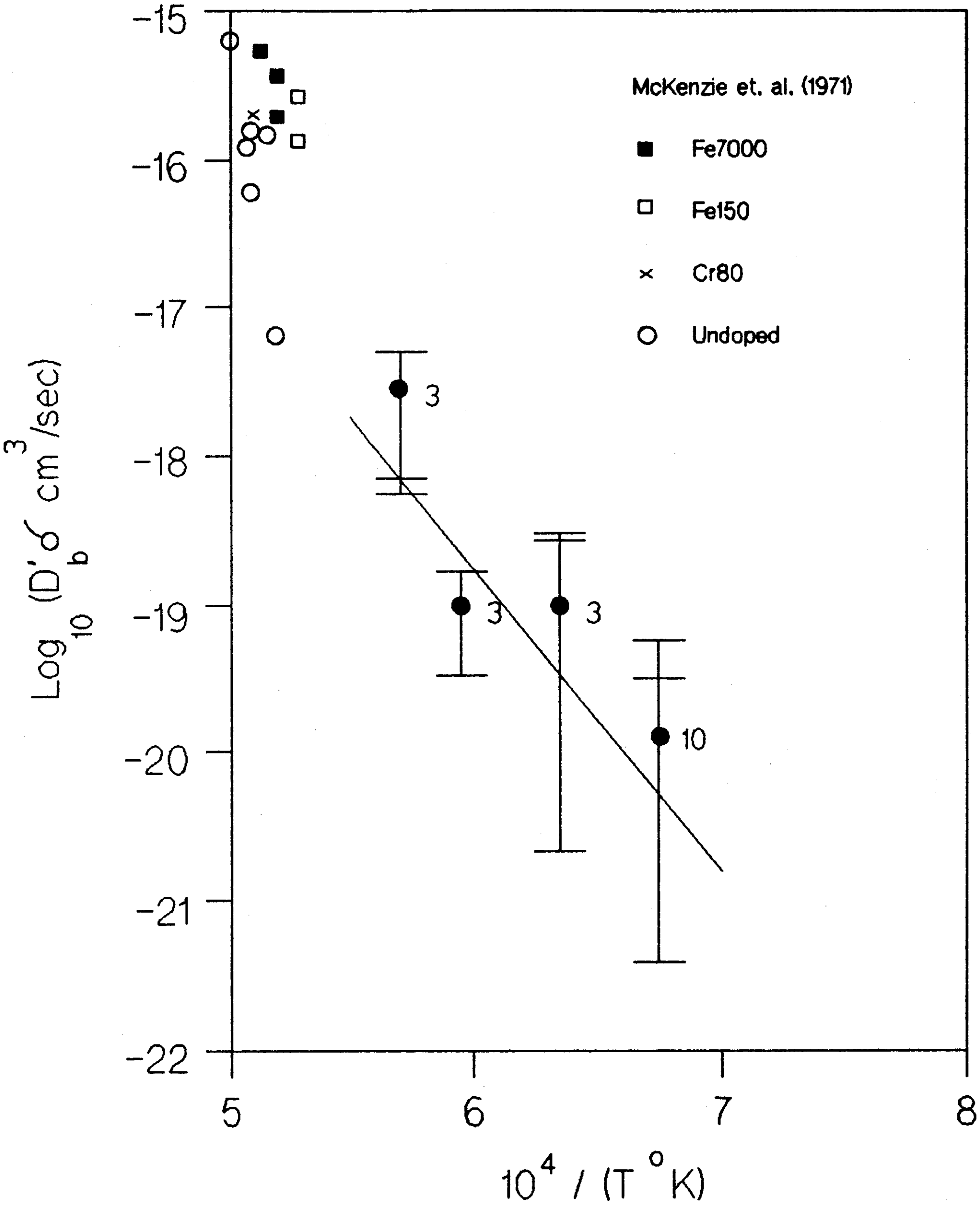

Fig. 20 Grain boundary oxygen diffusion parameter data of the present study with data of other authors. $D'_b\delta/D$ data of McKenzie et. al. was multiplied by the bulk oxygen diffusion data of the present study to conform to plot format.

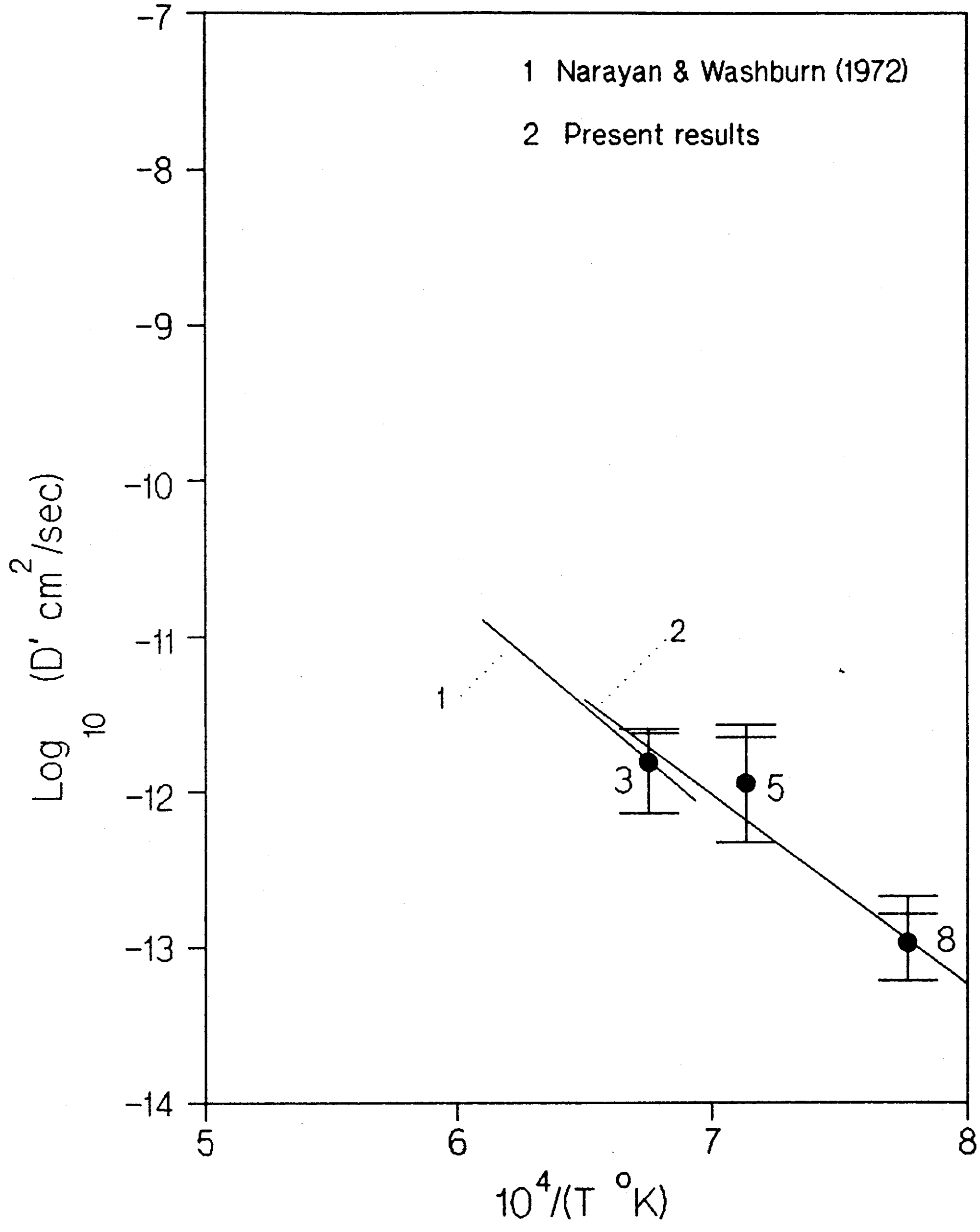

Fig. 21 Very short diffusion time (Type "C") data for undoped Oak Ridge, Norton, and MIT MgO. Samples with grain boundaries could not be distinguished from samples without grain boundaries. The data of Narayan and Washburn is also shown on the figure. It was obtained by TEM of dislocation loop shrinkage after successive heat treatments of a loop connected to the surface by a screw dislocation.

types of samples, error bars larger than the sample ranges shown may be more realistic, but the data are plotted using the same conventions used in other plots and described in section 5.2. From the regression line on the plot the following equation was solved.

$$D' = 3.57\times10^{-4}\ \exp\left(\frac{-2.43\ \text{eV}}{kT}\right) \qquad 1013\text{-}1209\,^{\circ}\text{C} \qquad (5.4)$$

This equation should be considered approximate due to the very narrow temperature range studied (200 °C) and the method used to calculate D' (Equation 4.13). Also shown in Figure 21 is the data of Narayan and Washburn[27] for diffusion in a screw dislocation. Their data agrees very well with that of the present study.

Dislocation densities were calculated from diffusion tail intercepts using equation 3.10 and as described in section 4.4. Table 6 lists the average calculated dislocation densities of intermediate diffusion time samples. These calculated dislocation densities are higher than the dislocation densities measured by etch pits (Table 4). Etch pits do not show all dislocations intersecting the surface,[59] and the many dislocations which are in grain boundaries are not counted in the etch pit density. Except for the Oak Ridge samples deformed 55%, the calculated dislocation densities exhibit the expected trend of being higher as the samples are deformed more. Also listed in Table 6 is the average area under the diffusion tails on the the $\log_e (C-.00204)$ vs channel number plots. More dislocations and grain boundaries will increase the amount of diffusant due to these paths and should increase the tail area. Except for the Oak Ridge sample deformed 55%, calculated areas follow the expected trend of greater area for more deformation.

Table 6

Dislocation Densities and Tail Areas Calculated from Diffusion Profiles

Sample Source	True Strain	Average Calculated Dislocation Density	Average Area Under Tails*
Oak Ridge	0%	1.99×10^{9} cm^{-2}	0.860×10^{-3}
"	6	4.53×10^{9}	2.20×10^{-3}
"	55	3.95×10^{9}	1.58×10^{-3}
Norton Co.	62	8.64×10^{9}	3.24×10^{-3}

*Areas were calculated for intermediate diffusion time samples using

$$\text{Area} = \frac{-\exp(b)\ p}{m\ (\#CN)}$$

where b = diffusion "tail" intercept
m = diffusion "tail" slope
p = calculated sputter pit depth, µm
#CN = total number of channels

The slope and intercept were calculated by linear regression. The pit depth and channel number had to be included so that the slope m for each sample would be based on the same x axis scale. Six to ten samples were used for each average. The same samples were used as those used to calculate the average dislocation density.

5.4 OXYGEN DIFFUSION IN Fe, Ca, Na, Ni DOPED MgO

In this section Fe, Ca, Ni and Na doped diffusion data are compared to undoped diffusion data. Ranges and standard deviations for doped samples are not shown to eliminate confusion. Only the type of dopant and number of SIMS samples is shown next to the mean of those samples. Fe and Ni doped samples were Spicer 4N crystals with 310ppm Fe and 370ppm Ni, respectively. No doped polycrystals were supplied by Carol Hadnwerker. Ca doped samples were deformed Oak Ridge single crystals annealed 22 days at 1400 °C in MgO powder doped with 2600 mole ppm Ca (see Section 4. 1).

Figure 22 contains data for doped MgO. Ni, Fe, and Ca have little effect on bulk diffusion. From only 2 samples, one cannot make conclusions about Na doped material. The Na doped samples were different than the others. They were small, curved, polycrystalline flakes.

Figure 23 contains oxygen diffusion in dislocation data for Fe, Ni and Ca doped MgO. There is no effect of these dopants within the observed experimental error.

Figure 24 contains oxygen diffusion in grain boundary data for Fe, Ni, Ca and Na doped MgO. There is no effect of Fe, Ni, Ca within the observed experimental error. Na may have an effect, but one cannot base conclusions on only two samples, especially since their polycrystalline structure of relatively large grain size was different from the other samples.

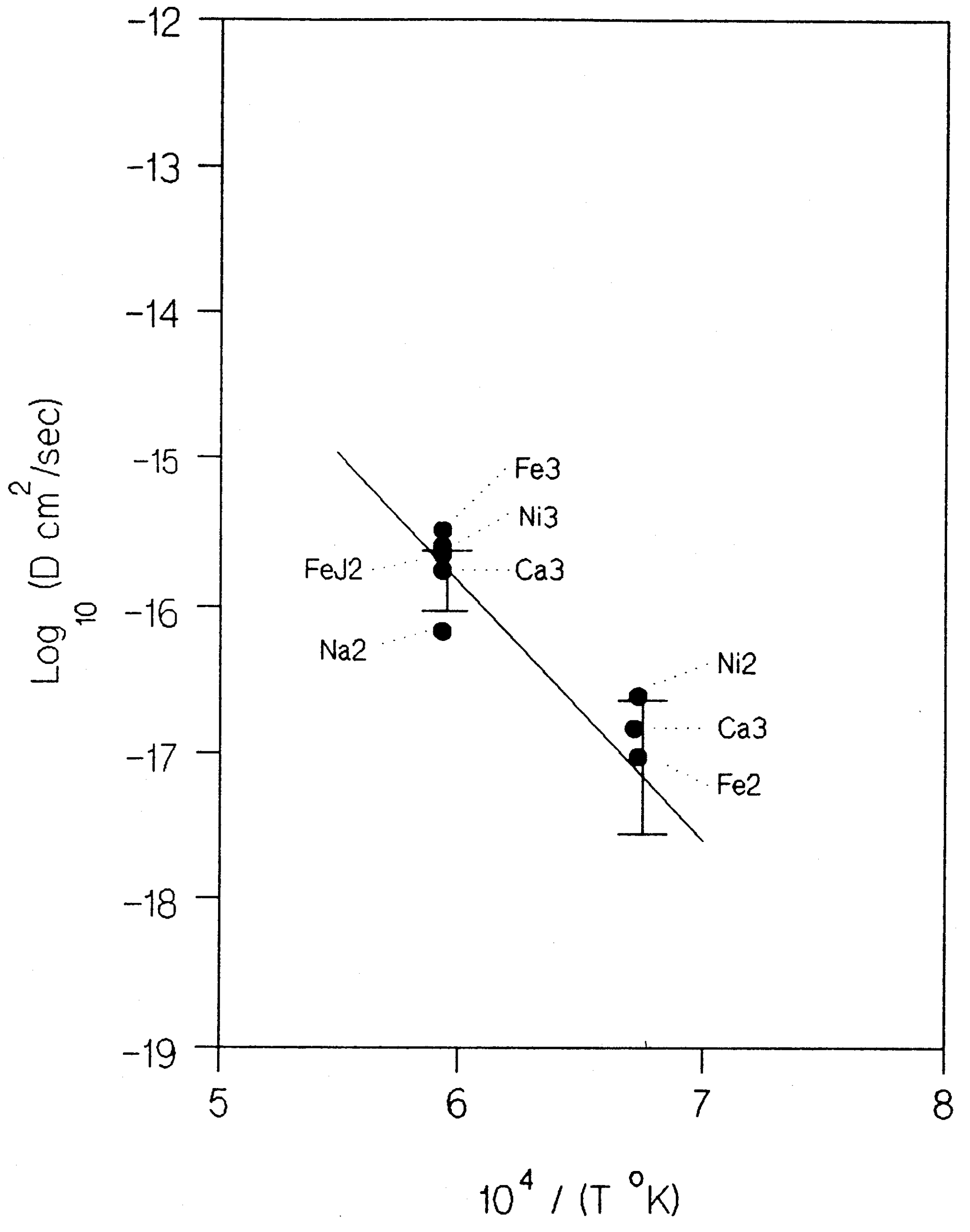

Fig. 22 Bulk diffusion in doped samples. Dopant and number of SIMS samples shown next to each mean. The ranges shown are for undoped samples (see Figure 15). FeJ refers to Fe doped samples supplied by Y. Oishi.

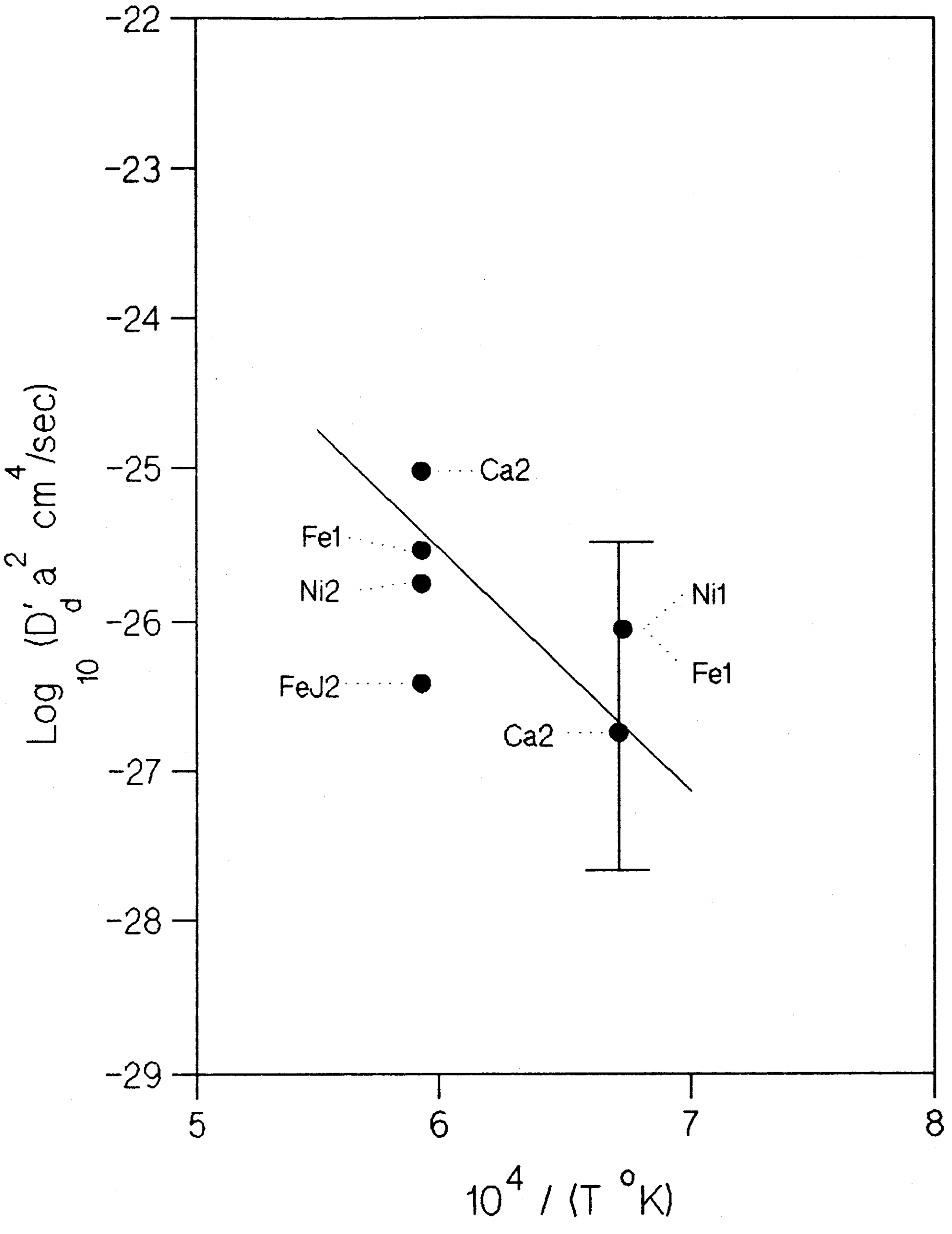

Fig. 23 Dislocation diffusion in doped samples. Dopant and number of SIMS samples shown next to each mean. The range shown is for undoped samples (see Figure 17).

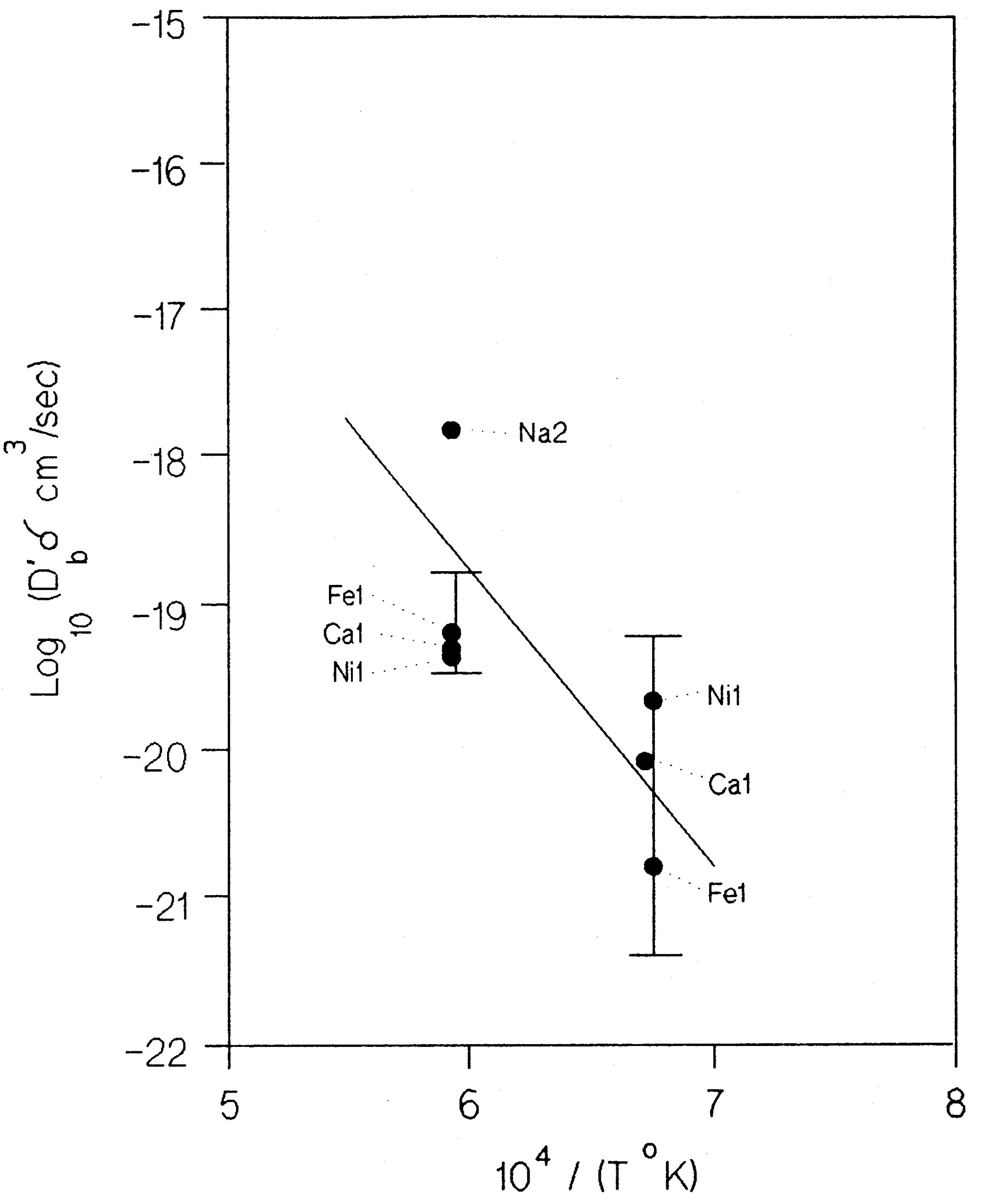

Fig. 24 Grain boundary diffusion in doped samples. Dopant and number of SIMS samples shown next to each mean. The ranges shown are for undoped samples (see Figure 19).

5.5 EVIDENCE OF Si CONTAMINATION

Even though precautions were taken to keep samples clean, all samples exhibited a Si signal which was highest at the specimen surface and then decreased as sputtering proceeded. The Si signal was monitored as an indicator of contamination as Si is particularly easy for the SIMS to detect. The Si signal cannot be converted to a concentration unless standards are made and tested. This is because Si and Mg may sputter differently. Even then surface contamination can overwhelm the actual bulk concentrations.

Figures 25, 26, and 27 are three raw data examples plotted as log # of counts versus channel number. Three distinct behaviors can be seen, each differently correlated to the O-18 signal. Figure 25 shows the raw data for an undeformed Oak Ridge single crystal. Its Si signal is confined to a shallower depth than the oxygen-18 bulk diffusion profile. Figure 26 shows the raw data for an MIT polycrystalline sample. All polycrystals had very large, very deep Si signals. These figures show that more processing steps (deformation, powder preparation and sintering) introduce more Si. Figure 28 shows the raw data for an Oak Ridge sample deformed 55%. Its Si signal extends much deeper than the oxygen-18 bulk diffusion profile. The Si signal also rises and falls. Perhaps this is due to precipatates containing Si. The effect of Si on oxygen diffusion cannot be well correlated with diffusion coefficients calculated from this data.

There are many possible sources of this contamination signal, including the as received Si concentration of 20ppm (Table 2), which may be segregating to the surface.

```
1  MASS=12  TIME(sec)=1  OFFSET(volts)=0
2  MASS=16  TIME(sec)=2  OFFSET(volts)=0
3  MASS=18  TIME(sec)=2  OFFSET(volts)=0
4  MASS=28  TIME(sec)=1  OFFSET(volts)=0
```

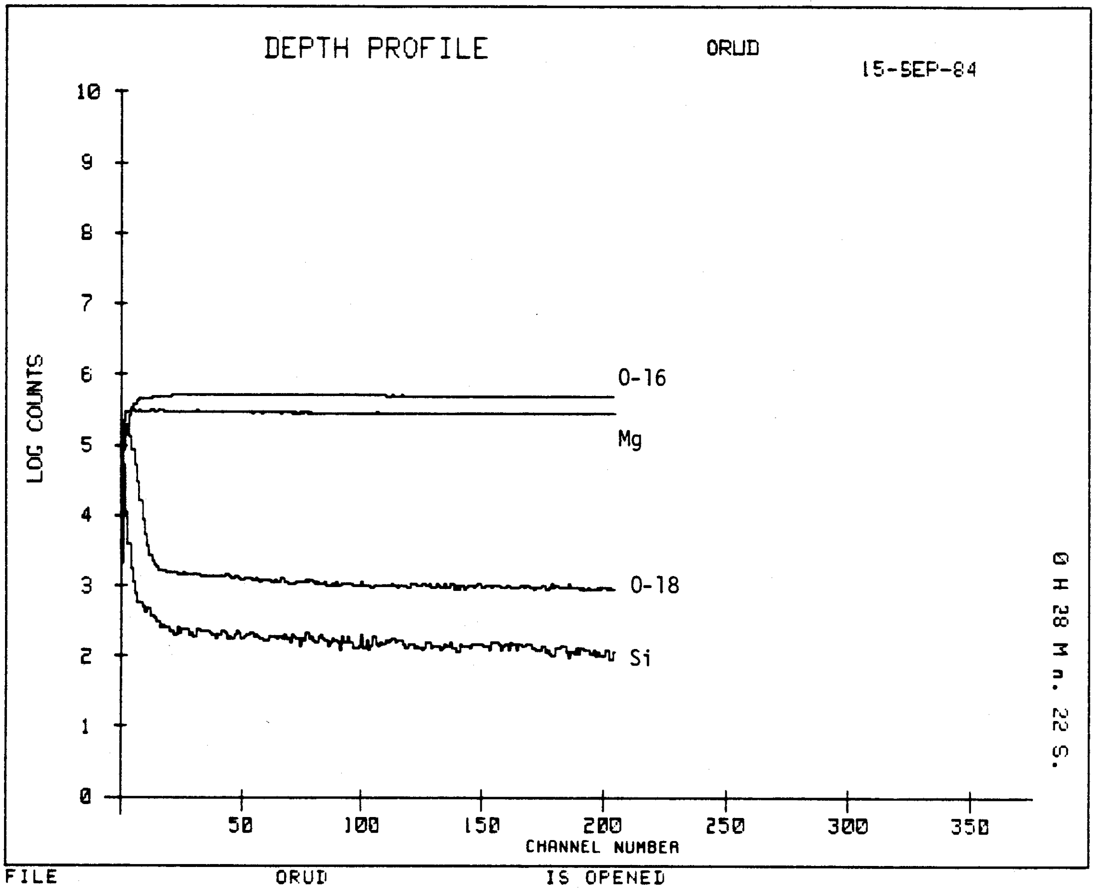

```
FILE                 ORUD                IS OPENED

                    MEASUREMENT CONDITIONS
SAMPLE REFERENCE: ORUD               DATE: 15-SEP-84
PRIMARY POLARITY: +    SECONDARY POLARITY: +
PRIMARY CURRENT: 8.23E-07 Amps.
PRIMARY VOLTAGE:  9.65  Kv.
RASTER:  500  Microns
IMAGE FIELD:  150  Microns
```

Figure 25. SIMS raw data for an undeformed Oak Ridge sample. Diffusion anneal 1210 °C, 64680 sec. Calculated sputter pit depth 0.72μm. SIMS analysis area 60μm diameter circle.

```
1  MASS=12  TIME(sec)=1  OFFSET(volts)=0
2  MASS=16  TIME(sec)=2  OFFSET(volts)=0
3  MASS=18  TIME(sec)=2  OFFSET(volts)=0
4  MASS=28  TIME(sec)=1  OFFSET(volts)=0
```

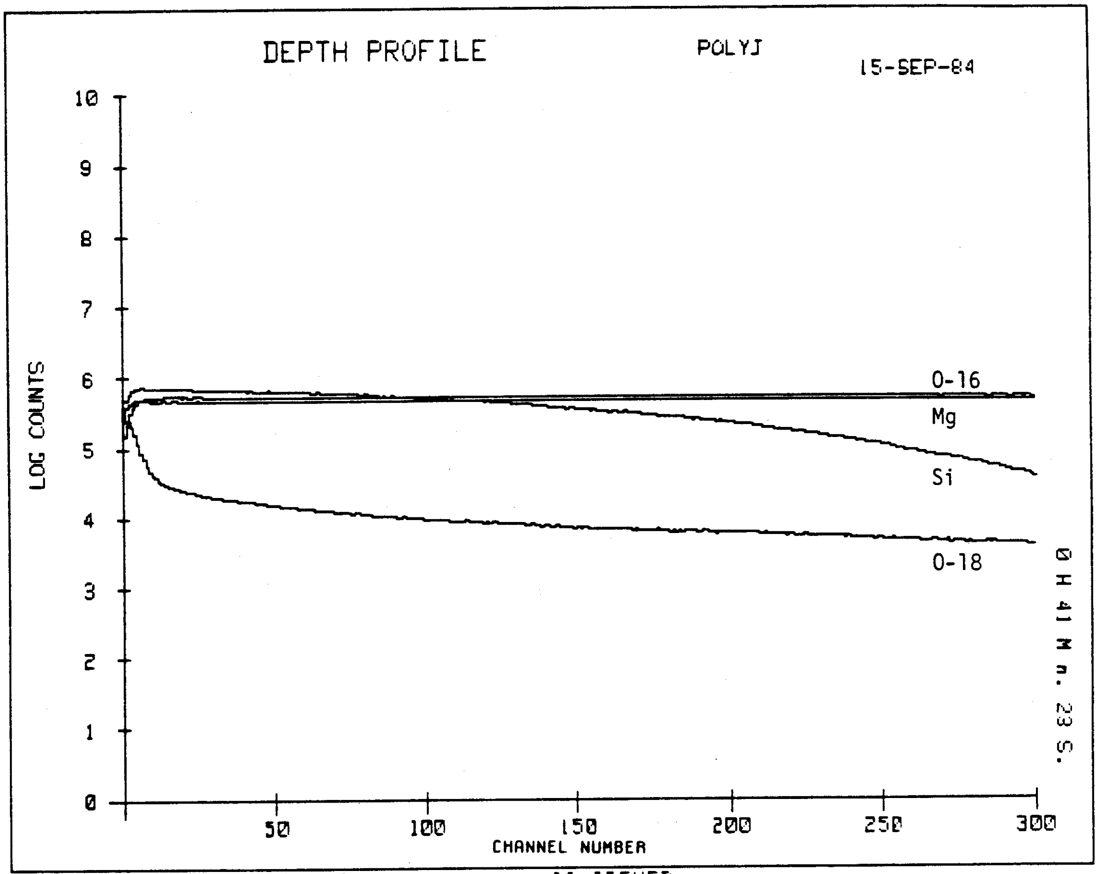

```
FILE                POLYJ                IS OPENED

                     MEASUREMENT CONDITIONS
SAMPLE REFERENCE: POLYJ                   DATE: 15-SEP-84
PRIMARY POLARITY: +    SECONDARY POLARITY: +
PRIMARY CURRENT: 8.54E-07 Amps.
PRIMARY VOLTAGE:   9.7  Kv.
RASTER:   500  Microns
IMAGE FIELD:   150  Microns
```

Figure 26. SIMS raw data for an MIT polycrystalline sample. Diffusion anneal 1304 °C, 40140 sec. Calculated sputter pit depth 1.05µm. SIMS analysis area 60µm diameter circle.

```
1  MASS=12  TIME(sec)=1  OFFSET(volts)=0
2  MASS=16  TIME(sec)=2  OFFSET(volts)=0
3  MASS=18  TIME(sec)=2  OFFSET(volts)=0
4  MASS=28  TIME(sec)=1  OFFSET(volts)=0
```

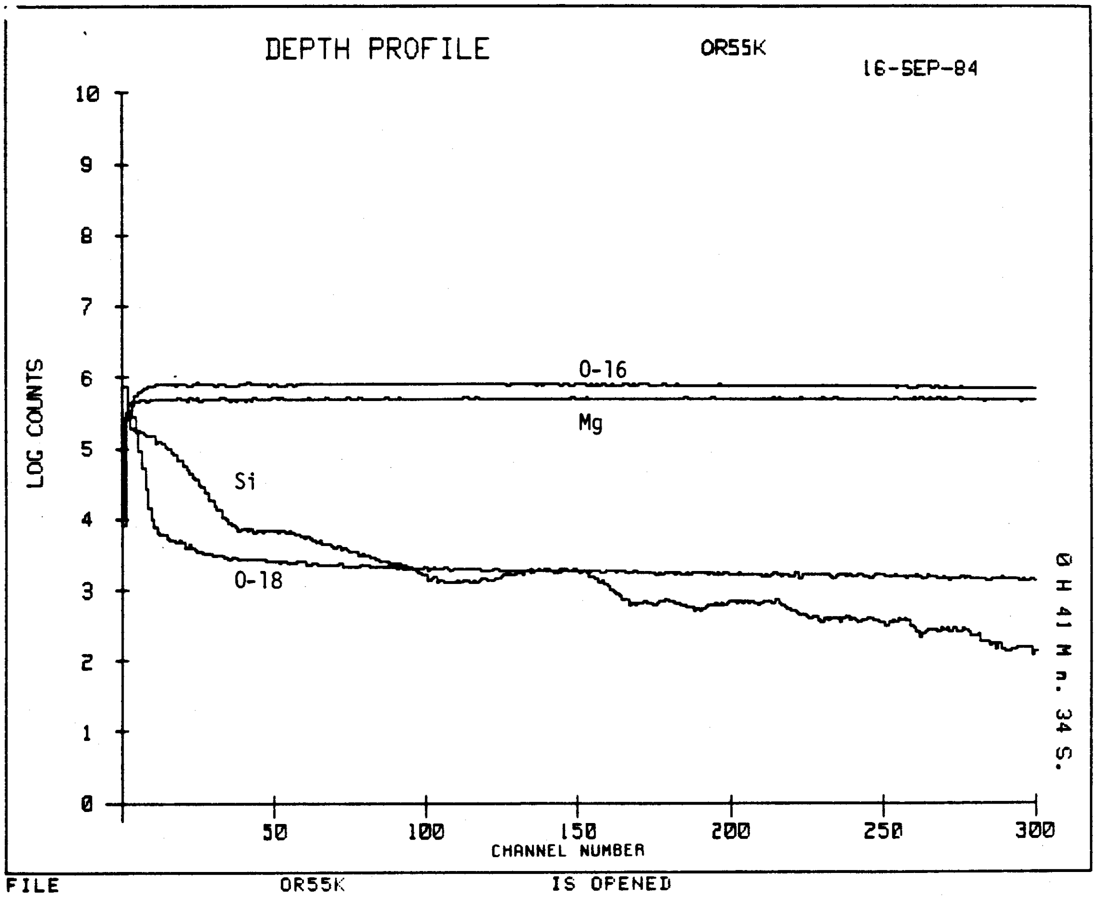

```
FILE                    OR55K                IS OPENED

                        MEASUREMENT CONDITIONS
SAMPLE REFERENCE: OR55K                    DATE: 16-SEP-84
PRIMARY POLARITY: +     SECONDARY POLARITY: +
PRIMARY CURRENT: 8.37E-07 Amps.
PRIMARY VOLTAGE:  9.67  Kv.
RASTER:  500  Microns
IMAGE FIELD:  150  Microns
```

Figure 27. SIMS raw data for an Oak Ridge single crystal deformed to 55% true strain. Diffusion anneal 1486 °C, 2755 sec. Calculated sputter pit depth 1.04µm. SIMS analysis area 60µm diameter circle.

We know that 99.8% Al_2O_3 furnace tubes can cause severe Si contamination as well as high surface evaporation (Figure 8). Other very common sources are solid, liquid or vapor particles suspended in the air. These come from such sources as kicked up dust, vaporization from silicones such as diffusion pump oils or sealants or high temperature gaskets. Even pure carbonaceous material such as rubber gaskets or pure virgin polyethylene contain Si as a major contaminant. (Qualitative spectrographic analysis ((at MIT by Walter Correia)) also showed Mg Al and Ca both on the surface and in the bulk of new VWR Van Lab Poly gloves.) Silicon may even be introduced on the sample surface just before or during SIMS analysis.

Although some of the following Si data appears diffusional it also can be due to surface or grain boundary segregation, or discreet surface contamination particles. These can be on or penetrating the surface (Figure 8). They can even be in the bulk of the material but segregated at all grain boundaries (Figure 7). Even if these profiles are evidence of Si diffusion, the boundary conditions, diffusion time and temperature would not be simple because Si could be introduced and diffuse during deformation, sintering, equilibration pre-annealing or during the diffusion anneal.

5.6 OXYGEN DIFFUSION IN SEVERELY CONTAMINATED UNDOPED MgO

This section contains oxygen-18 diffusion results for undoped Oak Ridge MgO. Diffusion anneals were performed in a McDanel 998 Al_2O_3 furnace tube which produced silicon containing lumps on the MgO surface as well as making the surface very rough, probably due to evaporation (see Figure 8).

Figure 28 contains bulk oxygen diffusion results for contaminated samples superimposed upon uncontaminated sample data. It is seen that contamination can produce a higher measured bulk diffusion coefficient. This may not be a result of enhanced diffusion in MgO but a result of $Si(O-18)_x$ or a related specie condensing on the MgO surface and increasing the amount of oxygen-18 transferred from the gas phase to the solid phase. The time dependence of the measured diffusion coefficient could be due to surface evaporation of Mg(O-18) or whichever specie is evaporating and producing the rough MgO surface.

Figure 29 contains dislocation diffusion results for contaminated Oak Ridge samples. One can see that the means fall within the experimental range of the 1200°C data (marked "11") whether that range is taken at 1200°C or moved up the regression line to the same temperature as the contaminated samples. One can conclude that there is no effect of contamination on dislocation diffusion, but these results must be interpreted with caution. A second phase silicate containing oxygen-18 may be diffusing or flowing down dislocations or grain boundaries. Sample surface evaporation may also distort results.

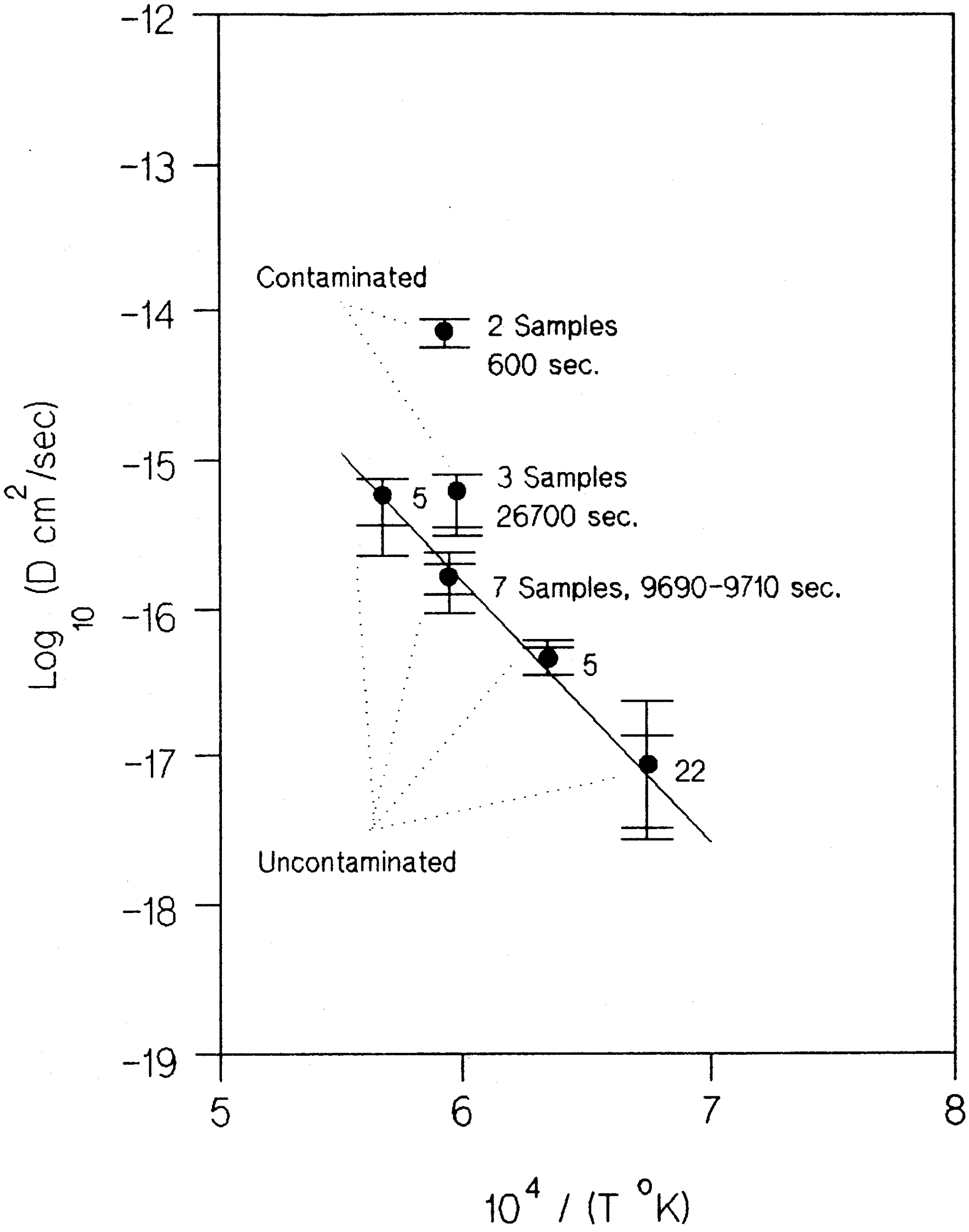

Fig. 28 Bulk oxygen diffusion data of contaminated, undoped Oak Ridge MgO. Results are superimposed on uncontaminated sample data. Diffusion anneal time is also shown on the figure.

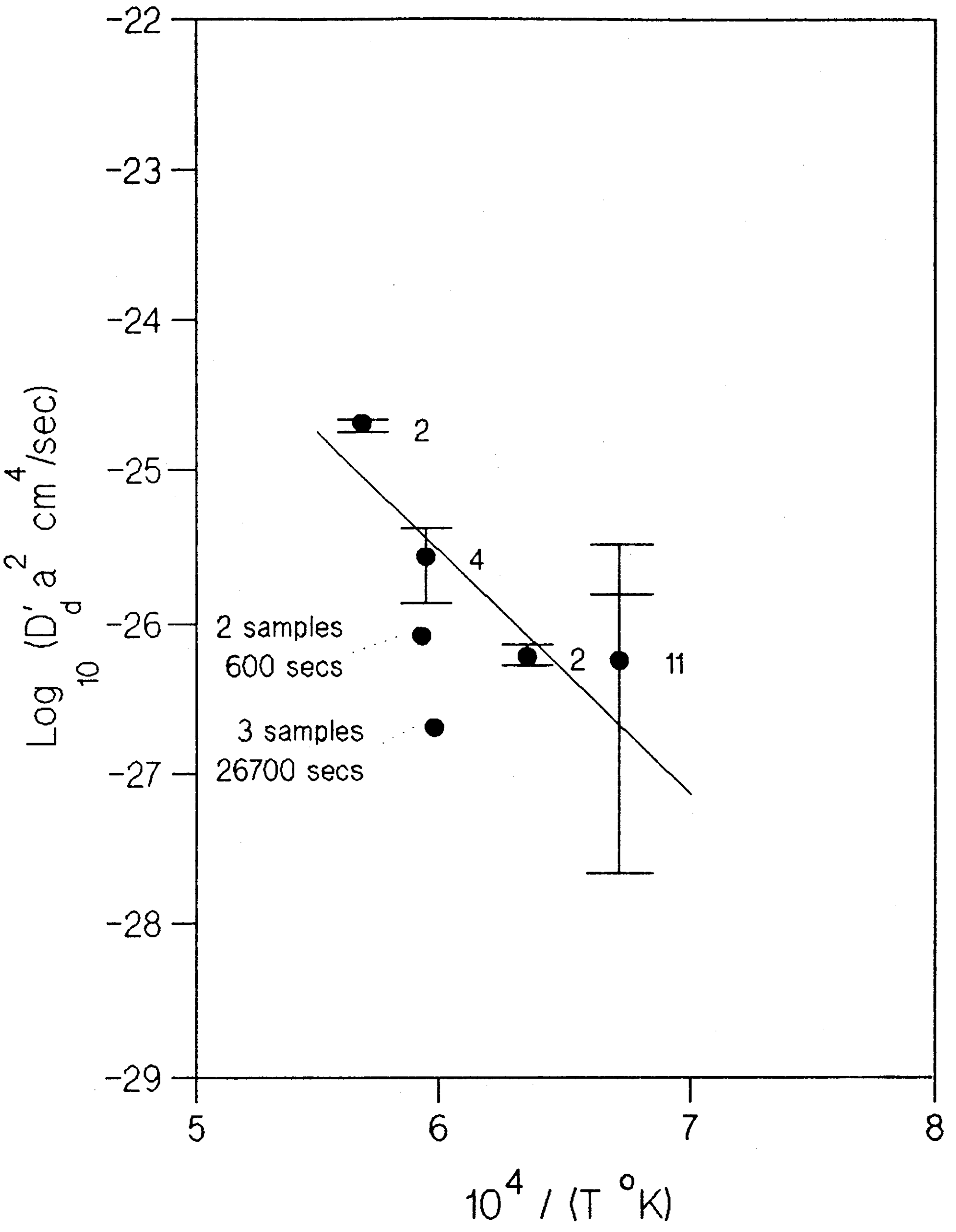

Fig. 29 Oxygen diffusion in dislocations in contaminated undoped Oak Ridge samples. Results are superimposed on uncontaminated sample data. Only means of contaminated sample data are shown for clarity. Diffusion anneal times are also shown on the figure.

6.0 DISCUSSION

6.1 OXYGEN DIFFUSION IN MgO

The data of this study for undoped MgO is weighted in favor of the purer Oak Ridge material. Out of the 77 data used in making Figures 15, 17 and 20, and calculating the equations for D, $D'_d a^2$ and $D'_b \delta$ (equations 5.1, 5.2 and 5.3), 53 data came from samples made from one Oak Ridge single crystal (Figure 2). However, no consistent difference was observed between data from Oak Ridge samples and data from other samples.

It is difficult to determine the mechanism for bulk oxygen diffusion in MgO. Table 7 lists various possible defect control regimes and the calculated activation energies for oxygen bulk diffusion which would result using the calculated enthalpies from Table 3. Intrinsic Frenkel defects are unlikely due to their high formation energies. Intrinsic Schottky vacancies are unlikely due to their high formation energy and the low purity of currently available MgO (section 2.2). Vacancies caused by monovalent impurity domination are unlikely due to the high Si, Fe and Al impurity levels in MgO (section 2.2). The anion vacancy concentration due to trivalent or quadravalent impurity domination are all very low because these impurities depress the oxygen vacancy concentration. It is apparent that all of the theoretically calculated enthalpies except the unlikely case of monovalent impurity domination are too large to be in agreement with the experimental value of 3.45 eV found in this study.

Oishi and Ando[6] have suggested that the vacancy pair mechanism is operative. The concentration of this defect will be independent of impurity concentration. Agreement between their data and this mechanism depends

Table 7

Possible Diffusion Mechanisms

Diffusing Specie	Specie Concentration	Defect Structure	Diffusion activation energy calculated from Table 3 eV
$O_i^{\circ\circ}$	$\exp\left(\frac{-H_f}{2kT}\right)$	Intrinsic Frenkel	$1/2H_f^F+H_m^i=7.4-10.2$
$V_O^{\circ\circ}$	$K_s^{1/2}=\exp\left(\frac{-H_s}{2kT}\right)$	Intrinsic Schottky	$1/2H_s+H_m^a=6.0-6.1$
$V_O^{\circ\circ}$	$[F'_{mg}]$	Schottky with monovalent impurity domination	$H_m^a=2.1-2.4$
$V_O^{\circ\circ}$	$\frac{2}{[F_{mg}^{\circ}]}K_s$	Schottky with substitution trivalent impurity domination	$H_s+H_m^a$ 9.8-9.9
$V_O^{\circ\circ}$	$\frac{K_s}{[F_{mg}^{\circ\circ}]}$	Schottky with substitutional quadravalent impurity domination	$H_s+H_m^a=9.8-9.9$
$V_O^{\circ\circ}$	$\frac{K_s}{2[F_i^{\circ\circ\circ\circ}]}$	Schottky with interstitial quadravalent impurity domination	$H_s+H_m^a=9.8-9.9$
$(V_O^{\circ\circ}V''_{mg})^X$	$K_s\ K_{association}$	this associate independent of defect structure	$H_s+H_f^p+H_m^p=7.2-7.9$

upon their experimentally determined activation energy of 5.6 eV to be correct and the calculated Schottky energy of 7-8 eV to be incorrect. Using their oxygen bulk diffusion activation energy value of 5.6 eV, association energy of -2.67eV and motion energy of 2.47eV (see Tables 3 and 7), they solve for a Schottky defect formation energy of 5.8 eV. This disagrees with most recent calculations of the Schottky defect formation energies in Table 3. However, Mackrodt[67] has stated that an activation energy of 5.5eV is not incompatible with theoretical calculations. Using Oishi and Ando's Schottky energy of 5.6eV and their association energy of -2.67eV (see Table 3), the concentration of vacancy pairs

$$[(V_O^{\circ\circ}\ V_{Mg}'')^{\times}]=SZ\ \exp\left(\frac{-(H_s+H_p^f)}{kT}\right) \tag{6.1}$$

where Z is the number of ways a vacancy pair can orient itself in the lattice

and S is an entropy factor assumed to be unity

would be $10^{-6.56}$ or 0.3ppm at 1700°C if Z=12. Even though this is very low, it is higher than intrinsic or impurity controlled free vacancies. Their diffusion activation energies of 2.2eV (1300-1500°C) and 5.6eV (1500-1750°C) disagree with the activation energy found in this study, 3.45eV (1200-1500°C) as well as the activation energy of Yoo[19], 3.24eV (1000-1650°C). They argue that their high temperature diffusion coefficient is intrinsic and their low temperature diffusion coefficient is extrinsic and structure sensitive. However the data of Yoo[19] does not shift to a high temperature intrinsic region even though Yoo's epitaxially grown MgO probably has a lower dislocation density than the arcfusion Norton and Oak Ridge MgO used by Oishi. In fact, Yoo's diffusion coefficient is lower than that of Oishi et. al.[5] (number 2 in Figure 1). If one is measuring intrinsic diffusion, the measured diffusion coefficient should be the lowest. The disagreement in activation energies at lower temperatures is puzzling. One would expect the activation energies to agree at lower temperatures. If the data of Oishi and Ando[6] is not broken up into high temperature and low temperature regions, the activation energy would agree with those of Yoo[19] and the present study. Even in view of the above discussion, the vacancy pair mechanism is more plausible than any others proposed, due both to its higher concentration than other possible defects and the impurity insensitiviy of oxygen diffusion observed by Ando et. al. [7] and the present author.

The difficulty of determining the diffusion mechanism of oxygen in MgO may be due to an overly simplistic view of the defect structure of MgO. Crawford[68] has stated that the only stable charge states for an oxygen vacancy are neutral (F center = $V_O^{\circ\circ} + 2e'$) or singly positive. Cation vacancies would also be singly charged. This would lower both the Schottky and anion Frankel defect formation energies as well as defect migration energies[68]. Taking electrons away from charged oxygen would decrease its effective radius. Carbon and hydrogen are known[69] to exist in MgO but are usually ignored in high temperature studies on the assumption they diffuse out readily. Perhaps they affect the high temperature defect structure more than has been thought. We have no idea how chlorine or nitrogen might behave in MgO. A specie no one has considered might even be responsible for oxygen diffusion.

The mechanism responsible for dislocation or grain boundary diffusion is as difficult to determine as for bulk diffusion. Kroger[70] has found no increase in electrical conductivity in Al_2O_3 due to grain boundaries, leading him to suggest that the neutral oxygen interstitial is responsible for oxygen diffusion in Al_2O_3 grain boundaries. This contrasts with metals where the vacancy mechanism is usually responsible for enhanced dislocation[1] and grain boundary[71] diffusion. The interstitial mechanism is not so improbable when one considers the relative openness of ceramic grain boundaries compared to metals[72], due both to vacant sites[73] and expansion of the lattice at ceramic grain boundaries[74]. A plausible form of an interstitial specie is a neutral oxygen interstitial with loosely associated electrons in the positive space charge region of MgO grain boundaries with Si, Fe and Al impurities. Another possibility is a neutral oxygen interstitial that has left two electrons in an oxygen vacancy (F center). If the grain boundary core has oxygen vacancies in it, the electrons may stay near the oxygen interstitial but be associated with oxygen vacancies. Or perhaps, an oxygen vacancy with associated electrons (F center) is the diffusing specie.

The data of this study shows that Fe, Ca, Ni and Na have no effect on oxygen diffusion in MgO. Also, no difference was observed among Oak Ridge, Norton, and MIT samples, which have different impurity contents (Table 2). This is the same result as Ando et. al.[7] who found no effect of Fe in the 1400-1700°C range, even up to 12900ppm. Henriksen et. al.[18] found no effect at 500 or 1400ppm Sc at 1400°C. This may be due to the fact that all MgO has enough Fe, Al, Si and other multivalent impurities to control the defect structure and make oxygen diffusion extrinsic (Table 2). As received material can only get more contaminated during experiments. Since as received impurities segregate to surfaces and grain boundaries in MgO[75], it is not surprising that additional dopants have no effect on grain boundary and dislocation diffusion in this study. Si and Ca, both major impurities in MgO (Table 2), segregate more strongly than other impurities[76] and may dominate grain boundary and dislocation diffusion in MgO. Extremely pure MgO has probably not been made yet and would be difficult to keep pure. However it would be necessary to study the effects of individual multivalent dopants. Current MgO can be used to study the affect of monovalent impurities such as Li and Na if the Li and Na chemical potential is controlled in the diffusion zone. The very fast redox kinetics in Li doped MgO[33] may be due to rapid Li diffusion to the sample surface where it can evaporate.

The activation energies for dislocation and grain boundary oxygen diffusion are the same as the activation energy for bulk oxygen diffusion within the experimental error.

Bulk	3.45±.17 eV
Dislocation	3.20±.58 eV
Grain Boundary	4.06±.78 eV

The large error range for the grain boundary activation energy indicates it may be the same as the bulk activation energy and not higher. In fact, the range of the bulk activation energy falls completely within the ranges of the dislocation and grain boundary activation energies. One must keep in mind the large errors associated with the measured activation energies. The stated error ranges are for 68% confidence based on a real, not estimated, calculated internal error.[*] There is therefore a 42% chance that the actual value for the activation energies are outside the stated ranges, a 21% chance that they are lower than the stated ranges.

To improve the confidence interval to 95%, multiply the standard deviation by two. If we do this to the grain boundary and dislocation diffusion activation energies, and assume the bulk energy is 3.45eV, there is a 2.5% chance that the activation energy for dislocation diffusion is less than 60% of the activation energy for bulk diffusion. Similarly there is a 2.5% chance that the activation energy for grain boundary diffusion is less than 72% of the

---

[*] Theoretically all calculations of errors are estimates until we approach an extremely large number of samples. The errors of this study are based on the theoretical equations of Section 3.2, and not arbitrarily or logically estimated from raw or intermediate data. The errors are true internal errors based upon a statistically significant number of diffusion coefficients or grain boundary/dislocation parameters.

activation energy for bulk diffusion.

The result that the activation energies for dislocation and grain boundary diffusion are similar to the activation energy of bulk diffusion is very different than results for metals[1,2] or for cations in ceramic systems[3]. Activation energies lower than bulk activation energies were found for Ni grain boundary diffusion in MgO grain boundaries with precipitates containing Ca and Si[77], for Cr grain boundary diffusion in MgO[39], and for Ni grain boundary diffusion in NiO[78]. Chen and Peterson[79] found similar activation energies for grain boundary and bulk diffusion of both Co and Cr in NiO, but this disagrees with the results of Atkinson and Taylor[80] for Co diffusion in NiO. The difference between the present anion results and others' cation results may be due to their difference in size. The boundary and associated space charges may be primarily due to changes in the cation sublattice while the anion sublattice remains relatively constant. The large size of the oxygen anion may make grain boundary and dislocation diffusion more difficult than for the smaller cation. It should be noted that similar activation energies among bulk, dislocation, and grain boundary diffusion does not necessarily mean that their mechanisms are the same.

The data of this study show that both the dislocation core radius as well as the grain boundary thickness should be measured in angstroms rather than microns. This is consistent with the dislocation diffusion data of Narayan and Washburn[26,27] as well as the grain boundary data of Holt and Condit[9]. In principle these can be measured by combining short time data for D'_d or D'_b with intermediate time data for $D'_d a^2$ or $D'_b \delta$ respectively. This has been done by Atkinson and Taylor for Ni diffusion in NiO where they found the dislocation core radius to be about 10 angstroms[55] and the grain boundary thickness to be 7 angstroms[78]. Figure 30 combines the bulk, dislocation, grain boundary, and very short time bulk diffusion data from undoped samples of this study, and graphically illustrates how the grain boundary and dislocation thicknesses were calculated. If the short time data used in this study is correct within a factor of 10, the core radius a and grain boundary thickness δ can be calculated as

$$\delta = .9^{+8}_{-.8}\ \text{Å} \tag{6.2}$$

$$a = 6^{+13}_{-4}\ \text{Å} \tag{6.3}$$

The data of this study also show that the magnitudes of the diffusion coefficients within the grain boundaries (D'_b) and within the dislocations (D'_d) to be similar. This is shown by the similarity of the very short time diffusion results for all samples. These results were all combined on Figure 21 and called D' because of their similarity. Also, if the dislocation diffusion data are treated as grain boundary diffusion data, the results agree with those of grain boundary diffusion samples. Similarly, if grain boundary diffusion data is treated as dislocation diffusion data, these results agree with the data from dislocation diffusion samples. However in both of these cases where data are treated in the "wrong" way, larger error scatter results than when the data are treated correctly. It should be noted that a difference may exist between dislocation and grain boundary oxygen diffusion but it may be lost within the experimental error.

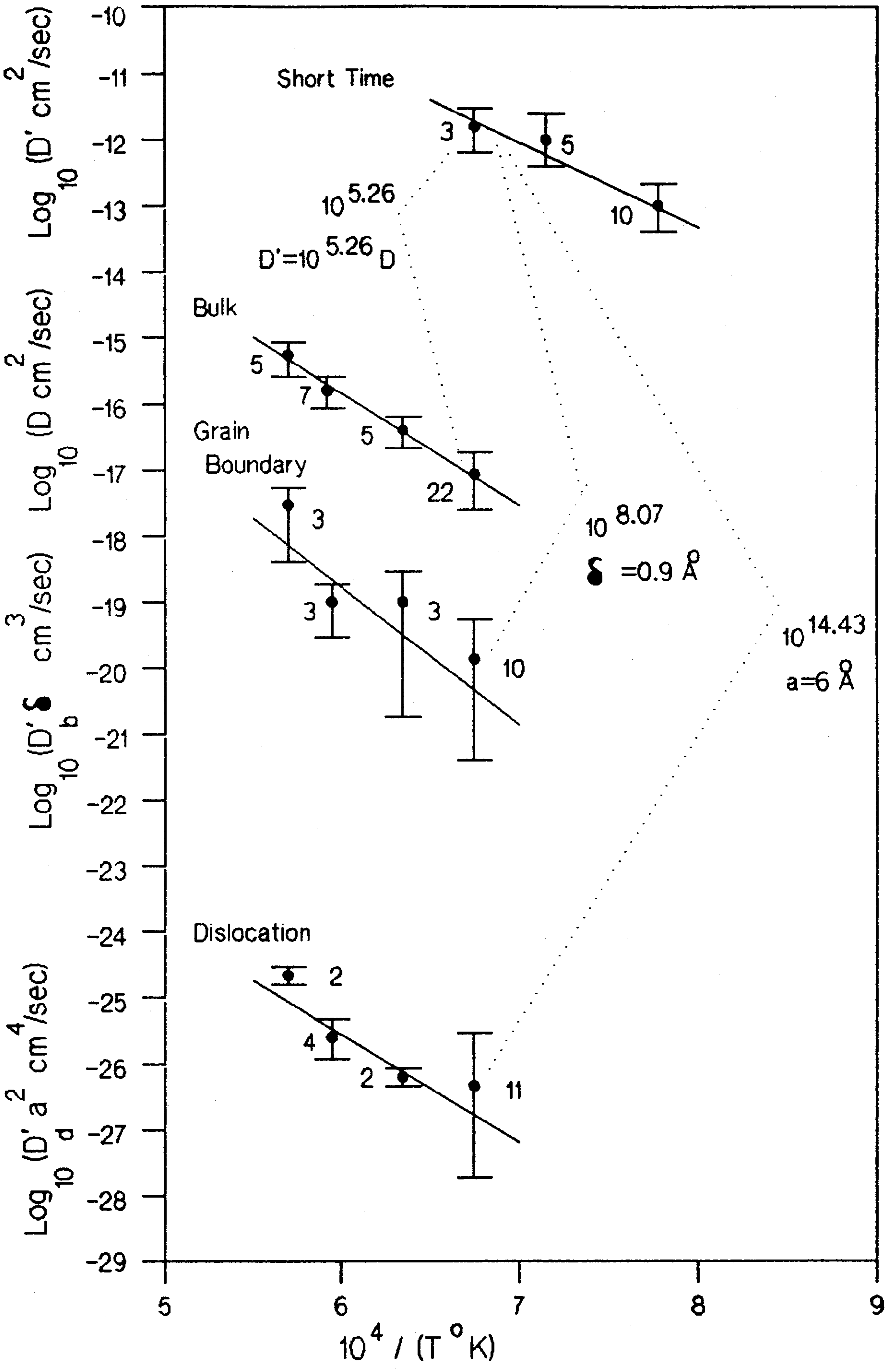

Fig. 30 Bulk, dislocation and grain boundary oxygen diffusion data in undoped MgO combined on one plot. Also shown are calculations based on the sample means indicated. Out of the 93 data used to make this plot, 62 came from SIMS profile data from samples made from one Oak Ridge single crystal. Measurement range is shown at each point.

No difference was observed among $D'_b\delta$ data from the different sample types. This was the case even though the Oak Ridge samples deformed 55% had clean low angle grain boundaries (Fig. 6), the Norton Company samples deformed 62% had low angle grain boundaries with precipitates (Fig. 7), and the MIT polycrystals had high angle grain boundaries. All of the boundaries probably had similar impurity segregation due to as received impurity levels (Table 2), so differences in total impurity content may not cause consistent differences in grain boundary diffusion behavior among samples. The lack of observable difference in $D'_b\delta$ data between low angle boundary samples and high angle boundary samples may mean both have similar transport properties. However, differences due to impurities or boundary type may be lost in the experimental error. These differences may even be the cause of the observed scatter.

The present results suggest that oxygen grain boundary or dislocation diffusion in MgO is slower than magnesium grain boundary or dislocation diffusion. The magnesium bulk diffusion data of Wuensch et. al.[81] for Norton and Spicer MgO, which is below that of others[81], is

$$D_{mg} = 4.19^{+2.45}_{-1.55} \times 10^{-4} \exp\left(\frac{-(2.76\pm.08\text{ eV})}{kT}\right) \text{cm}^2/\text{sec} \quad 1400\text{-}2400^\circ\text{C} \qquad (6.4)$$

When evaluated at 1209°C it is 1.73×10^{-13} cm^2/sec. The magnesium vacancy is responsible for magnesium diffusion and its bulk diffusion coefficient is

$$D_{V_{mg}} = (0.38\pm0.15) \exp\left(\frac{-(2.28\pm.21\text{ eV})}{kT}\right) \text{cm}^2/\text{sec} \quad 1200\text{-}1600^\circ\text{C} \qquad (6.5)$$

as determined by Sempolinski and Kingery[36]. At 1209°C its value is 6.74×10^{-9} cm^2/sec. At 1209°C the present study found the diffusion coefficient of oxygen in a dislocation or grain boundary, D', to be 9.42×10^{-13} cm^2/sec. This value is comparable to that of Wuensch et. al.[81] for magnesium bulk diffusion and much less than that of Sempolinski and Kingery[36] for magnesium vacancy bulk diffusion. If magnesium grain boundary and dislocation diffusion are faster than magnesium bulk diffusion, then they must be faster than oxygen dislocation or grain boundary diffusion. The dislocation and grain boundary diffusion parameters for magnesium, $D'_{d,Mg}a^2$ and $D'_{d,Mg}\delta$, must also be larger than the dislocation and grain boundary diffusion parameters for oxygen. This disagrees with creep and sintering data interpretations which imply the opposite[82]. This discrepancy between diffusion data and creep/sintering interpretation was also noted by Atkinson[3] in his review of diffusion in ceramic dislocations and grain boundaries.

Dislocation or grain boundary diffusion will increase the total amount of oxygen-18 exchange. If only the total amount of oxygen-18 exchanged is used to calculate a bulk diffusion coefficient, D, the result will be erroneously high. This will be especially true if diffusion times are relatively short and if excess dislocations are introduced by crushing the sample. This is probably one of the reasons for the disagreement between various authors in their measurements of oxygen bulk diffusion (Figure 1). This study determined D from bulk diffusion profiles in surface regions where the contribution from grain boundaries and dislocations was less than 2%. In some samples from short to intermediate time diffusion anneals, uptake due to dislocations and grain boundaries was about half of the total uptake. A factor of two increase in the total oxygen-18 uptake could easily increase a bulk diffusion coefficient calculated from the total uptake by a factor of 5-10 (see Crank[29]).

Another possible source of increased amount of oxygen-18 exchange (and hence errors if only this is used to calculate D) is contamination. The present study has found that a

99.8% Al_2O_3 furnace tube can contaminate the surface of MgO with silicon. This was probably from a volatile silicate from the grain boundary second phase in the furnace tube. When the silicate specie is gaseous, it can equilibrate its oxygen-18 concentration with the atmosphere. Then when it reacts with the MgO surface it will bring that oxygen-18 with it. Contamination from other sources could also increase the amount of oxygen-18 exchange. For example, the surface may become contaminated with something which has a higher diffusion coefficient than MgO. This could be a silicate from dust or some other source which can melt on the MgO surface at the diffusion anneal temperature. A second phase at grain boundaries or dislocations could also have a higher diffusion coefficient than MgO and increase the amount of oxygen-18 exchange. Since impurities tend to segregate to grain boundaries and dislocations, contamination, impurities, dislocations and grain boundaries can all combine to increase the total amount of gas exchange and may be the reason for the lack of agreement between various authors' bulk oxygen diffusion measurements (Figure 1).

The combined effects of contamination, dislocations and grain boundaries, especially for very short time diffusion suggest that the attempts of other authors to break up bulk diffusion log(D) vs 1/T curves into intrinsic high temperature and extrinsic (impurity or defects) low temperature regions may be incorrect. Curvature in Arrhenius plots can easily be caused by contamination or dislocation/grain boundary effects. This is especially apparent if one looks at Yoo's[19] bulk diffusion data obtained in a similar manner as the data in this study. He studied a wider temperature range than other authors. His data showed no tendency for curve break up. Even at high temperatures (1650°C) his data do not shift to a higher activation energy slope even though his data are lower than all other authors' measurements at this temperature. In fact, the only lower published bulk diffusion result is that extrapolated from Narayan and Washburn[12]. However they did not measure any diffusion profiles, their method was an indirect TEM one on relatively impure Muscle Shoals MgO (Table 2) subject to assumptions made as mentioned in the literature survey. Attempts of other authors to make their high temperature bulk diffusion data agree with that of Narayan & Washburn[12] by breaking up their log D versus $1/T\,^{\circ}K$ curve should be discouraged.

Some[83] have suggested that the reason why Narayan and Washburn's[12] bulk diffusion results are well below those of others is because of surface evaporation of others' samples. However, surface evaporation is probably not important in these measurements for several reasons. First, Yoo[19] performed both interdiffusion as well as gas exchange at 1100 °C and 1200 °C and the results agreed. Second, the data of this study and that of Yoo used very different diffusion times (those of Yoo were 7-32 times those of this study) which should result in different evaporation amounts, yet the present results agree with those of Yoo in pre-exponential factor, activation energy, and magnitude. (The present results are no lower than 0.4 times those of Yoo.) Third, the results of Narayan and Washburn[12] tend to agree more with those of others at higher temperatures. The opposite would be the case if evaporation was appreciable. Dislocation and grain boundary diffusion profiles should be relatively immune to evaporation even if it was happening.

In order to discuss sources of error in determining D, $D'_d a^2$, and $D'_b \delta$, it useful to reexamine equations 4.6,4.9, and 4.12 which were used to calculate those quantities.

$$D = \frac{1}{t}\left(2\,\frac{d\,\mathrm{erf}^{-1}(C')}{dCN}\,\frac{\#CN}{p}\right)^{-2}\ \mathrm{cm}^2/\mathrm{sec} \qquad (4.6)$$

t=diffusion anneal time
#CN=number of channels sputtered
p=calculated sputter pit depth

$$D'_d a^2 = A^2 D \left(\frac{d\ \ln(C-C_b)}{dCN} \frac{\#CN}{p} \right)^{-2} + Da^2 \quad cm^4/sec \qquad (4.9)$$

A=a constant approximately equal to 1
D=bulk oxygen diffusion coefficient
(calculated from equation 5.1)
a=dislocation core radius

$$D'_b \delta = 0.66 \left(\frac{d\ \ln(C-C_b)}{dCN^{1.2}} \frac{\#CN^{1.2}}{p^{1.2}} \right)^{-5/3} \left(\frac{4D}{t}\right)^{1/2} \quad cm^3/sec \qquad (4.12)$$

In order to calculate D from Equation 4.6 we must measure the diffusion time t, the slope $d\ erf^{-1}(C')/dCN$, the number of channels #CN, and the sputter pit depth p. There is no error in counting the number of channels and the error in measuring diffusion time is only a few percent or less, due mostly to uncertainty as to exact time the samples reach temperature. Therefore the major sources of error in calculating D are the error in measuring the slope and the error in measuring the sample pit depth. The relative slope errors, calculated by linear regression, ranged from 1% to 13% and averaged 3% for undoped MgO samples (Figure 15). The error in measuring pit depths was calculated by taking the ordinary sum of errors in the pit depth versus sputter time regression, or in other words, by applying Equation 3.21 to Equation 4.7. (The slope and intercept errors are not random and independent of each other so Equation 3.20 cannot be used.) The relative pit depth errors ranged from 10% to 26% and averaged 13% for undoped MgO samples (Figure 15). Therefore the major source of error in calculating D is in measuring the sputter pit depths. There may also be systematic error in the pit depth regression Equation 4.7 and this may be the reason why the present results are lower than Yoo's[19] by a factor of 1/2. (Yoo[19] measured pit depths in the same way as the present author but his epitaxially grown MgO surfaces were less smooth with less curvature than the present study's chemically polished surfaces.)

In discussing the sources of error in determining $D'_d a^2$ and $D'_b \delta$, it is useful to compare Equations 4.12 and 4.9 to Equation 4.6. It is interesting to note that the bulk diffusion coefficient D appears in Equations 4.9 and 4.12 for calculating $D'_d a^2$ and $D'_b \delta$, so that any error in D will add to the errors in $D'_d a^2$ and $D'_b \delta$. The value of D calculated from the linear regression of $\log(D)$ versus $1/T$ (Equation 5.1) was used in Equations 4.9 and 4.12. However, since the same value of D is used for all samples annealed at the same temperature, the value of D is not a source of observed experimental error. In a very similar manner as in Equation 4.6 for D, the major sources of error in calculating $D'_d a^2$ and $D'_b \delta$ are in measuring a slope and a sputter pit depth. (The term Da^2 in Equation 4.9 is insignificant in the present results.) In fact in all three Equations 4.6, 4.9, and 4.12, the slope and pit depths are weighted very similarly. The relative pit depth errors for undoped MgO averaged 14% and 12% for samples used to calculate $D'_d a^2$ (Figure 17) and $D'_b \delta$ (Figure 19) respectively. These errors are essentially the same as the 13% error for samples used to calculate D (Figure 15). The relative slope errors from linear regression results for calculating $D'_d a^2$ and $D'_b \delta$ were 5% and 3 % respectively. These are similar to or slightly higher than the 3% relative slope error for calculating D.

Considering the similarity of Equations 4.6, 4.9, and 4.12, this marginal increase in slope error does not account for the large increase in scatter in comparing D results (Figure 15) to $D'_d a^2$ (Figure 17) and $D'_b \delta$ (Figure 19) results. A contributing factor to this increased error is that grain boundary and dislocation diffusion models assume the grain boundaries and dislocations are perpendicular to the sample surface. The low angle grain boundaries in highly deformed samples tended to be perpendicular to the diffusion sample surface. In general, dislocations and grain boundaries are more or less randomly oriented. In the Oak Ridge sample deformed 6%, many of the free dislocations are glide dislocations which may have preferred orientations.

Nevertheless, the variability of dislocation and grain boundary diffusion results may indicate inherent differences in diffusion behavior among dislocations and grain boundaries. The sample taken by SIMS is very small; basically a 60µm diameter by 1µm thick surface disk. Dislocation and grain boundary diffusion behavior may vary between such small areas. Impurity segregation effects may vary among dislocations and grain boundaries. In general, every grain boundary has a different structure. In metals,[71] diffusivities increase and activation energies decrease progressively from lattice to dissociated dislocation to grain boundary and undissociated dislocation to surface diffusion. Dislocations and grain boundaries might add their effects together to produce a whole range of behaviour. Wide data scatter was also found by Reddy[15,16] for oxygen diffusion in Al_2O_3, McKenzie et. al.[24] for oxygen diffusion in MgO, and Chen and Peterson[79] for Cr diffusion in NiO. Even though scatter can be high, high scatter is preferable to not seeing any dislocation or grain boundary diffusion at all even though it is taking place. This author assumes this has happened many times because dislocation and grain boundary diffusion tail signals can be very low, in fact lost in the noise level of many techniques, unless gross second phase contamination has occurred.

Secondary Ion Mass Spectrometry of oxygen-18 profiles in MgO is a good technique for studying bulk oxygen diffusion. The agreement of this study's bulk diffusion coefficient with that of Yoo[19], also determined by SIMS, is excellent. The data of this study is no less than 0.4 of Yoo's, and the activation energy and pre-exponential are essentially the same. This agreement exists even though the studies used different single crystal starting materials (Yoo-epitaxial MgO made by him, present study-Oak Ridge, Norton and MIT polycrystalline MgO). Also good agreement exists even though the diffusion times of Yoo in the temperature range of this study were from 7-32 times the diffusion times of this study. Also, Yoo found agreement between interdiffusion and gas exchange samples.

SIMS may not be as good a technique for studying oxygen dislocation and grain boundary diffusion as for studying bulk diffusion, but it may be the best technique used so far. At least the grain boundary and dislocation "tails" have been observed and not inferred from "bulk diffusion" measurements. SIMS of MgO is in itself an interesting subject. The observed emission of oxygen from the surface due to electron bombardment alone is an interesting result, probably related to the charge suppression process. SIMS is a very complicated technique and the physics of much of it, for instance secondary ion production, is poorly understood.

Finally, this author would like to suggest that other processes might compete with or mimic grain boundary or dislocation diffusion effects. Grain boundary penetration of a liquid phase from the surface might cause concentration profiles to appear like grain boundary diffusion. Gas phase contamination of sintering particles might produce significantly different grain boundary chemistry after sintering, resulting in unusual extrinsic properties.

6.2 CONTAMINATION OF MgO

The data of this study suggest that silicon contamination may be more prevalent and important than previously expected. Even though precautions were taken, all samples showed high surface or near surface Si signals. The silicon signal was monitored to check for contamination because it was easy for the SIMS instrument to detect. Other impurities might also be contaminating MgO surfaces, but silicon is different because of its prevalence, high charge, and unique chemistry.

Almost everything contains silicon. Twenty-six percent of the earth's crust is silicon[84], second in abundance only to oxygen. Analysis of talc free polyethylene gloves made from pure virgin polyethylene showed it to contain silicon both on its surface and in the bulk. All MgO used in diffusion studies probably contains silicon as a major impurity (Table 2). A one microgram particle of SiO_2 can contaminate a one micron deep by one cm^2 area of MgO to about 10 mole %Si. Silicon contamination will not only occur in dusty (i.e. all) air but also in closed atmosphere apparatus such as gas exchange or epitaxial MgO growth apparatus[13]. Trapped water, acids, oils, etc., which recirculate through the system can increase Si evaporation by leaching or forming hydrated silicate species.

Unlike other elements which form solid solutions, silicon likes to form glassy more volatile phases. Iron, for example, will dissolve in MgO or produce solid magnesiowustite. However, the solubility limit for Si in MgO is very low[85], 340 ppm at 1800 °C. It can easily form a glassy grain boundary phase in either MgO or Al_2O_3. Silicon together with Ca, also segregates to MgO grain boundaries in a narrower region than other impurities[76]. This may mean that grain boundary and dislocation diffusion in MgO are dominated by as received levels of Si, even though as received levels of Al or Fe are usually greater and control the overall defect structure.

A polycrystalline Al_2O_3 furnace tube will contaminate a sample if it has a glassy second phase. If it doesn't have a glassy second phase, it will probably not be dense and will therefore be weak and less useful. In gas exchange diffusion experiments silicate evaporation can cause an apparently higher "bulk diffusion coefficient". A silicate specie can become volatile, equilibrate its O-18 concentration with the gas phase, and then deposit itself on the diffusion sample. This will increase the amount of O-18 exchange measured by either gas composition change, sample composition change, or oxygen-18 SIMS signal. Once the silicate contamination is on the surface, it can then diffuse into or penetrate as a second phase into grain boundaries.

Even though Si contamination was observed in all samples, the samples could very well be cleaner than those used in other studies. Many precautions were taken to keep the samples clean. In this study, Si contamination was looked for on all samples. The sensitivity of SIMS for Si detection is high. In the literature there are many references to firings, heat treatments, etc., with no mention of what type of furnace apparatus was used. Many of these heat treatments probably introduce Si and other contaminants, and no mention is made that they were looked for.

To sum up, silicon is everywhere, has unique chemical properties, and is volatile at high temperatures. New methods may have to be developed to avoid silicon contamination when studying ceramics at high temperatures.

7.0 SUMMARY AND CONCLUSIONS

Diffusion of oxygen in MgO single crystals, deformed single crystals and polycrystals was studied by high temperature oxygen-18 gas exchange followed by secondary ion mass spectrometry to determine concentration profiles. Silicon contamination was observed on all samples, probably coming from a glassy phase in the furnace tube, but perhaps coming from elsewhere, such as dust particles. Effort was concentrated on analyzing the low concentration, deep penetration part of the diffusion profile often called a "tail", which is dominated by dislocation and grain boundary diffusion.

The oxygen bulk diffusivity, D, in undoped MgO made at Oak Ridge, Norton Co., and MIT, was found to be

$$D=(3.9\ {}^{+10.5}_{-2.9}) \times 10^{-6} \ \exp(-\frac{3.45 \pm 0.17 \text{ eV}}{kT}) \ \text{cm}^2/\text{sec} \quad 1200\text{-}1500°\text{C} \qquad (7.1)$$

The dislocation diffusion parameter was found to be

$$D'_d a^2 = 10^{-(15.9\pm1.9)} \exp(-\frac{3.20 \pm 0.58 \text{ eV}}{kT}) \ \text{cm}^4/\text{sec} \quad 1200\text{-}1500°\text{C} \qquad (7.2)$$

where D'_d = oxygen diffusion coefficient within a dislocation

a = dislocation core radius

The grain boundary diffusion parameter was found to be

$$D'_b\delta = 10^{-(6.5\pm2.2)} \exp(-\frac{4.06 \pm 0.78}{kT}) \ \text{cm}^3/\text{sec} \quad 1200\text{-}1500°\text{C} \qquad (7.3)$$

where D'_b = oxygen diffusion coefficient within a grain boundary
δ = grain boundary thickness

Stated errors are for 68% confidence based on standard deviations of constants calculated by linear regression of Arrhenius plot data. The activation energies of oxygen diffusion in the bulk, dislocations and grain boundaries are the same within the experimental error.

At 1200 °C, the dislocation core radius and grain boundary thickness are under 10 angstroms, and the oxygen diffusion coefficients within grain boundaries and dislocations, D'_b and D'_d respectively, were found to be $10^{5.3}$ times the bulk diffusion coefficient D

a < 10 angstroms
δ < 10 angstroms 1200 °C
$D'_b \sim D'_d \sim 10^{5.3}$ D

All of the above data are summarized in Figure 30.

Secondary Ion Mass Spectrometry is a good technique to study oxygen-18 bulk diffusion profiles in MgO.

8.0 SUGGESTIONS FOR FURTHER WORK

1. Study bulk diffusion with the present study's experimental apparatus at 1500°C-1750°C or higher to compare the activation energy with Oishi's[4,5,6] data and with Narayan and Washburn's extrapolated data[12]. An interdiffusion sample should be included to elimate the possibility of evaporation. This will produce more data which may answer the question of intrinsic slope shift.

2. Oxygen diffusion experiments on MgO with no impurities would be hard to do, but of great scientific value. Pure polycrystals as well as pure single crystals have not yet been produced.

3. Oxygen diffusion in Lithium doped MgO as well as Lithium diffusion in MgO can be studied. Anomalous redox kinetics[33] may be explained. Lithium diffusion in dislocations or grain boundaries may be responsible. Oxygen diffusion in monovalent ion doped samples where the chemical potential of that ion is controlled in the diffusion zone may shed new light on the mechanism of oxygen diffusion.

4. Cation grain boundary and dislocation diffusion should be done to compare with oxygen diffusion data. The cation diffusion data may be more easily obtained with greater precision than the oxygen diffusion data.

5. Oxygen grain boundary and dislocation diffusion data should be compared to inferences about it made from creep data.

6. The study of evaporation of MgO and the condensation of impurities on MgO may lead to improved understanding of ceramics. Basic scientific knowledge may be gained as well as information which may be of use in ceramics processing. SIMS may also be done on

Si doped, dust contaminated and finger residue contaminated MgO to compare to previous work.

7. Continued improvement of SIMS of insulating materials should be used to improve the precision and accuracy of SIMS data.

8. Used samples from this study could be analyzed by CO_2 gas mass spectrometry to correlate with the present SIMS results as well as with most previous oxygen diffusion data.

9.0 REFERENCES

1. R.W. Balluffi, Phys. Stat. Sol. 42, 11,1970.

2. G. Martin & B. Perraillon, J. de Phy., Paris Suppl., 36, C4-165, 1975.

3. A. Atkinson, Solid State Ionics, 12, 309,1984.

4. Y. Oishi & W.D. Kingery, J. Chem. Phys. 33, 905, 1960

5. Y. Oishi, K. Ando, H. Kurokawa, & Y. Hiro, J. Am. Ceram. Soc., 66, c-60, 1983

6. Y. Oishi & K. Ando, in Structure & Properties of MgO and Al_2O_3 Ceramics, Advances in Ceramics, Vol. 10, edited by W.D. Kingery, The American Ceramic Society, Inc., Columbus, OH, 1984, pp379-393.

7. K. Ando, Y. Kurokawa & Y. Oishi, J. Chem. Phys., 78, 6890, 1983

8. R. H. Condit & J. B. Holt, J. Electrochemical Soc., 111, 1192, 1964

9. J. B. Holt & R. H. Condit, in Materials Science Research Vol. 3, eds. W. W. Kriegel & H. Palmour III, Plenum Press, New York, 1966, p13

10. L.H. Rovner, Ph.D. Thesis, Department of Physics, Cornell University, 1966, quoted from other ref 56

11. H. Hashimoto, M. Hama, S. Shirasaki, J. Appl. Phys., 43, 4828, 1972

12. J. Narayan & J. Washburn, Acta Metall., 21, 533, 1973

13. Y. Ko, K. Ando & Y. Oishi, presentation at the Sixteenth Ceramics Conference, Tokyo, Japan, 1978, Conference Report 7A05, quoted from reference 32.

14. Y. Moriyoshi, H. Haneda & S. Shirasaki, presentation at the Sixteenth Ceramics Conference, Tokyo, Japan, 1978, Conference report 7A04, quoted from reference 32.

15. K.P.R. Reddy, Ph.D. Thesis, Department of Metallurgy and Materials Science, Case Western Reserve U. 1979

16. K.P.R. Reddy & A.R. Cooper, J. Am. Ceram. Soc., 66, 664, 1983

17. Y. Moriyoshi, T. Ikegami, S. Matsuda, Y. Bando, Y. Sekikawa, & S. Shirasaki, Z. Phys. Chem. N.F., 118, 187, 1979

18. A.F. Henriksen, Y.M. Chiang, W.D. Kingery & W.T. Petuskey, J. Am. Ceram. Soc., 66, c-144, 1983

19. H.I. Yoo, PhD Thesis, MIT 1979

20. S. Shirasaki & Y. Oishi, Japan J. Appl., Phys., 10, 1109, 1971

21. S. Shirasaki & M. Hama, Chem. Phys. Letts., 20, 361, 1973

22. S. Shirasaki, H. Yamamura, M. Hama, H. Hashimoto, Japan J. Appl. Phys., 12, 1654, 1973

23. S. Shirasaki, S. Matsuda, H. Yamamura& H. Haneda, in Structure & Properties of MgO and Al_2O_3 Ceramics, Advances in Ceramics, Vol. 10, edited by W.D. Kingery, The American Ceramic Society, Inc., Columbus, OH, 1984, pp464-489.

24. D. R. McKenzie, A. W. Searcy, J. B. Holt & R. H. Condit, J. Am. Ceram. Soc., 54, 188, 1971

25. G.W. Groves & A. Kelly, J. Appl. Phys. Suppl 33, 456, 1962.

26. J. Narayan & J. Washburn, Phil. Mag. 26, 1179, 1972.

27. J. Narayan & J. Washburn, Crystal Lattice Defects 3, 91, 1972.

28. Y.A. LeQuinio, MS Thesis, MIT 1977

29. J. Crank "The Mathematics of Diffusion", 2nd ed., Clarendon Press, Oxford England, 1975.

30. Y. Oishi & W.D. Kingery, J. Chem. Phys. 33, 480,1960

31. W.D. Kingery, J. Am. Ceram. Soc. 57, 74,1974

32. K.W. Cheng, Sc.D. Thesis MIT 1980

33. Y. Chen, N. Dudney. J. Narayan & V.M. Orera, Phil. Mag. A 44, 63, 1981.

34. G.S. White, K.H. Lee and J.H. Crawford, Jr., Appl. Phys. Lett., 35, 1, 1979.

35. B.J. Wuensch in Mass Transport in Solids, edited by F. Beniere & C.R.A. Catlow, Plenum Press, New York, New York, 1983, pp 353-376

36. D.R. Sempolinski & W.D. Kingery, J. Am. Ceram. Soc., 63, 664, 1980.

37. M.M. Abraham, C.T. Butler, & Y. Chen, J. Chem. Phys., 55, 3752, 1971.

38. J.R. Booth, W.D. Kingery & H.K. Bowen, J. Cryst. Growth, 29, 257, 1975.

39. J.W. Osenbach & V.S. Stubican, J. Am. Ceram. Soc., 66, 191,1983.

40. R.A. Weeks & E. Sonder, Rev. Int. Hautes Temp. Ref., Fr., 17 154, 1980.

41. F. Sato & K. Sumino, J. Mat. Sci., 15, 1625, 1980.

42. P.C. Dokko & J.A. Pask, J. Am. Ceram. Soc., 62, 433, 1979.

43. B.C. Harding, D.M. Price & A.J. Mortlock, Phil. Mag., 23, 399, 1971.

44. C.T. Butler, B.J Sturm & R.B. Quincy Jr., J. Cryst. Growth, 8, 197, 1971.

45. W.C. Mackrodt & R.F. Stewart, J. Phys. C. Solid State Phys., 12, 5015, 1979.

46. M.J.L. Sangster & D.K. Rowell, Phil. Mag. A, 44, 613, 1981.

47. C.R.A. Catlow, I.D. Faux & M.J. Norgett, J. Phys. C., 9, 419, 1976.

48. W.H. Gourdin & W.D. Kingery, J. Mater. Sci., 14, 2053, 1979.

49. W.C. Mackrodt, in Structure & Properties of MgO and Al_2O_3 Ceramics, Advances in Ceramics, Vol. 10, edited by W.D. Kingery, The American Ceramic Society, Inc., Columbus, OH, 1984, pp62-78.

50. K. Tharmalingam & A.B. Lidiard, Phil. Mag., 6, 1157, 1961.

51. A.D. LeClaire & A. Rabinovitch, J. Phys. C: Solid State Phys., 14, 3863, 1981.

52. A.D. LeClaire, Brit. J. Appl. Phys., 14, 351, 1963.

53. L.G. Harrison, Trans. Faraday Soc., 57, 1191, 1961.

54. G. Martin & B. Perraillon, in Grain Boundary Structure and Kinetics, American Society for Metals, Metals Park, Ohio 1980, pp 239-293.

55. A. Atkinson & R.I. Taylor, Phil. Mag. A, 39, 581, 1979.

56. B.J. Wuensch, in Mass Transport Phenomena in Ceramics, edited by A.R. Cooper & A.H. Heuer, Plenum Press, New York, New York, 1975, pp 211-231

57. J.R. Taylor, "An Introduction to Error Analysis", University Science Books, Mill Valley California, 1982.

58. J.B. Lacy, M.M. Abraham, J.L. Boldú, Y. Chen, J. Narayan, & H.T. Tohver, Phys. Rev. B, 18, 4136, 1978.

59. W. Hüther & B. Reppich, Phil. Mag., 28, 363, 1973.

60. Yasumichi Oishi, Kyushu University, private communication. Jules Routbort, Argonne National Laboratory, private communication.

61. M. Fujimoto, Y.M. Chiang & W.D. Kingery, unpublished.

62. M. Fujimoto, personal communication.

63. Y. Oishi, K. Ando, N. Suga, J. Am. Ceram. Soc., 66, c130, 1983

64. Unpublished work with Prof. R.M. Cannon, MIT, 1978-1979.

65. E. Giraldez, W.T. Petuskey, L. Dolhert & W.D. Kingery, to be published in J. Am. Ceram. Soc. Comm.

66. D. Lewis III, Ceramic Bulletin, 57, 434,1978.

67. W.C. Mackrodt, personal communication.

68. J.H. Crawford Jr., in Structure & properties of MgO and Al_2O_3 Ceramics, Advances in Ceramics, Vol. 10, edited by W.D. Kingery, The American Ceramic Society, Inc., Columbus, OH, 1984, pp793-798.

69. F. Freund, B. King, R. Knobel & H. Kathrein, in Structure & Properties of MgO and Al_2O_3 Ceramics, Advances in Ceramics, Vol. 10, edited by W.D. Kingery, The American Ceramic Society, Inc., Columbus, OH, 1984, pp119-138.

70. F.A. Kroger, in Structure & Properties of MgO and Al_2O_3 Ceramics, Advances in Ceramics, Vol. 10, edited by W.D. Kingery, The American Ceramic Society, Inc., Columbus, OH, 1984, pp1-15.

71. R.W. Balluffi, Met. Trans. B, 13B, 527, 1982.

72. W.D. Kingery, Pure & Appl. Chem., 56, 1703, 1984

73. D.M. Duffy & P.W. Tasker, J. Am. Ceram. Soc., 67, C-176, 1984.

74. J. Eastman, F. Schmückle, M.D. Vaudin & S.L. Sass, in Structure & properties of MgO and Al_2O_3 Ceramics, Advances in Ceramics, Vol. 10, edited by W.D. Kingery, The American Ceramic Society, Inc., Columbus, OH, 1984, pp324-346.

75. W.D. Kingery, Sol. State Ionics, 12, 299, 1984.

76. Y.M. Chiang, A.F. Henriksen, W.D. Kingery & D. Finello, J. Am. Ceram. Soc., 64, 385, 1981.

77a. B.J. Wuensch & T. Vasilos, J. Am. Ceram. Soc., 47, 63,1964.
b. B.J. Wuensch & T. Vasilos, J. Am. Ceram. Soc., 49, 433, 1966.

78. A. Atkinson & R.I. Taylor, Phil. Mag. A, 43, 979,1981.

79. W.K. Chen & N.L. Peterson, J. Am. Ceram. Soc., 63, 566,1980.

80. A. Atkinson & R.I. Taylor, Phil. Mag. A, 45, 583, 1982.

81. B.J. Wuensch, W.C. Steele & T. Vasilos, J. Chem. Phys., 58, 5258, 1973.

82. J. Philibert, J. Phys. Paris, 36, C4-411, 1975.

83. N.L. Peterson, personal communication.

84. W.D. Kingery, H.K. Bowen & D.R. Uhlmann, Introduction to Ceramics, John Wiley & Sons, New York, 1976.

85. A. Henriksen, Sc.D. Thesis, MIT 1978

APPENDIX I-Oxygen Diffusion in Contaminated Li & Cr Doped MgO

Diffusion results for Spicer 800ppm Cr MgO and Oak Ridge .03-.05a% Li doped MgO were only obtained from diffusion anneals performed in the McDanel 998 Al_2O_3 furnace tube which contaminated MgO surfaces with silicon containing lumps (Figure 8) and increased the apparent bulk diffusion coefficient (section 5.6). Unfortunately one cannot separate the effect of contamination from the effect of doping. Figure I-A shows bulk oxygen diffusion data for contaminated Cr and Li doped MgO superimposed on Figure 28. Figure I-B shows dislocation oxygen diffusion data for contaminated Cr and Li doped MgO superimposed on Figure 29.

Shirasaki et. al.[22] found Li increased bulk diffusion coefficients while Rovner's[10] data shows no increase. Rovner[10] found Cr increased the bulk oxygen diffusion coefficient (Figure 1 and Table 1).

Measured sputter pit depths for Li doped MgO were as high or higher than for similarly sputtered undoped MgO. Sputter rate for Li doped MgO may be higher than for undoped MgO, but not enough sputter pits were measured in Li doped MgO to accurately determine its sputter rate.

The measurement of oxygen diffusion in Li doped MgO is further complicated by Li diffusion. Lithium is probably being lost from the sample surfaces as the profiles of Appendix II show.

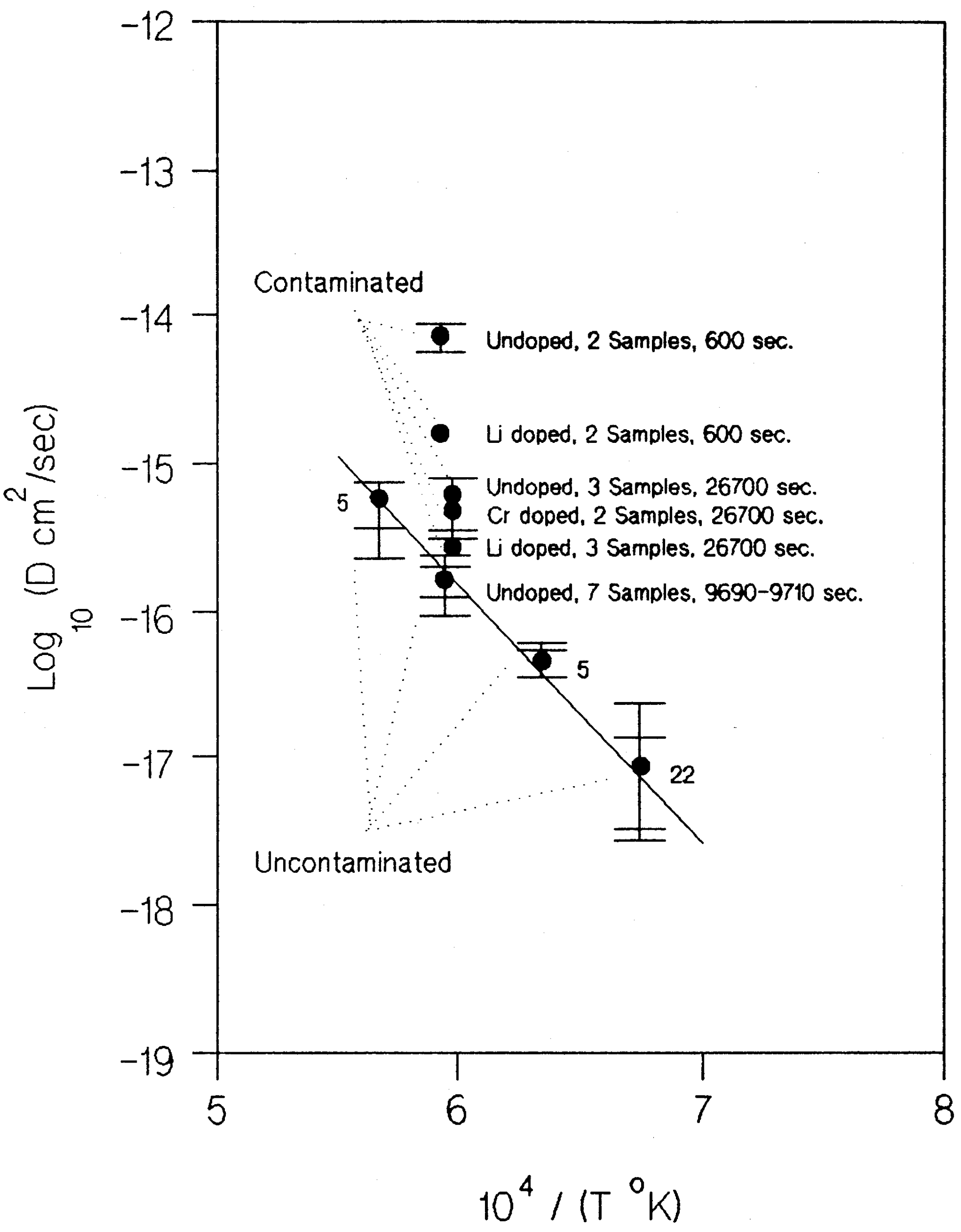

Figure I-A Bulk oxygen diffusion data of contaminated Li and Cr doped MgO. Results are superimposed on Figure 28. Diffusion anneal time is also shown on the figure.

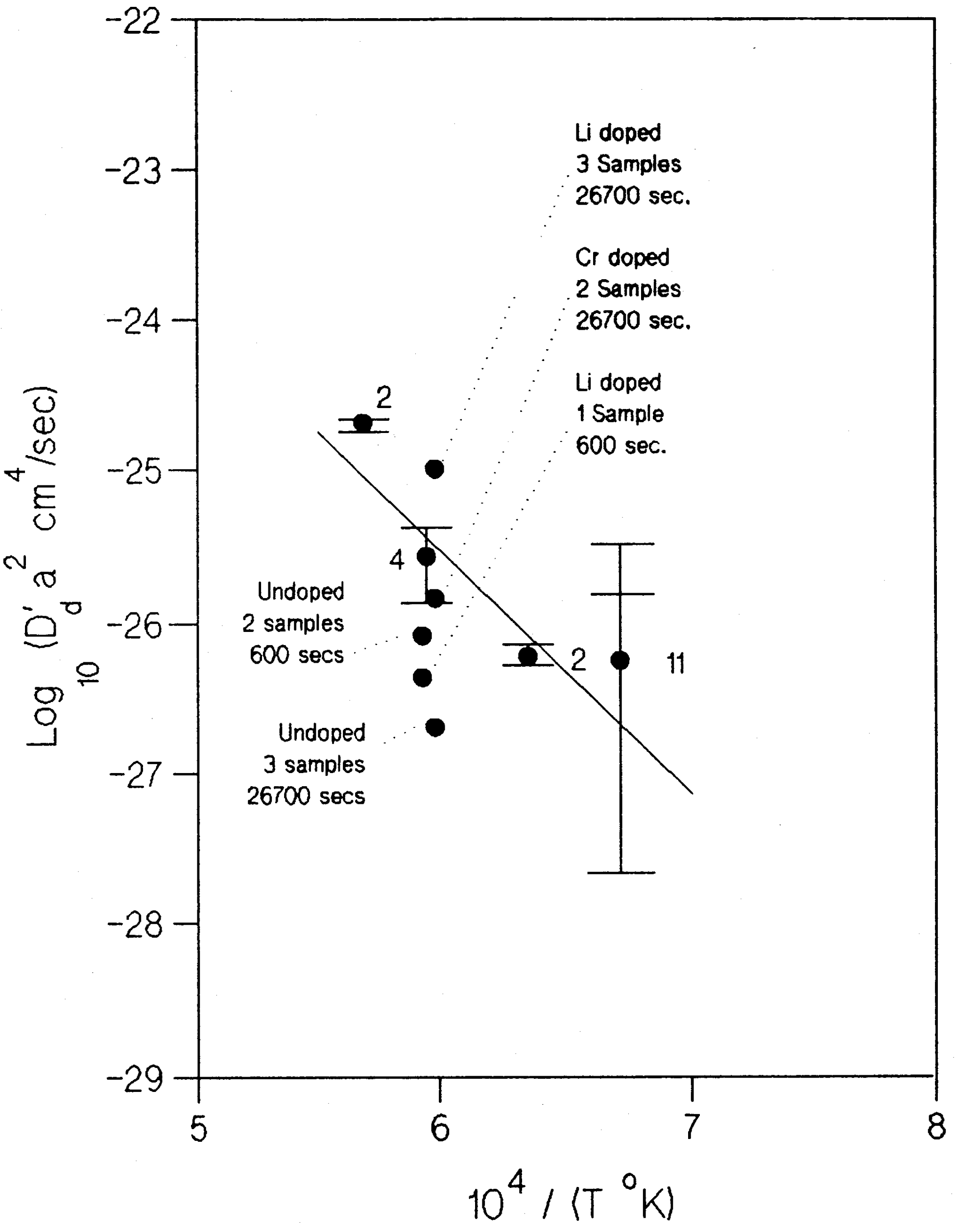

Figure I-B Oxygen diffusion in dislocations in contaminated Li and Cr doped MgO. Results are superimposed on Figure 29. Diffusion anneal time is also shown on the figure.

APPENDIX II-Evidence of Li Diffusion

This section contains two SIMS raw data plots of profiles of 3-5% Li doped Oak Ridge MgO. These show evidence that lithium is diffusing out of the sample during high temperature anneals in air. Figure II-A shows a diffusion profile for Li diffusing out of the sample. Figure II-B shows an unusual profile which might be an indicator of Li_2O precipitates.

```
1  MASS=7   TIME(sec)=.5   OFFSET(volts)=0
2  MASS=12   TIME(sec)=.5   OFFSET(volts)=0
3  MASS=16   TIME(sec)=1   OFFSET(volts)=0
4  MASS=18   TIME(sec)=1   OFFSET(volts)=0
5  MASS=28   TIME(sec)=.5   OFFSET(volts)=0
```

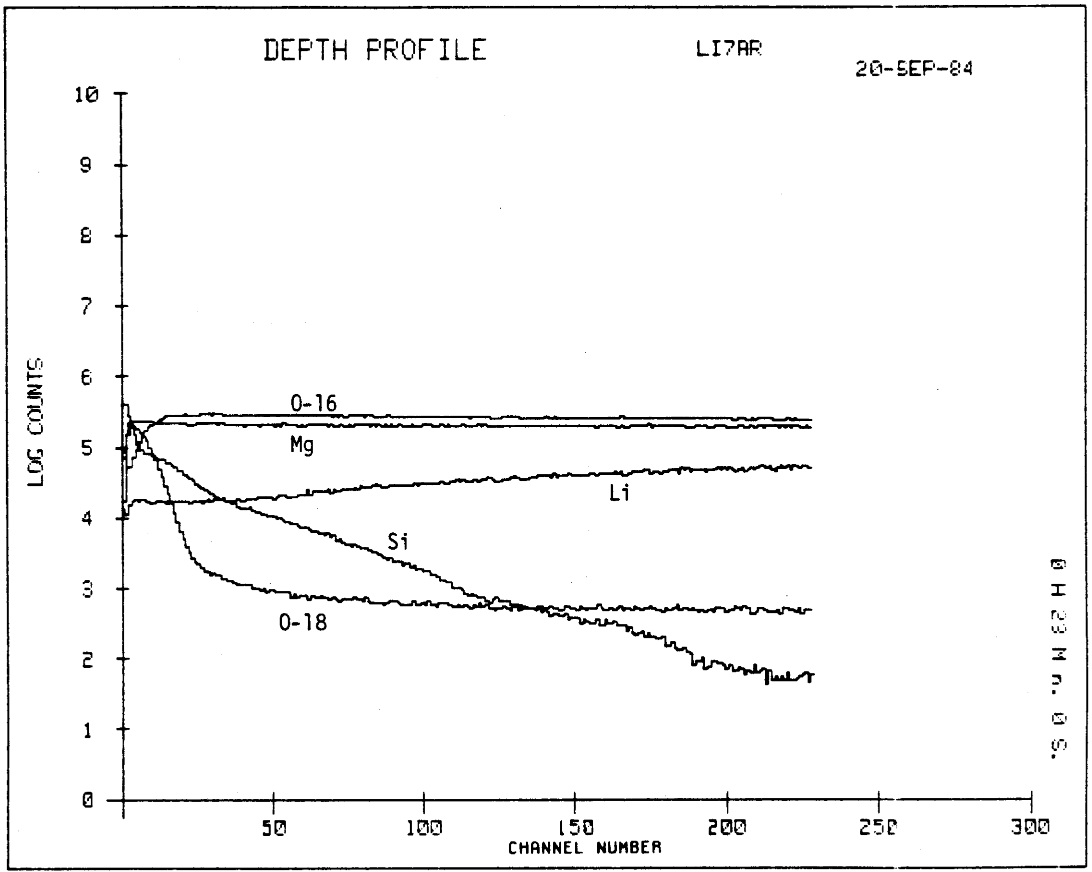

```
FILE                LI7AR              IS OPENED

                     MEASUREMENT CONDITIONS
SAMPLE REFERENCE: LI7AR                 DATE: 20-SEP-84
PRIMARY POLARITY: +     SECONDARY POLARITY: +
PRIMARY CURRENT: 8.76E-07 Amps.
PRIMARY VOLTAGE:  9.71  Kv.
RASTER:  500  Microns
IMAGE FIELD:  150  Microns
```

Fig. II-A SIMS raw data of a Li doped MgO sample. This sample was not given an equilibration pre-anneal. Diffusion anneal-1398 °C, 26700 sec. Calculated sputter pit depth-0.63μm. SIMS analysis area-60μm diameter circle.

```
1  MASS=6   TIME(sec)=.5   OFFSET(volts)=0
2  MASS=12   TIME(sec)=.5   OFFSET(volts)=0
3  MASS=16   TIME(sec)=1   OFFSET(volts)=0
4  MASS=18   TIME(sec)=1   OFFSET(volts)=0
5  MASS=28   TIME(sec)=.5   OFFSET(volts)=0
```

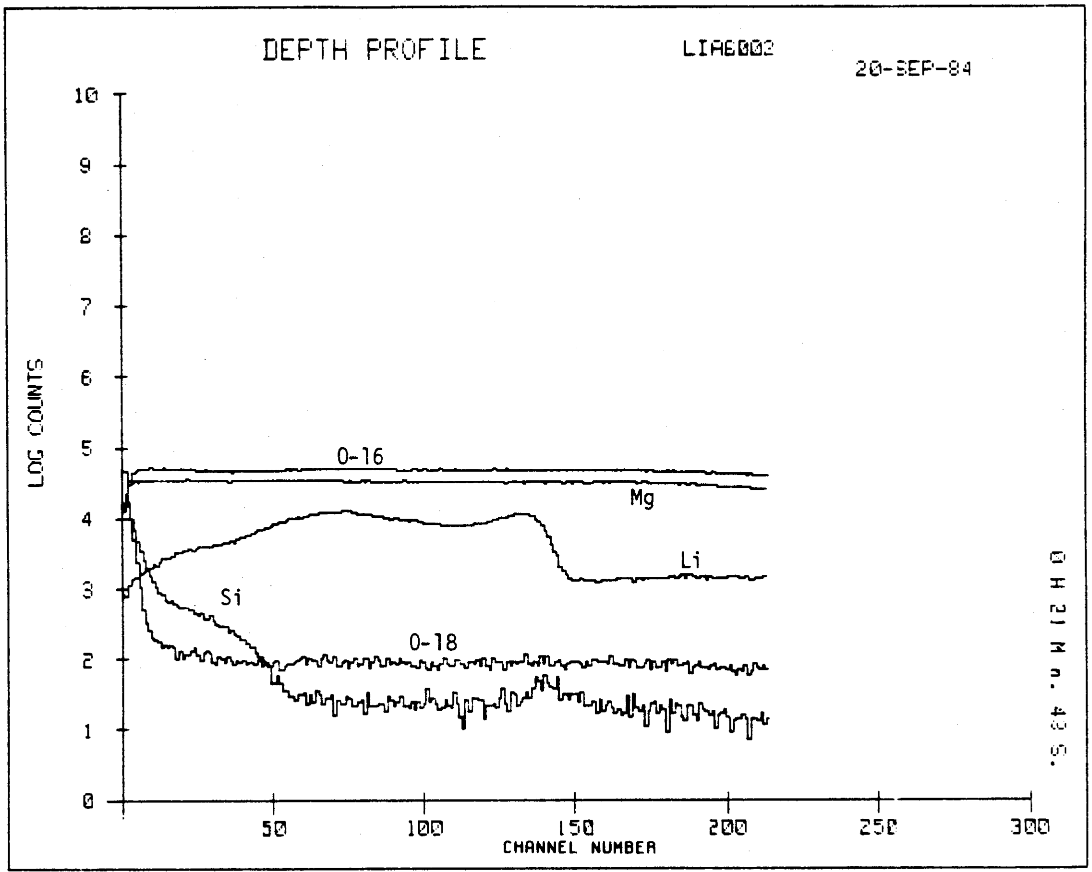

```
FILE                    LIA602                  IS OPENED

                         MEASUREMENT CONDITIONS
SAMPLE REFERENCE: LIA6002                        DATE: 20-SEP-84
PRIMARY POLARITY: +     SECONDARY POLARITY: +
PRIMARY CURRENT: 8.85E-07 Amps.
PRIMARY VOLTAGE:   9.71  Kv.
RASTER:   500   Microns
IMAGE FIELD:   150   Microns
```

Fig. II-B SIMS raw data of a Li doped MgO sample. This sample was not given an equilibration pre-anneal. Diffusion anneal 1412 °C, 600 sec. Calculated sputter pit depth 0.61 µm. SIMS analysis area 60 µm diameter circle.

APPENDIX III-Electron Sputtering or Stimulated Desorption

Figure III-A illustrates that bombardment of an MgO surface by an electron beam is enough to cause the sputtering or desorption of oxygen. When the surface was bombarded by the electron beam, an oxygen-16 signal was detected by the mass spectrometer. This phenomenon may be related to the reduction in SIMS charging which the electron beam allows.

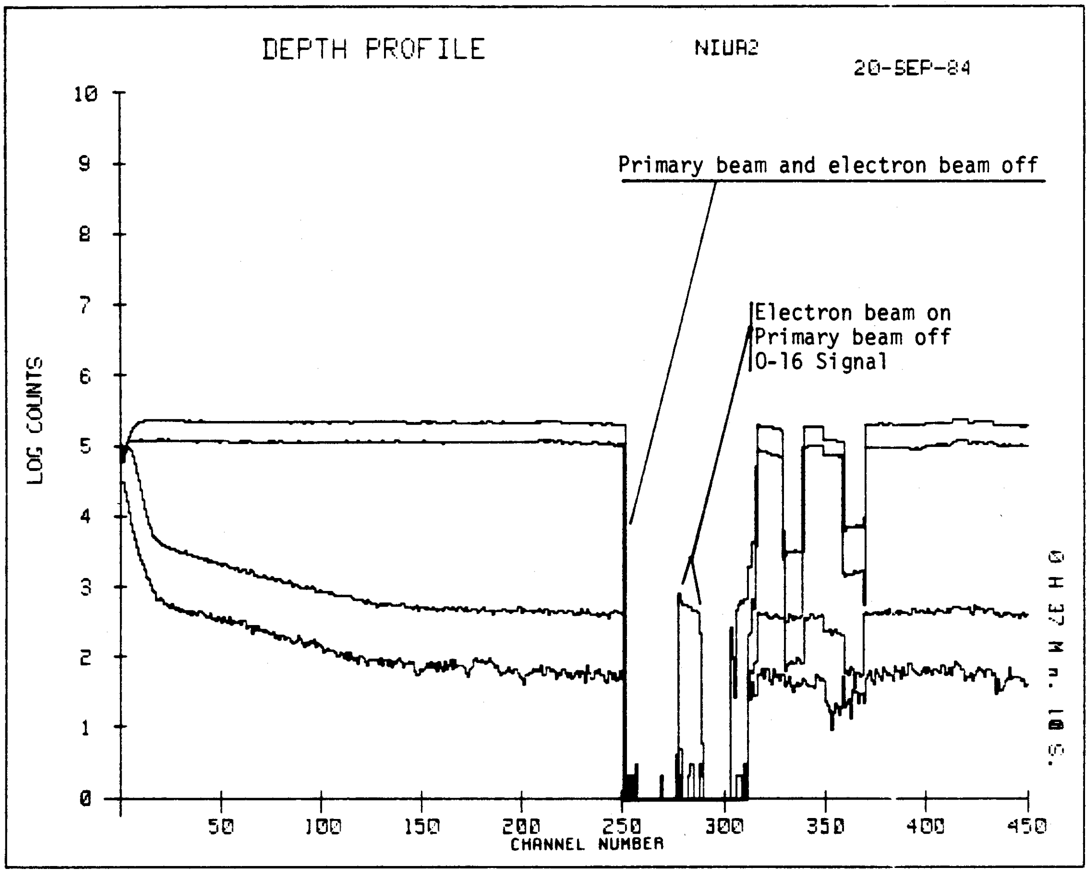

Fig. III-A SIMS raw data plot. During analysis, both the primary beam and the electron beam were turned off around channel 250. When only the electron beam was turned on, an oxygen-16 signal was observed. The oxygen-16 signal is always the highest signal on this plot.

APPENDIX IV-Tail Slope Time Dependence at 1200 °C

Figure IV-A is a plot of "tail" slopes versus diffusion time at 1200 °C for the various samples indicated. As described in section 3.1, equation 3.13, these plots should have a slope of -0.3 for grain boundary diffusion. As can be seen in the figure, the error associated with these measurements is too high to decide which diffusion mechanism is dominant in the tail region. There is a downward trend for the polycrystalline sample data and a flat trend for the undeformed and 6% deformed sample data as is to be expected. However the upward trend for the 55% and 62% deformed samples was unexpected. Instead of using these plots, samples were divided for subsequent analysis on the basis of microstructure. Single crystals and the Oak Ridge sample deformed 6% had few grain boundaries and were analyzed using dislocation diffusion mathematics. Polycrystals and highly deformed samples with low angle grain boundaries were analyzed using grain boundary diffusion mathematics.

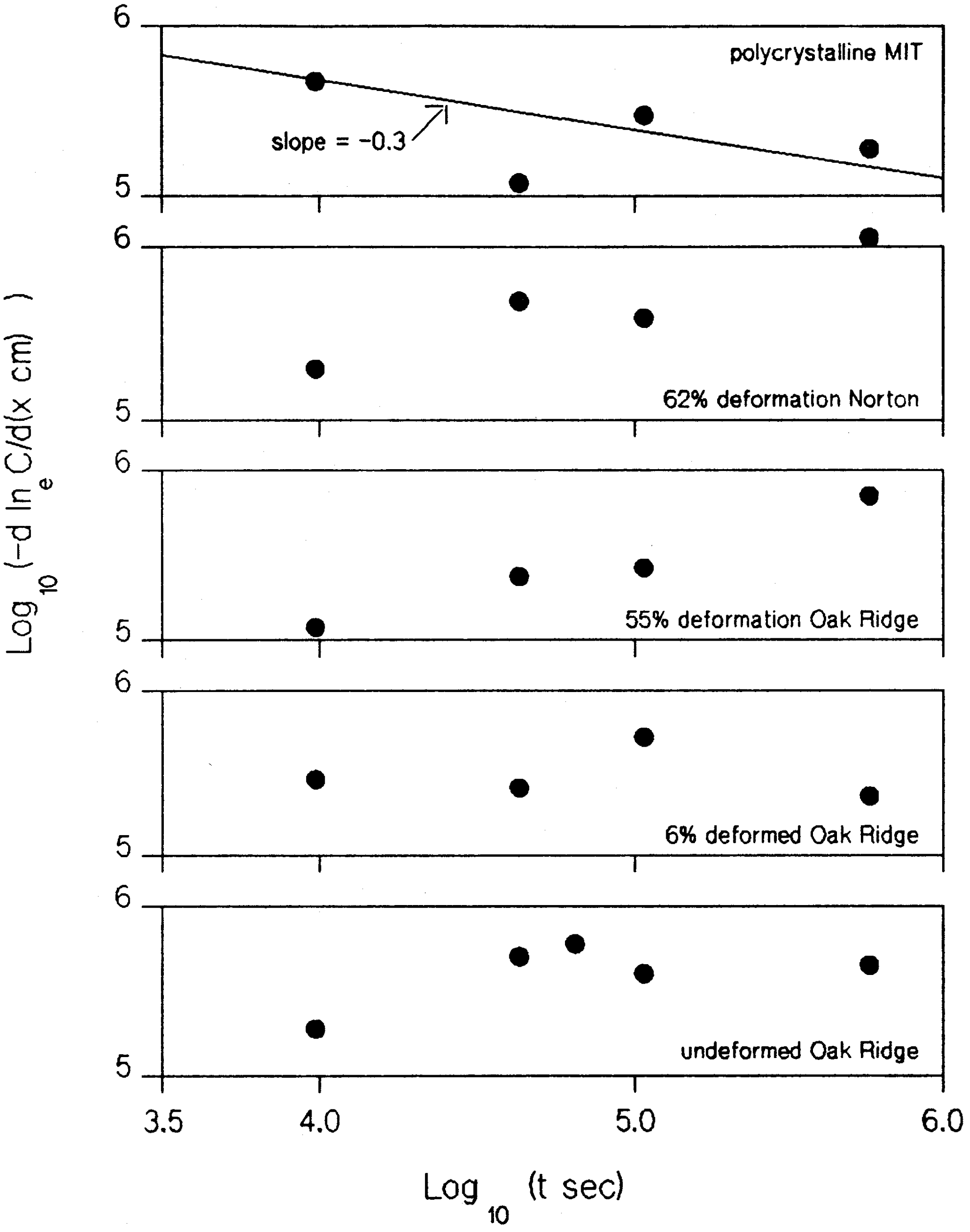

Fig. IV-A Diffusion time dependence of "tail" slope from $\ln_e$ C versus $x^{1.2}$ plots. 1200°C diffusion samples. Slope should be -0.3 for grain boundary diffusion.

APPENDIX V-Data and Data used in Plots and Calculations

```
APPENDIX 5 TABLE 1

THIS TABLE SHOWS THE SAMPLES USED FOR EACH FIGURE AND  TABLE LISTED.
    LISTS FOR DIFFUSION PLOT FIGURES SHOW THE TEMPERATURE (DEGREES CENTIGRADE),
    POINT LABEL, AND SAMPLES USED TO MAKE THAT POINT.
    LINEAR REGRESSION INFORMATION IS ALSO LISTED FOR CERTAIN PLOTS.

FIG. 11 DATA EXAMPLE
        OR6A2

FIG. 12 DATA EXAMPLE
        POLYE

FIG. 13 DATA EXAMPLE
        NC62B

FIG. 15 LOG D VS. 1/T
1486 5 ORUK OR6K OR55K NC62K POLYK
1411 7 ORUA ORUI OR6A OR6A2 OR55A NC62I POLYA
1304 5 ORUJ OR6J OR55J NC62J POLYJ
1210 22 ORUE ORUH ORUH2 ORUH3 ORUD ORUC OR6E OR6C OR6C2 OR6C3 OR6H OR55C OR55C2
        OR55C3 OR55E OR55H NC62C NC62E NC62H POLYE POLYC POLYH
        LINEAR REGRESSION SLOPE=-17414+/-877 INTERCEPT=-5.4030+/-0.5634
        CORRELATION COEFFICIENT=-0.956

FIG. 17 LOG DAA VS. 1/T
1486 2 ORUK OR6K
1411 4 ORUA ORUI OR6A OR6A2
1304 2 ORUJ OR6J
1210 11 ORUC ORUD ORUE ORUH ORUH2 ORUH3 OR6C OR6C2 OR6C3 OR6E OR6H
        LINEAR REGRESSION SLOPE=-16129+/-2912 INTERCEPT=-15.859+/-1.872
        CORRELATION COEFFICIENT=-0.80215

FIG. 19 LOG DD VS 1/T
1486 3 OR55K NC62K POLYK
1410 3 OR55A NC62I POLYA
1304 3 OR55J NC62J POLYJ
1210 10 OR55C OR55C2 OR55E OR55H NC62C NC62E NC62H POLYC POLYE POLYH
        LINEAR REGRESSION SLOPE=-20469+/-3920 INTERCEPT=-6.4935+/-2.5075
        CORRELATION COEFFICIENT=-0.785

FIG. 21 LOG D' VS 1/T
1209 3 NC62L ORUL OR6L
1127 5 OR55G NC62G POLYG OR6G OR6G2
1013 8 OR55B NC62B NC62B2 POLYB POLYB2 ORCLB ORCUTB OR6B
        LINEAR REGRESSION SLOPE=-12250 INTERCEPT=-3.448

FIG. 22 LOG D VS 1/T FOR DOPED SAMPLES
1411 CA3 CA55I CA6I CA6I2
1216 CA3 CA6C CA6C2 CA55C
1411 NA2 MGONA MGONA2
1410 NI3 NIUA NIUA2 NI27A
1210 NI2 NIUD NI27D
1411 "FEJ2" FEJ FEJ2
1410 FE3 FE35A FEUA FEUA2
1210 FE2 FE35D FEUD
```

APPENDIX 5 TABLE 1 (cont.)

FIG. 23 LOG DAA VS 1/T FOR DOPED SAMPLES
1411 CA2 CA6I CA6I2
1216 CA2 CA6C CA6C2
1410 NI2 NIUA NIUA2
1210 NI1 NIUD
1411 "FEJ2" FEJ FEJ2
1410 FE1 FEUA2
1210 FE1 FEUD

FIG. 24 LOG DD VS 1/T FOR DOPED SAMPLES
1411 CA1 CA55I
1216 CA1 CA55C
1411 NA2 MGONA MGONA2
1410 NI1 NI27A
1210 NI1 NI27A
1410 FE1 FE35A
1210 FE1 FE35D

FIG. 25 SIMS RAW DATA EXAMPLE
ORUD

FIG. 26 SIMS RAW DATA EXAMPLE
POLYJ

FIG. 27 SIMS RAW DATA EXAMPLE
OR55K

FIG. 28 LOG D VS 1/T FOR CONTAMINATED SAMPLES
1412 2 OR600 OR6600
1398 3 OR7PRE OR7PR2 6ORPR7

FIG. 29 LOG DAA VS 1/T FOR CONTAMINATED SAMPLES
1412 2 OR600 OR6600
1398 3 OR7PRE OR7PR2 6ORPR7

TABLE 6 DISLOCATION DENSITY AND AREA CALCULATIONS
OAK RIDGE 0% ORUA ORUC ORUD ORUE ORUH ORUH2 ORUH3 ORUI ORUJ ORUK
OAK RIDGE 6% OR6A OR6A2 OR6C OR6C2 OR6C3 OR6E OR6H OR6J OR6K
OAK RIDGE 55% OR55A OR55C OR55C2 OR55C3 OR55E OR55H OR55J OR55K
NORTON CO. 62% NC62C NC62E NC62H NC62I NC62J NC62K

FIG I-A LOG D VS 1/T FOR CONTAMINATED CR AND LI DOPED SAMPLES
1412 LI2 LIA60084 LIA60284
1398 LI3 LI7PRE84 LI7PR284 LI7AR84
1398 CR2 MGOCR MGOCR2

FIG. I-B LOG DA VS 1/T FOR CONTAMINATED CR AND LI DOPED SAMPLES
1412 LI1 LIA60084
1398 LI3 LI7PRE84 LI7PR284 LI7AR84
1398 CR2 MGOCR MGOCR2

FIG. II-A SIMS RAW DATA EXAMPLE
LI7AR84

FIG II-B SIMS RAW DATA EXAMPLE
LIA60284

FIG III-A SIMS RAW DATA EXAMPLE
NIUA2

FIG. IV-A TAIL SLOPE TIME DEPENDENCE AT 1200C
POLYCRYSTALLINE POLYF POLYE POLYC POLYH
NORTON CO. 62% NC62F NC62E NC62C NC62H
OAK RIDGE 55% OR55F OR55E (AVERAGE OF OR55C AND OR55C2) OR55H
OAK RIDGE 6% OR6F OR6E (AVERAGE OF OR6C, OR6C2 AND OR6C3) OR6H
OAK RIDGE 0% ORUF ORUE ORUD ORUC (AVERAGE OF ORUH, ORUH2 AND ORUH3)

APPENDIX V TABLE 2

THIS TABLE LISTS THE SAMPLES USED IN ALL DIFFUSION ANNEALS (SEE TABLE 5) UNDER EACH RUN NUMBER OR LETTER IS LISTED THE SQUARE ROOT OF (DT) IN ANGSTROMS, WHERE D IS THE BULK DIFFUSION COEFFICIENT CALCULATED BY EQUATION 5.1 AND T IS THE DIFFUSION ANNEAL TIME (TABLE 5). UNDER THIS, THE DIMENSIONLESS NUMBER BETA IS LISTED WHICH WAS CALCULATED USING EQUATIONS 5.1 AND 5.3, AND THE DIFFUSION ANNEAL TIME IN EQUATION 3.12. SAMPLE MAKER KEY: OR=OAK RIDGE, SP=SPICER, NC=NORTON, MIT=MADE AT MIT FORMAT FOR EACH SAMPLE: MAKER, DOPANT, TRUE STRAIN %, COMMENTS

```
RUN 4A   NC
  275A
  4.14

RUN 4B   NC
  628A
  181

RUN 11   OR      LI DOPED   NOT PRE-ANNEALED
  406A   OR      LI DOPED
  289    OR
         OR      6%
         SP      310PPM FE  NOT PRE-ANNEALED
         SP      310PPM FE
         SP      800PPM CR

RUN 12   OR      LI DOPED
   67A   OR      LI DOPED   NOT PRE-ANNEALED
  1808   OR      6%
         OR

RUN  A   OR
   267A  OR      6%
   454   OR      55%
         MIT     POLYCRYSTAL
         SP      370PPM NI
         SP      370PPM NI     27%
         SP      310PPM FE
         SP      310PPM FE     35%

RUN  B   OR
    4A   OR       6%
   7532  OR      55%
         MIT     POLYCRYSTAL
         OR      DIAMOND SAW CUT SURFACE
         NC      62%
         SP      370PPM NI         27%
         SP      310PPM FE         35%

RUN  C   OR      (2 PIECES)
   188A  OR      6%
    373  OR      55%
         MIT     POLYCRYSTAL
         OR      CA DOPED          6%  ANNEALED IN 2600APPM CA MGO POWDER FOR
         --      --------              22 DAYS, 1400C
         OR      CA DOPED         55%  SAME AS ABOVE
         OR      6%          LONG PRE-ANNEAL 22 DAYS 1400C IN PURE MGO POWDER
         OR      55%         SAME AS ABOVE
         NC      62%
```

APPENDIX V TABLE 2 (cont.)

```
RUN D     OR
   139A   SP      370PPM NI
   495    SP      370PPM NI       27%
          SP      310PPM FE
          SP      310PPM FE       35%

RUN E     OR
  107A    OR       6%
  628     OR      55%
          MIT     POLYCRYSTAL
          NC      62%

RUN F     OR
  51A     OR       6%
  1316    OR      55%
          MIT     POLYCRYSTAL
          NC      62%

RUN G     OR
  6A      OR       6%
  8592    OR      55%
          MIT     POLYCRYSTAL
          NC      62%

RUN H     OR
  419A    OR       6%
  165     OR      55%
          MIT     POLYCRYSTAL
          NC      62%

RUN I     OR
  269A    OR    CA DOPED    6%    ANNEALED IN 2600APPM CA DOPED MGO POWDER FOR
  451     --    --------          22 DAYS AT 1400C
          OR    CA DOPED   55%    SAME AS ABOVE
          OR       6%      LONG PRE-ANNEAL 22 DAYS AT 1400C IN PURE MGO POWDER
          OR      55%      SAME AS ABOVE
          NC      62%
          SP    310PPM FE   SUPPLIED BY Y. OISHI

RUN J     OR
  244A    OR       6%
  374     OR      55%
          MIT     POLYCRYSTAL
          NC      62%        (2 PIECES)

RUN K     OR
  238A    OR       6%
  611     OR      55%
          MIT     POLYCRYSTAL
          NC      62%

RUN L     OR
  8A      OR       6%
  8164    OR      55%
          NC      62%

RUN MGO:NA    MIT  NA DOPED POLYCRYSTALS (2 PIECES)
  299A
  406
```

APPENDIX 5 TABLE 3

THIS TABLE IS A KEY TO THE SIMS SAMPLE NAMES USED IN THE FOLLOWING 2 TABLES.
COLUMN 1: SIMS SAMPLE NAME
" 2: MATERIAL SOURCE OR=OAK RIDGE,NC=NORTON CO.,SP=SPICER,MIT=MIT
" 3: DOPANT
" 4: TRUE STRAIN %
" 5: DIFFUSION ANNEAL (SEE TABLE 5)
" 6: SIMS RUN (FIRST,ETC.) OF THE PARTICULAR MGO SAMPLE
" 7: COMMENTS
ALL SIMS SAMPLES 500 SQUARE MICRON RASTERS UNLESS OTHERWISE NOTED.

1	2	3	4	5	6	7
2MGO21	NC	--	0	4B	2	250 MICRON RASTER
MGO212	NC	--	0	4B	3	250 MICRON RASTER
2MGO4	NC	--	0	4A	2	250 MICRON RASTER
3MGO4	NC	--	0	4A	3	250 MICRON RASTER
4MGO4	NC	--	0	4A	4	250 MICRON RASTER
2A1421	NC	--	0	4B	4	250 MICRON RASTER
LI7AR1	OR	LI	0	11	1	300-500APPM LI NOT PRE-ANNEALED 250 MICRON RASTER
LI7PR1	OR	LI	0	11	1	300-500APPM LI 250 MICRON RASTER
LI7AR2	OR	LI	0	11	2	300-500APPM LI NOT PRE-ANNEALED 250 MICRON RASTER
OR7PRE	OR	--	0	11	1	250 MICRON RASTER
OR7PR2	OR	--	0	11	2	250 MICRON RASTER
FEAR7	SP	FE	0	11	1	310PPM FE NOT PRE-ANNEALED 250 MICRON RASTER
FEPR7	SP	FE	0	11	1	310PPM FE 250 MICRON RASTER
FEAR72	SP	FE	0	11	2	310PPM FE 250 MICRON RASTER
LIP600	OR	LI	0	12	1	300-500APPM LI 250 MICRON RASTER
LIA600	OR	LI	0	12	1	300-500APPM LI NOT PRE-ANNEALED 250 MICRON RASTER
6ORPR7	OR	--	6	11	1	250 MICRON RASTER
OR6600	OR	--	6	12	1	250 MICRON RASTER
OR600	OR	--	0	12	1	250 MICRON RASTER
OR55C2	OR	--	55	C	2	250 MICRON RASTER
ORUC	OR	--	0	C	1	
OR6C	OR	--	6	C	1	
OR6C2	OR	--	6	C	2	
OR55C	OR	--	55	C	1	
OR55C3	OR	--	55	C	3	
POLYC	MIT	--	--	C	1	POLYCRYSTAL
NC62C	NC	--	62	C	1	
CA55C	OR	CA	55	C	1	22 DAYS @ 1400C IN 2600APPM CA MGO POWDER
LN55C	OR	--	55	C	1	22 DAYS @ 1400C IN PURE MGO POWDER
LN55C2	OR	--	55	C	2	SAME AS ABOVE
LN6C	OR	--	6	C	1	SAME AS ABOVE
CA6C	OR	CA	6	C	1	22 DAYS @ 1400C IN 2600APPM CA MGO POWDER
CA6C2	OR	CA	6	C	2	SAME AS ABOVE
OR6C3	OR	--	6	C	3	
NC62B	NC	--	62	B	1	
NC62B2	NC	--	62	B	2	
NC62B3	NC	--	62	B	3	
ORCUTB	OR	--	--	B	1	DIAMOND SAW CUT SURFACE
FE35B	SP	FE	35	B	1	310PPM FE
OR6B	OR	--	6	B	1	
OR55B	OR	--	55	B	1	
ORCLB	OR	--	--	B	1	CLEAVED MGO SURFACE
POLYB	MIT	--	--	B	1	POLYCRYSTAL
POLYB2	MIT	--	--	B	2	POLYCRYSTAL
ORUA	OR	--	0	A	1	
OR55A	OR	--	55	A	1	
POLYA	MIT	--	--	A	1	POLYCRYSTAL
OR6A	OR	--	6	A	1	

APPENDIX 5 TABLE 3 (cont.)

OR6A2	OR	--	6	A	2	
MGOCR	SP	CR	0	11	1	800PPM CR
MGOCR2	SP	CR	0	11	2	800PPM CR
ORUD	OR	--	0	D	1	
NIUD	SP	NI	0	D	1	370PPM NI
NI27D	SP	NI	27	D	1	370PPM NI
ORUJ	OR	--	0	J	1	
OR6J	OR	--	6	J	1	
OR55J	OR	--	55	J	1	
NC62J	NC	--	62	J	1	
POLYJ	MIT	--	--	J	1	POLYCRYSTAL
NC62K	NC	--	62	K	1	
ORUK	OR	--	0	K	1	
OR6K	OR	--	6	K	1	
POLYK	MIT	--	--	K	1	POLYCRYSTAL
OR55K	OR	--	55	K	1	
ORUE	OR	--	0	E	1	
NC62E	NC	--	62	E	1	
OR55E	OR	--	55	E	1	
POLYE	MIT	--	--	E	1	POLYCRYSTAL
OR55F	OR	--	55	F	1	
ORUF	OR	--	0	F	1	
OR6F	OR	--	6	F	1	
POLYF	MIT	--	--	F	1	POLYCRYSTAL
OR6E	OR	--	6	E	1	
NC62F	NC	--	62	F	1	
OR55H	OR	--	55	H	1	
OR6H	OR	--	6	H	1	
ORUH	OR	--	0	H	1	
ORUH2	OR	--	0	H	2	
POLYH	MIT	--	--	H	1	POLYCRYSTAL
NC62H	NC	--	62	H	1	
ORUH3	OR	--	0	H	3	
NC62G	NC	--	62	G	1	
ORUG	OR	--	0	G	1	
POLYG	MIT	--	--	G	1	POLYCRYSTAL
OR6G	OR	--	6	G	1	
OR6G2	OR	--	6	G	2	
OR55G	OR	--	55	G	1	
ORUL	OR	--	0	L	1	
NC62L	NC	--	62	L	1	
OR55L	OR	--	55	L	1	
OR6L	OR	--	6	L	1	
ORUI	OR	--	0	I	1	
NC62I	NC	--	62	I	1	
LN55I	OR	--	55	I	1	22 DAYS @ 1400C IN PURE MGO POWDER
CA55I	OR	CA	55	I	1	22 DAYS @ 1400C IN 2600APPM CA MGO POWDER
CA6I	OR	CA	6	I	1	SAME AS ABOVE
LN6I	OR	--	6	I	1	22 DAYS @ 1400C IN PURE MGO POWDER
LN6I2	OR	--	6	I	2	SAME AS ABOVE
CA6I2	OR	CA	6	I	2	22 DAYS @ 1400C IN 2600APPM CA MGO POWDER
FEJ	SP	FE	0	I	1	SUPPLIED BY Y. OISHI
FEJ2	SP	FE	0	I	2	SUPPLIED BY Y. OISHI
LN55I2	OR	--	55	I	2	22 DAYS @ 1400C IN PURE MGO POWDER
LN6C94	OR	--	6	C	2	SAME AS ABOVE
MGONA	MIT	NA	--	NA	1	NA DOPED POLYCRYSTAL
MGONA2	MIT	NA	--	NA	1	SECOND NA DOPED POLYCRYSTAL
FE35D	SP	FE	35	D	1	310PPM FE
FEUD	SP	FE	0	D	1	310PPM FE
FE35A	SP	FE	35	A	1	310PPM FE
FEUA	SP	FE	0	A	1	310PPM FE
FEUA2	SP	FE	0	A	2	310PPM FE
NI27A	SP	NI	27	A	1	370PPM NI
NIUA	SP	NI	0	A	1	370PPM NI
NIUA2	SP	NI	0	A	2	370PPM NI
LI7PRE84	OR	LI	0	11	2	300-500APPM LI
LI7PR284	OR	LI	0	11	3	300-500APPM LI
LI7AR84	OR	LI	0	11	3	300-500APPM LI NOT PRE-ANNEALED
LIA60084	OR	LI	0	12	2	300-500APPM LI
LIA60284	OR	LI	0	12	3	300-500APPM LI
NI27B	SP	NI	27	B	1	370PPM NI

APPENDIX 5 TABLE 4

THIS TABLE CONTAINS VARIOUS INFORMATION FOR EACH SIMS PROFILE SAMPLE IN THE FOLLOWING ORDER-SIMS SAMPLE NAME,DIFFUSION ANNEAL TEMPERATURE IN DEGREES CENTIGRADE, DIFFUSION ANNEAL TIME IN SECONDS, SIMS SPUTTER CURRENT IN NANOAMPS, SIMS SPUTTER TIME IN SECONDS, TOTAL NUMBER OF CHANNELS DURING SIMS SPUTTERING, THE CONSTANT A USED IN DISLOCATION DIFFUSION PARAMETER CALCULATIONS (EQUATION 4.9), SPUTTER PIT DEPTH IN MICRONS CALCULATED BY EQUATION 4.7, ERROR IN SPUTTER PIT DEPTH IN MICRONS CALCULATED BY APPLYING 3.21 TO 4.7 AND ASSUMING NEGLIGIBLE ERROR IN SPUTTER CURRENT AND TIME, FRACTIONAL SPUTTER PIT DEPTH ERROR, AND THE CHANNEL NUMBER USED TO CALCULATE THE DIFFUSION DEPTH FOR TYPE C VERY SHORT TIME DIFFUSION ANNEALS.

SIMS	DIFFUSION		SIMS							
SAMPLE	ANNEAL		CONDITIONS							
NAME	TEMP	TIME	I	TIME	#CN	A	P	SP	SP/P	
	(C)	(SEC.)	(NA)	(SEC.)	-	-	MICRONS		-	
2MGO21	1386.	75780.	184.	3827.	403.	0.70	1.38	0.14	0.10	
MGO212	1386.	75780.	657.	1404.	184.	0.70	1.94	0.29	0.15	
2MGO4	1386.	14580.	167.	966.	102.	0.79	0.36	0.06	0.18	
3MGO4	1386.	14580.	167.	957.	101.	0.79	0.35	0.06	0.18	
4MGO4	1386.	14580.	150.	1994.	211.	0.79	0.61	0.08	0.13	
2A1421	1386.	75780.	260.	1747.	400.	0.70	0.93	0.12	0.13	
LI7AR1	1398.	26700.	250.	2423.	400.	0.75	1.21	0.14	0.12	
LI7PR1	1398.	26700.	256.	1162.	112.	0.75	0.64	0.10	0.16	
LI7AR2	1398.	26700.	218.	1106.	182.	0.75	0.52	0.09	0.17	
OR7PRE	1398.	26700.	216.	858.	141.	0.75	0.42	0.08	0.19	
OR7PR2	1398.	26700.	127.	1443.	237.	0.75	0.38	0.06	0.15	
FEAR7	1398.	26700.	278.	2684.	250.	0.75	1.48	0.16	0.11	
FEPR7	1398.	26700.	261.	620.	102.	0.75	0.39	0.09	0.23	
FEAR72	1398.	26700.	255.	1504.	250.	0.75	0.80	0.11	0.14	
LIP600	1412.	600.	162.	1010.	300.	1.01	0.36	0.06	0.17	
LIA600	1412.	600.	179.	1018.	300.	1.01	0.40	0.07	0.17	
6ORPR7	1398.	26700.	231.	1220.	200.	0.75	0.60	0.10	0.16	
OR6600	1412.	600.	212.	1212.	200.	1.01	0.55	0.09	0.16	
OR600	1412.	600.	182.	1223.	200.	1.01	0.48	0.07	0.16	
OR55C2	1216.	106560.	589.	1369.	129.	0.84	1.70	0.25	0.15	
ORUC	1216.	106560.	607.	2419.	400.	0.84	0.74	0.08	0.12	
OR6C	1216.	106560.	519.	1650.	156.	0.84	0.44	0.06	0.14	
OR6C2	1216.	106560.	552.	2617.	244.	0.84	0.72	0.08	0.11	
OR55C	1216.	106560.	593.	2436.	231.	0.84	0.72	0.08	0.12	
OR55C3	1216.	106560.	593.	897.	84.	0.84	0.30	0.06	0.19	
POLYC	1216.	106560.	790.	3977.	377.	0.84	1.53	0.15	0.10	
NC62C	1216.	106560.	762.	2214.	210.	0.84	0.85	0.10	0.12	
CA55C	1216.	106560.	787.	2421.	400.	0.84	0.95	0.11	0.12	
LN55C	1216.	106560.	786.	225.	36.	0.84	0.15	0.06	0.38	
LN55C2	1216.	106560.	777.	2420.	400.	0.84	0.94	0.11	0.12	
LN6C	1216.	106560.	802.	2007.	330.	0.84	0.82	0.10	0.12	
CA6C	1216.	106560.	808.	2392.	393.	0.84	0.97	0.11	0.12	
CA6C2	1216.	106560.	813.	2053.	337.	0.84	0.85	0.10	0.12	
OR6C3	1216.	106560.	810.	2420.	400.	0.84	0.98	0.11	0.12	
NC62B	1013.	4050.	810.	3309.	400.	2.83	1.32	0.14	0.10	178.
NC62B2	1013.	4050.	818.	2476.	400.	2.83	1.01	0.12	0.11	162.
NC62B3	1013.	4050.	825.	2581.	270.	2.83	1.06	0.12	0.11	-
ORCUTB	1013.	4050.	830.	2028.	400.	2.83	0.85	0.11	0.12	247.
FE35B	1013.	4050.	801.	2146.	400.	2.83	0.87	0.11	0.12	173.
OR6B	1013.	4050.	821.	2480.	400.	2.83	1.02	0.12	0.11	140.
OR55B	1013.	4050.	807.	2489.	400.	2.83	1.00	0.11	0.11	113.
ORCLB	1013.	4050.	788.	2499.	400.	2.83	0.98	0.11	0.11	127.
POLYB	1013.	4050.	815.	1790.	328.	2.83	0.75	0.10	0.13	161.
POLYB2	1013.	4050.	808.	1882.	344.	2.83	0.78	0.10	0.13	175.
ORUA	1410.	9690.	803.	2133.	350.	0.79	0.87	0.11	0.12	
OR55A	1410.	9690.	821.	2125.	350.	0.79	0.88	0.11	0.12	
POLYA	1410.	9690.	803.	2419.	400.	0.79	0.97	0.11	0.12	
OR6A	1410.	9690.	799.	2119.	350.	0.79	0.86	0.10	0.12	

APPENDIX 5 TABLE 4 (cont.)

OR6A2	1410.	9690.	709.	1929.	318.	0.79	0.70	0.09	0.13	
MGOCR	1398.	26700.	815.	2200.	362.	0.75	0.90	0.11	0.12	
MGOCR2	1398.	26700.	809.	2834.	350.	0.75	1.14	0.12	0.11	
ORUD	1210.	64680.	818.	1702.	204.	0.89	0.72	0.10	0.13	
NIUD	1210.	64680.	604.	2409.	202.	0.89	0.73	0.08	0.12	
NI27D	1210.	64680.	1040.	2511.	238.	0.89	1.30	0.15	0.11	
ORUJ	1304.	40140.	822.	1425.	171.	0.80	0.61	0.09	0.15	
OR6J	1304.	40140.	826.	2487.	300.	0.80	1.03	0.12	0.11	
OR55J	1304.	40140.	858.	1608.	194.	0.80	0.71	0.10	0.14	
NC62J	1304.	40140.	900.	1298.	156.	0.80	0.62	0.09	0.15	
POLYJ	1304.	40140.	849.	2483.	300.	0.80	1.05	0.12	0.11	
NC62K	1486.	2755.	860.	2249.	271.	0.80	0.97	0.12	0.12	
ORUK	1486.	2755.	844.	2494.	300.	0.80	1.05	0.12	0.11	
OR6K	1486.	2755.	854.	2493.	300.	0.80	1.06	0.12	0.11	
POLYK	1486.	2755.	859.	2478.	297.	0.80	1.06	0.12	0.11	
OR55K	1486.	2755.	835.	2494.	300.	0.80	1.04	0.12	0.11	
ORUE	1205.	42600.	625.	2492.	300.	0.93	0.78	0.09	0.11	
NC62E	1205.	42600.	801.	2208.	265.	0.93	0.89	0.11	0.12	
OR55E	1205.	42600.	850.	1933.	232.	0.93	0.84	0.11	0.13	
POLYE	1205.	42600.	856.	2487.	300.	0.93	1.06	0.12	0.11	
OR55F	1205.	9720.	853.	2494.	300.	1.08	1.06	0.12	0.11	
ORUF	1205.	9720.	844.	1494.	300.	1.08	0.66	0.09	0.14	
OR6F	1205.	9720.	848.	1617.	325.	1.08	0.71	0.10	0.14	
POLYF	1205.	9720.	876.	1616.	325.	1.08	0.73	0.10	0.14	
OR6E	1205.	42600.	848.	1865.	225.	0.93	0.81	0.10	0.13	
NC62F	1205.	9720.	838.	1487.	300.	1.08	0.65	0.09	0.14	
OR55H	1211.	579600.	888.	2914.	351.	0.75	1.28	0.14	0.11	
OR6H	1211.	579600.	880.	2304.	277.	0.75	1.02	0.12	0.12	
ORUH	1211.	579600.	865.	493.	57.	0.75	0.27	0.07	0.26	
ORUH2	1211.	579600.	871.	536.	84.	0.75	0.29	0.07	0.25	
POLYH	1211.	579600.	882.	2077.	250.	0.75	0.93	0.11	0.12	
NC62H	1211.	579600.	860.	2090.	253.	0.75	0.91	0.11	0.12	
ORUH3	1211.	579600.	885.	2488.	300.	0.75	1.10	0.13	0.11	
NC62G	1127.	605.	881.	2329.	319.	2.46	1.03	0.12	0.12	107.
ORUG	1127.	605.	903.	2186.	298.	2.46	1.00	0.12	0.12	-
POLYG	1127.	605.	877.	2305.	314.	2.46	1.02	0.12	0.12	104.
OR6G	1127.	605.	893.	2339.	319.	2.46	1.05	0.12	0.12	257.
OR6G2	1127.	605.	874.	2272.	310.	2.46	1.00	0.12	0.12	167.
OR55G	1127.	605.	853.	2072.	282.	2.46	0.90	0.11	0.12	121.
ORUL	1209.	241.	869.	1854.	252.	2.11	0.82	0.11	0.13	113.
NC62L	1209.	241.	864.	2377.	325.	2.11	1.03	0.12	0.12	159.
OR55L	1209.	241.	855.	1282.	175.	2.11	0.58	0.09	0.15	-
OR6L	1209.	241.	848.	1296.	176.	2.11	0.58	0.09	0.15	82.
ORUI	1411.	9710.	862.	2406.	289.	0.79	1.04	0.12	0.12	
NC62I	1411.	9710.	868.	2488.	300.	0.79	1.08	0.12	0.11	
LN55I	1411.	9710.	851.	1313.	158.	0.79	0.59	0.09	0.15	
CA55I	1411.	9710.	880.	2154.	259.	0.79	0.96	0.12	0.12	
CA6I	1411.	9710.	845.	2449.	295.	0.79	1.04	0.12	0.11	
LN6I	1411.	9710.	870.	2488.	300.	0.79	1.08	0.12	0.11	
LN6I2	1411.	9710.	904.	2488.	300.	0.79	1.12	0.13	0.11	
CA6I2	1411.	9710.	883.	2489.	300.	0.79	1.10	0.13	0.11	
FEJ	1411.	9710.	876.	450.	50.	0.79	0.26	0.07	0.27	
FEJ2	1411.	9710.	875.	2277.	274.	0.79	1.00	0.12	0.12	
LN55I2	1411.	9710.	871.	2119.	383.	0.79	0.93	0.11	0.12	
LN6C94	1216.	106560.	903.	2151.	425.	0.84	0.98	0.12	0.12	
MGONA	1411.	12015.	857.	2247.	450.	0.79	0.97	0.12	0.12	
MGONA2	1411.	12015.	865.	1775.	355.	0.79	0.79	0.10	0.13	
FE35D	1210.	64680.	878.	2066.	414.	0.89	0.92	0.11	0.12	
FEUD	1210.	64680.	898.	1740.	348.	0.89	0.80	0.11	0.13	
FE35A	1410.	9690.	881.	1522.	304.	0.79	0.70	0.10	0.14	
FEUA	1410.	9690.	883.	158.	31.	0.79	0.14	0.06	0.45	
FEUA2	1410.	9690.	879.	2240.	450.	0.79	0.99	0.12	0.12	
NI27A	1410.	9690.	872.	227.	45.	0.79	0.16	0.06	0.38	
NIUA	1410.	9690.	887.	2232.	450.	0.79	1.00	0.12	0.12	
NIUA2	1410.	9690.	892.	2230.	450.	0.79	1.00	0.12	0.12	
LI7PRE84	1398.	26700.	858.	478.	72.	0.75	0.26	0.07	0.26	
LI7PR284	1398.	26700.	860.	1465.	242.	0.75	0.66	0.09	0.14	
LI7AR84	1398.	26700.	864.	1380.	228.	0.75	0.63	0.09	0.15	
LIA60084	1412.	600.	887.	199.	32.	1.01	0.16	0.06	0.41	
LIA60284	1412.	600.	885.	1303.	213.	1.01	0.61	0.09	0.15	
NI27B	1013.	4050.	811.	2028.	400.	2.83	0.83	0.10	0.12	119.

APPENDIX 5 TABLE 5

THIS TABLE LISTS DATA FOR THE SIMS SAMPLES LISTED.
COLUMN 1: SIMS SAMPLE NAME
" 2: BULK DIFFUSION COEFFICIENT OR OR DISLOCATION/GRAIN BOUNDARY DIFFUSION COEFFICIENT FOR VERY SHORT TIME DIFFUSION ANNEALS
" 3: DISLOCATION DIFFUSION PARAMETER
" 4: DISLOCATION DENSITY CALCULATED FROM TAIL INTERCEPT BY EQN 3.10 NUMBER PER SQUARE CENTIMETER
" 5: GRAIN BOUNDARY DIFFUSION PARAMETER
" 6: BETA CALCULATED FROM EQNS. 3.12 & 5.1,DIFFUSION TIME & COLUMN 5
" 7: LOG(C-0.00204) VS. DIFFUSION DISTANCE(CM.) TO THE 1.2 POWER SLOPE
" 8: LOG(C-0.00204) VS. DIFFUSION DISTANCE(CM.) TAIL SLOPE
SOME NUMBERS NOT CALCULATED FOR VERY SHORT TIME DIFFUSION ANNEALS OR FOR SIMS SAMPLES WITH UNRELIABLE TAILS
FORMAT: 0.AAAE-XX REPRESENTS 0.AAA TIMES 10 TO THE -XX POWER

SIMS SAMPLE NAME	BULK D	DISLOC. DAA	DISLOC. DENSITY CALCULATED	GRAIN BOUNDARY DD	BETA	SLOPE 6/5 POWER X AXIS	SLOPE LINEAR X AXIS
2MG021	0.994E-15	0.305E-25	0.135E+11	0.393E-19	0.478E+02	-0.307E+06	-0.458E+05
MG0212	0.161E-15	----------					-0.148E+05
2MG04	0.111E-15	0.225E-26	0.731E+10	0.531E-20	0.148E+02	-0.167E+07	-0.190E+06
3MG04	0.359E-13	0.220E-25	0.106E+12	0.456E-19	0.127E+03	-0.459E+06	-0.608E+05
4MG04	0.286E-14	0.242E-25	0.728E+11	0.501E-19	0.139E+03	-0.435E+06	-0.581E+05
2A1421	0.606E-15	0.213E-25	0.184E+11	0.260E-19	0.317E+02	-0.392E+06	-0.547E+05
LI7AR1	0.154E-13	----------					-0.421E+05
LI7PR1	0.932E-15	0.413E-26	0.326E+11	0.101E-19	0.160E+02	-0.997E+06	-0.145E+06
LI7AR2	0.270E-15	0.308E-26	0.726E+10	0.727E-20	0.115E+02	-0.122E+07	-0.168E+06
OR7PRE	0.771E-15	0.116E-26	0.141E+12	0.316E-20	0.499E+01	-0.201E+07	-0.274E+06
OR7PR2	0.660E-15	0.112E-26	0.138E+12	0.296E-20	0.469E+01	-0.208E+07	-0.279E+06
FEAR7	0.698E-15	0.127E-24	0.286E+10	0.210E-18	0.333E+03	-0.161E+06	-0.262E+05
FEPR7	0.188E-15	0.484E-26	0.359E+10	0.103E-19	0.163E+02	-0.985E+06	-0.134E+06
FEAR72	0.274E-15	0.189E-24	0.339E+09	0.290E-18	0.459E+03	-0.133E+06	-0.215E+05
LIP600	0.378E-14	0.405E-26	0.495E+12	0.242E-19	0.189E+03	-0.196E+07	-0.218E+06
LIA600	0.773E-14	0.109E-26	0.102E+13	0.907E-20	0.709E+02	-0.353E+07	-0.421E+06
6ORPR7	0.321E-15	0.389E-26	0.104E+11	0.862E-20	0.136E+02	-0.110E+07	-0.150E+06
OR6600	0.557E-14	0.112E-25	0.118E+12	0.749E-19	0.586E+03	-0.994E+06	-0.131E+06
OR600	0.879E-14	0.591E-26	0.321E+12	0.406E-19	0.317E+03	-0.144E+07	-0.181E+06
OR55C2	0.244E-16	0.868E-26	0.971E+10	0.253E-19	0.164E+04	-0.157E+06	-0.259E+05
ORUC	0.115E-16	0.186E-26	0.363E+10	0.521E-20	-0.406E+06	0.337E+03	-0.560E+05
OR6C	0.376E-17	0.150E-26	0.196E+10	0.405E-20	-0.472E+06	0.262E+03	-0.623E+05
OR6C2	0.725E-17	0.350E-25	0.352E+10	0.687E-19	-0.864E+05	0.445E+04	-0.129E+05
OR55C	0.113E-16	0.254E-26	0.526E+10	0.613E-20	-0.368E+06	0.397E+03	-0.478E+05
OR55C3	0.133E-16	0.182E-20	0.230E+10	0.313E-15	-0.552E+03	0.203E+08	-0.566E+02
POLYC	0.105E-16	0.311E-26	0.162E+11	0.901E-20	-0.292E+06	0.584E+03	-0.432E+05
NC62C	0.816E-17	0.176E-26	0.555E+10	0.540E-20	-0.398E+06	0.350E+03	-0.575E+05
CA55C	0.746E-17	0.347E-26	0.134E+10	0.843E-20	-0.304E+06	0.546E+03	-0.409E+05
LN55C	0.993E-17	0.218E-27	0.111E+11	0.669E-21	-0.139E+07	0.433E+02	-0.163E+06
LN55C2	0.468E-17	0.551E-26	0.434E+10	0.142E-19	-0.223E+06	0.917E+03	-0.325E+05
LN6C	0.810E-17	0.148E-27	0.371E+10	0.585E-21	-0.151E+07	0.379E+02	-0.198E+06
CA6C	0.155E-16	0.361E-26	0.259E+10	0.109E-19	-0.260E+06	0.708E+03	-0.402E+05
CA6C2	0.200E-16	0.809E-27	0.422E+10	0.274E-20	-0.598E+06	0.177E+03	-0.848E+05
OR6C3	0.102E-16	0.117E-25	0.369E+10	0.298E-19	-0.143E+06	0.193E+04	-0.222E+05
NC62B	0.212E-12	----------				0.352E+07	-0.205E+05
NC62B2	0.104E-12	----------				0.540E+08	-0.363E+04
NC62B3	----------					0.119E+10	-0.661E+03
ORCUTB	0.172E-12	----------				0.150E+09	-0.197E+04
FE35B	0.871E-13	----------				0.553E+09	-0.921E+03
OR6B	0.778E-13	----------				0.173E+09	-0.196E+04
OR55B	0.497E-13	----------				0.207E+09	-0.163E+04
ORCLB	0.603E-13	----------				0.180E+10	-0.488E+03
POLYB	0.832E-13	----------				0.487E+07	-0.148E+05
POLYB2	0.963E-13	----------				0.279E+08	-0.532E+04
ORUA	0.164E-15	0.148E-25	0.483E+10	0.368E-19	-0.656E+06	0.747E+02	-0.881E+05
OR55A	0.133E-15	0.134E-25	0.324E+10	0.344E-19	-0.683E+06	0.698E+02	-0.927E+05
POLYA	0.240E-15	0.759E-25	0.285E+11	0.163E-18	-0.268E+06	0.332E+03	-0.389E+05
OR6A	0.150E-15	0.343E-25	0.117E+11	0.832E-19	-0.402E+06	0.169E+03	-0.579E+05

APPENDIX 5 TABLE 5 (cont.)

OR6A2	0.943E-16	0.139E-25	0.408E+10	0.336E-19	-0.693E+06	0.682E+02	-0.911E+05
MGOCR	0.543E-15	0.856E-26	0.193E+11	0.165E-19	-0.744E+06	0.261E+02	-0.101E+06
MGOCR2	0.397E-15	0.195E-25	0.577E+10	0.343E-19	-0.479E+06	0.543E+02	-0.670E+05
ORUD	0.137E-16	0.937E-27	0.181E+10	0.322E-20	-0.609E+06	0.315E+03	-0.790E+05
NIUD	0.298E-16	0.881E-26	0.805E+10	0.290E-19	-0.163E+06	0.284E+04	-0.258E+05
NI27D	0.217E-16	0.695E-26	0.752E+10	0.239E-19	-0.183E+06	0.234E+04	-0.290E+05
ORUJ	0.375E-16	0.513E-26	0.587E+09	0.126E-19	-0.503E+06	0.139E+03	-0.680E+05
OR6J	0.388E-16	0.659E-26	0.114E+10	0.162E-19	-0.433E+06	0.179E+03	-0.600E+05
OR55J	0.391E-16	0.791E-27	0.623E+10	0.221E-20	-0.143E+07	0.245E+02	-0.173E+06
NC62J	0.619E-16	0.289E-26	0.287E+11	0.740E-20	-0.692E+06	0.818E+02	-0.906E+05
POLYJ	0.483E-16	0.129E-24	0.909E+10	0.293E-18	-0.762E+05	0.324E+04	-0.135E+05
NC62K	0.614E-15	0.253E-23	0.137E+10	0.502E-17	-0.682E+05	0.408E+04	-0.114E+05
ORUK	0.709E-15	0.196E-24	0.865E+09	0.464E-18	-0.285E+06	0.377E+03	-0.411E+05
OR6K	0.651E-15	0.209E-24	0.213E+10	0.571E-18	-0.251E+06	0.464E+03	-0.398E+05
POLYK	0.645E-15	0.147E-23	0.171E+11	0.322E-17	-0.890E+05	0.261E+04	-0.150E+05
OR55K	0.235E-15	0.231E-24	0.768E+09	0.591E-18	-0.246E+06	0.480E+03	-0.378E+05
ORUE	0.487E-17	0.163E-26	0.151E+10	0.548E-20	-0.489E+06	0.758E+03	-0.599E+05
NC62E	0.425E-17	0.121E-26	0.450E+10	0.528E-20	-0.500E+06	0.731E+03	-0.695E+05
OR55E	0.126E-16	0.513E-26	0.280E+10	0.189E-19	-0.232E+06	0.262E+04	-0.337E+05
POLYE	0.125E-16	0.139E-25	0.867E+10	0.575E-19	-0.119E+06	0.795E+04	-0.205E+05
OR55F	0.195E-16	0.253E-25	0.298E+10	0.124E-18	-0.117E+06	0.359E+05	-0.176E+05
ORUF	0.354E-16	0.161E-25	0.371E+10	0.600E-19	-0.181E+06	0.174E+05	-0.221E+05
OR6F	0.314E-16	0.615E-26	0.441E+10	0.281E-19	-0.285E+06	0.815E+04	-0.358E+05
POLYF	0.418E-16	0.197E-26	0.413E+11	0.121E-19	-0.472E+06	0.352E+04	-0.631E+05
OR6E	0.127E-16	0.450E-26	0.122E+11	0.169E-19	-0.249E+06	0.234E+04	-0.360E+05
NC62F	0.240E-16	0.104E-25	0.174E+11	0.515E-19	-0.198E+06	0.149E+05	-0.274E+05
OR55H	0.263E-17	0.417E-27	0.121E+10	0.806E-21	-0.729E+06	0.256E+02	-0.101E+06
OR6H	0.368E-17	0.376E-26	0.391E+09	0.596E-20	-0.219E+06	0.190E+03	-0.336E+05
ORUH	0.636E-17	0.390E-27	0.322E+10	0.717E-21	-0.781E+06	0.228E+02	-0.104E+06
ORUH2	0.319E-17	0.117E-26	0.802E+09	0.158E-20	-0.486E+06	0.504E+02	-0.602E+05
POLYH	0.643E-17	0.471E-26	0.790E+10	0.768E-20	-0.188E+06	0.244E+03	-0.300E+05
NC62H	0.274E-17	0.206E-27	0.996E+10	0.379E-21	-0.115E+07	0.121E+02	-0.143E+06
ORUH3	0.414E-17	0.211E-27	0.146E+10	0.409E-21	-0.109E+07	0.130E+02	-0.142E+06
NC62G	0.494E-12	--------	--------	--------	--------	0.203E+09	-0.118E+04
ORUG	--------	--------	--------	--------	--------	--------	-0.114E+04
POLYG	0.477E-12	--------	--------	--------	--------	0.605E+08	-0.241E+04
OR6G	0.294E-11	--------	--------	--------	--------	0.259E+07	-0.172E+05
OR6G2	0.119E-11	--------	--------	--------	--------	0.351E+08	-0.341E+04
OR55G	0.605E-12	--------	--------	--------	--------	0.109E+10	-0.441E+03
ORUL	0.140E-11	--------	--------	--------	--------	0.142E+08	-0.367E+04
NC62L	0.262E-11	--------	--------	--------	--------	0.804E+08	-0.129E+04
OR55L	--------	--------	--------	--------	--------	--------	-0.123E+04
OR6L	0.765E-12	--------	--------	--------	--------	0.768E+07	-0.486E+04
ORUI	0.157E-15	0.410E-25	0.120E+10	0.769E-19	-0.423E+06	0.153E+03	-0.533E+05
NC62I	0.187E-15	0.375E-25	0.157E+10	0.930E-19	-0.377E+06	0.185E+03	-0.557E+05
LN55I	0.106E-15	0.453E-25	0.267E+10	0.110E-18	-0.342E+06	0.218E+03	-0.507E+05
CA55I	0.524E-16	0.231E-25	0.668E+09	0.536E-19	-0.525E+06	0.107E+03	-0.711E+05
CA6I	0.241E-15	0.111E-24	0.304E+10	0.190E-18	-0.246E+06	0.377E+03	-0.324E+05
LN6I	0.356E-15	0.571E-25	0.719E+10	0.135E-18	-0.302E+06	0.268E+03	-0.452E+05
LN6I2	0.182E-15	0.218E-24	0.212E+10	0.366E-18	-0.166E+06	0.728E+03	-0.231E+05
CA6I2	0.249E-15	0.715E-25	0.484E+10	0.141E-18	-0.294E+06	0.280E+03	-0.404E+05
FEJ	0.315E-15	0.584E-26	0.631E+10	0.162E-19	-0.108E+07	0.322E+02	-0.141E+06
FEJ2	0.162E-15	0.203E-26	0.221E+10	0.567E-20	-0.202E+07	0.113E+02	-0.240E+06
LN55I2	0.695E-16	0.112E-23	0.135E+09	0.180E-17	-0.638E+05	0.357E+04	-0.102E+05
LN6C94	0.439E-17	--------	--------	--------	--------	--------	-0.108E+05
MGONA	0.775E-16	0.540E-25	0.273E+10	0.844E-19	-0.375E+06	0.151E+03	-0.465E+05
MGONA2	0.667E-16	0.362E-23	0.135E+10	0.319E-17	-0.425E+05	0.569E+04	-0.568E+04
FE35D	0.763E-17	0.405E-27	0.409E+10	0.162E-20	-0.921E+06	0.158E+03	-0.120E+06
FEUD	0.118E-16	0.869E-26	0.715E+10	0.299E-19	-0.160E+06	0.292E+04	-0.259E+05
FE35A	0.152E-15	0.289E-25	0.619E+10	0.646E-19	-0.468E+06	0.131E+03	-0.630E+05
FEUA	0.668E-15	--------	--------	--------	--------	--------	-0.250E+05
FEUA2	0.172E-15	0.287E-25	0.138E+11	0.685E-19	-0.452E+06	0.139E+03	-0.633E+05
NI27A	0.521E-15	0.232E-25	0.102E+11	0.478E-19	-0.561E+06	0.970E+02	-0.704E+05
NIUA	0.103E-15	0.231E-25	0.715E+10	0.480E-19	-0.559E+06	0.975E+02	-0.706E+05
NIUA2	0.110E-15	0.112E-25	0.716E+10	0.236E-19	-0.855E+06	0.480E+02	-0.101E+06
LI7PRE84	0.452E-15	0.157E-25	0.223E+10	0.286E-19	-0.534E+06	0.452E+02	-0.745E+05
LI7PR284	0.274E-15	0.288E-24	0.289E+09	0.406E-18	-0.109E+06	0.643E+03	-0.174E+05
LI7AR84	0.734E-16	0.386E-26	0.146E+10	0.785E-20	-0.116E+07	0.124E+02	-0.150E+06
LIA60084	0.275E-14	0.435E-26	0.300E+12	0.294E-19	-0.174E+07	0.230E+03	-0.211E+06
LIA60284	0.497E-15	--------	--------	--------	--------	--------	-0.387E+05
NI27B	0.377E-13	--------	--------	--------	--------	0.268E+08	-0.546E+04